



DISSERTATION

Ab initio calculation of the spin-lattice relaxation time T_1 in the negatively charged nitrogen vacancy center in diamond

Ausgeführt zum Zwecke der Erlangung des akademischen Grades eines
Doktors der technischen Wissenschaften unter der Leitung von

UNIV.PROF. DR. TECHN. PETER MOHN

INSTITUT FÜR ANGEWANDTE PHYSIK E134

CENTER FOR COMPUTATIONAL MATERIALS SCIENCE

eingereicht an der Technischen Universität Wien
Fakultät für Physik

von

DIPL.-ING. JOHANNES GUGLER

e1026727

Währingerstrasse 108/9

1180 Wien

Wien, am 6. November 2018

Kurzfassung

Diese Doktorarbeit behandelt die *ab initio* Berechnung der Spin-Gitter Relaxationszeit T_1 im negativ geladenen Stickstoff-Fehlstellen Zentrum (NV^- Zentrum) in Diamant. Spin-Gitter Relaxation ist der Vorgang durch den die Energie zwischen einem Spin-System und der Umgebung ausgetauscht wird. Im Fall eines Festkörpers tritt als stärkster Kopplungsmechanismus die Wechselwirkung zwischen dem Spin-System und den bewegten Ionen, welche das Gitter des Festkörpers aufbauen, auf. Die Eigenschaften des hier untersuchten NV^- Zentrums und die Anwendungen dieses Farbzentrum in der Messtechnik und Quantenmechanik werden in Kapitel 1 eingeführt und die Bedeutung dieser Arbeit wird motiviert. Das theoretische Fundament für die Behandlung eines allgemeinen quantenmechanischen Viel-Teilchen-Systems im Falle eines Festkörpers wird in Kapitel 2 gelegt: Ausgehend vom Hohenberg-Kohn Theorem wird die Dichtefunktionaltheorie und deren Anwendung im Kohn-Sham-System eingeführt. Diverse Approximationen für die Beschreibung der Vielteilcheneffekte werden vorgestellt und hinsichtlich ihrer Genauigkeit und Rechenintensität analysiert. Um die Relaxationszeit auszurechnen, ist eine Modellierung der Bewegung der Ionen unabdingbar. Zu deren Zweck wird in Kapitel 3 eine quantenmechanische Beschreibung der Gitterschwingungen, Phononen genannt, in harmonischer Näherung gegeben. In Kapitel 4 wird die Historie der theoretischen Beschreibungen der Spin-Gitter-Relaxation präsentiert und es werden den historischen Beschreibungen folgend Ausdrücke für die Spin-Gitter-Relaxationszeit T_1 abgeleitet. Dies geschieht ausgehend von zwei unterschiedlichen Kopplungsmechanismen: Der erste Mechanismus resultiert aus der Änderung der magnetischen Spin-Spin Wechselwirkung, welche durch Ionenbewegung induziert wird. Der zweite Mechanismus entsteht durch die induzierte Änderung der Spin-Bahn Wechselwirkung. Die Relaxationszeiten für den ersten Mechanismus werden in Kapitel 5 *ab initio* mithilfe von Computerprogrammen berechnet und ein theoretisches Verständnis der langen Relaxationszeiten für das ausgewählte Spin-System wird erlangt: Aufgrund der hohen Steifigkeit von Diamanten existieren wenige Gitterschwingungen, welche der niedrigen Übergangsfrequenz des Spin-Systems entsprechen. Wie

weitere Simulationen zeigen, resultiert eine Beschädigung des Diamantgitters in niederfrequenteren Gitterschwingungen, was eine Verkürzung der Relaxationszeit nach sich zieht. Die berechneten Daten erlauben den Schluss, dass die langen Relaxationszeiten aus der Kopplung über die Spin-Spin Wechselwirkung resultieren. Abschließend werden in Kapitel 6 die wichtigsten Aussagen dieser Arbeit zusammengefasst und ein Ausblick auf mögliche zukünftige Forschungsarbeit geboten.

Abstract

This work is concerned with an *ab initio* calculation of the spin lattice relaxation time T_1 of the negatively charged nitrogen vacancy center (NV^- center) in diamond. Spin lattice relaxation is the mechanism by which the energy between a spin system and its surrounding is transferred. In the case of a solid, the most important mechanism for spin coupling is given by the interaction of a spin system with the moving ions which constitute the lattice of the material. The NV^- center in diamond as the spin system of choice and its applications in measurement technology and quantum theory are introduced and the implications of this thesis are pointed out in Chapter 1. The theoretical foundations for the treatment of a quantum mechanical many body problem in a solid are laid in Chapter 2: Starting from the Hohenberg-Kohn theorem, the machinery of density functional theory for the Kohn-Sham system with its different levels of approximations for a treatment of the many body effects is presented. For the calculation of the relaxation time T_1 , the dynamics of the ions have to be modeled: Chapter 3 is dedicated to the quantum mechanical calculation of the lattice dynamics in the harmonic approximation, where a proper description of phonons, the quantized vibrations in solids, is derived. In Chapter 4, electron spins and phonons are coupled. At the beginning of this Chapter, we will introduce the history of the treatment of spin-lattice relaxation. Subsequently, the expressions of relaxation rates via first and second order time dependent perturbation theory are deduced and two different mechanisms of spin-phonon coupling are considered: Coupling via the magnetic spin-spin interaction and coupling via the spin-orbit interaction. Expressions for the relaxation time T_1 are given for both coupling cases. The relaxation rates are calculated *ab initio* in Chapter 5, where the electronic and ionic properties of the NV^- center are simulated and effects of the local vibrations are taken into account. The simulations show that the measured relaxation times may be explained by the changes of the spin-spin interaction, when the ions start to move. The excellent spin properties of the NV^- center are explained by the strong covalent bonds in diamond, which result in high frequency phonons, way above the spin transition frequency. Further simulations show that induced crystal damage alters

the phononic properties of the system and reduces T_1 . Chapter 6 concludes and gives a small outlook for possible future investigations.

Dedication

This work is dedicated to my family and my girlfriend Stephanie, who have always been there for me and supported me, no matter how difficult it was. Without their dedicated education and love, I would never have been able to concentrate on my studies.

Declaration

I hereby declare that except where specific reference is made to the work of others, the contents of this dissertation are original and have not been submitted in whole or in part for consideration for any other degree or qualification in this, or any other university. This dissertation is my own work and contains nothing which is the outcome of work done in collaboration with others, except as specified in the text and acknowledgements.

Acknowledgement

I acknowledge all the people and institutions that supported this work:

- My collaborators from the Atominstitut of TU Vienna, Thomas Astner, Andreas Angerer, Johannes Majer and Jörg Schmiedmayer for performing excellent experiments that lay the foundation of this research.
- All my colleagues from the Center for Computational Materials Science, Michael Wolloch, Jakub Planer, Martin Pimon, Jacqueline Atanelov, Wernfried Mayr-Schmölzer and Professor Josef Redinger for fruitful discussions and pleasant social interaction. I am especially thankful to Wernfried for always helping me with software issues.
- My supervisor Professor Peter Mohn for endless support, patience and for giving me the possibility to deal with subjects I am interested in. I am very thankful for his introduction to the life of a scientist and the philosophical requirements one needs to work in the field of gaining knowledge.
- The austrian science fund FWF and the ViCoM project for the funding and the opportunity to attend international conferences.

Contents

1	Introduction	1
1.1	History of the NV center	1
1.2	Applications of the NV ⁻ center	4
1.2.1	Sensing	4
1.2.2	NV ⁻ centers in quantum information technology	5
1.3	Sample production	5
2	Introduction to density functional theory (DFT)	9
2.1	The Born-Oppenheimer Approximation and the Hellmann-Feynman theorem	9
2.2	Hartree and Hartree-Fock theory	12
2.3	Hohenberg-Kohn theorem	15
2.4	Thomas-Fermi theory	16
2.5	Kohn-Sham theory	17
2.6	The exchange and correlation Energy E_{xc}	18
2.6.1	The local density approximation (LDA)	21
2.6.2	Gradient expansion approximation (GEA)	22
2.6.3	Generalized gradient approximations (GGA)	23
2.6.4	MetaGGAs	24
2.6.5	Hybrid functionals	25
2.6.6	Semi-empirical functionals	26
2.7	Solid state systems	26
2.7.1	Periodic systems - crystals structures and Bloch's theorem	26
2.8	Wannier functions	30
2.9	Software package	33
3	The theory of lattice vibrations	36
3.1	The harmonic approximation	36
3.2	Calculating the phonon dispersion	41
3.2.1	Diamond phonons	41

4	Spin-lattice relaxation theory	48
4.1	Introduction	48
4.2	The first investigation on spin-lattice relaxation - Ivar Waller . .	48
4.3	Putting spin-orbit coupling in the game - Gorter, Kronig and Van Vleck	50
4.4	Spin relaxation in metals - Overhauser	52
4.5	Elliott and Yafet's theories of spin relaxation	53
4.6	Dyakonov-Perel	55
4.7	The Bir-Aronov-Pikus mechanism - relaxation by hole scattering	55
4.8	Higher order processes I: Raman processes	56
4.8.1	Raman processes in first order perturbation theory . . .	57
4.8.2	Raman processes in second order perturbation theory . .	60
4.9	Higher order processes II: Localized phonons - the Orbach process	61
4.10	The phonon-bottleneck	62
4.11	Measurements of T_1 in the NV^- center	62
4.11.1	Elevated temperature measurements	62
4.11.2	Low temperature measurements	64
4.12	Spin-lattice relaxation in the Nitrogen-Vacancy center	65
4.12.1	Waller's process revised	65
4.12.2	Elliott-Yafet relaxation rate calculation	71
5	<i>Ab initio</i> calculation of Γ_0	77
5.1	Ab initio Calculation of Γ_0 for a Waller process	77
5.1.1	Accuracy of the calculations	78
5.1.2	The phononic properties of the NV^- center	78
5.2	The electronic properties of the NV^- center	90
5.2.1	Maximally localized Wannier functions at the NV^- center	92
5.3	Moving orbitals	92
5.3.1	Bader analysis	93
5.3.2	Geometrical separation	94
5.3.3	Results for the Waller process	94
5.4	Ab initio Calculation of Γ_0 for the Elliott-Yafet process	95
5.4.1	Comparison with experiment	96
6	Summary and outlook	100
	Appendices	101

A	Response functions	101
A.1	Linear Response	101
A.2	Properties of response functions	104
B	A short introduction to group theory	105
C	Time-dependent perturbation theory	108
D	2nd order diagrams	113
E	Additional data for Chapter 5	118
E.1	Eigenvectors and group velocities	118
E.2	Localized phonon modes	118

List of Figures

1.1	NV center structure	2
1.2	NV^- level scheme	3
2.1	Self consistency cycle	14
2.2	2d Bravais lattice	27
2.3	Diamond unit cells	28
2.4	Bandstructure diamond	31
2.5	Diamond Bloch and Wannier functions	32
3.1	Phonons: spring model	37
3.2	Diamond lattice constant	42
3.3	Diamond phonon bands and DOS	43
3.4	Diamond: Functional variation for bands and DOS	44
3.5	Diamond: polarization vectors	45
4.1	Debye functions	59
4.2	Elevated temperature T_1 measurement for the NV^- center	63
4.3	Waller relaxation sketch	65
4.4	Relaxation rates measurement	70
5.1	Cutoff convergence NV^- center	79
5.2	Lattice constant NV^- center	79
5.3	Relaxation in the NV^- center	80
5.4	Phonon DOS and BANDS with NV^- center	82
5.5	NV^- supercell 2x2x2 vs. 1x1x1 : Bandstructure and DOS	83
5.6	NV^- density comparison	84
5.7	NV^- phonons supercell convergence	86
5.8	NV^- phonons supercell convergence	87
5.9	0.1 THz isosurface and group velocity	88
5.10	The localization of phonon modes	89
5.11	Bandstructure of the NV^- center	91
5.12	Electronic orbitals of the NV^- center	91

5.13	Maximally localized Wannier functions	92
5.14	Electronic density of states at the nitrogen atom	93
5.15	Bader volume and charge density	94
5.16	Wigner-Seitz cell of the nitrogen atom	95
5.17	Rate comparison with experiment	97
E.1	Phonons supercell convergence	119

List of acronyms

NV nitrogen-vacancy

LCAO linear combination of atomic orbitals

HPHT high pressure high temperature

PBE Perdew-Burke-Ernzerhof

LDA local density approximation

HSE Heyd-Scuseria-Ernzerhof

LSDA local spin density approximation

GEA gradient expansion approximation

GGA generalized gradient approximation

DFT density functional theory

ZPL zero phonon line

ESR electron spin resonance

ODMR optically detected magnetic resonance

MLWF maximally localized Wannier function

VASP Vienna *ab initio* Simulation Package

NMR nuclear magnetic resonance

MRI magnetic resonance imaging

DOS density of states

List of symbols

Symbol	Description	Si-unit
T_1	Spin-lattice relaxation time	s
Γ_1	Spin-lattice relaxation rate	s^{-1}
\mathbf{S}	Spin vector	$\text{kgm}^2\text{s}^{-1}$
m_s	Magnetic quantum number for S_z	1
\mathbf{L}	Angular momentum	$\text{kgm}^2\text{s}^{-1}$
m_l	Magnetic quantum number for L_z	1
\mathbf{J}	Total angular momentum	$\text{kgm}^2\text{s}^{-1}$
m_j	Magnetic quantum number for J_z	1
g	Gyromagnetic ratio	1
\mathbf{B}	Magnetic field	T
\mathbf{E}	Electric field	NC^{-1}
D	Zero field splitting constant	Hz
t	Time	s
$\hat{\mathcal{H}}$	Hamilton operator	J
E	Energy	J
\hat{T}	Kinetic energy operator	J
\hat{v}	Potential energy operator	J
\mathbf{R}	Ion position	m
\mathbf{Q}	Ion displacement vector	m
\mathbf{P}	Ion momentum	kgms^{-1}
\mathbf{r}	Electron position	m
\mathbf{r}_{ij}	Electron distance vector	m
n	Electron density	m^{-3}
\mathbf{a}_i	Lattice basis vector	m
\mathbf{b}_i	Reciprocal lattice basis vector	m^{-1}
\mathbf{G}_i	Reciprocal lattice vector	m^{-1}
V	Crystal volume	m^3
\mathcal{T}	Translation operator	1
\mathbf{k}	Bloch state label	1
$D_q^{\mu\nu,ij}$	Dynamical matrix	$\text{Jm}^{-2}\text{kg}^{-1}$
c	Phonon group velocity (not to be confused with the speed of light)	ms^{-1}
ν	Frequency	s^{-1}
ω	Angular frequency	s^{-1}
Ψ	Wavefunction	s^{-1}
Φ	Wavefunction	s^{-1}
ϕ	Orbital	s^{-1}
σ	Spin label / Pauli Matrix	m
γ_i	i particle density matrix	m^{-3i}
ρ_i	Spin free i particle density matrix	m^{-3i}
μ	Chemical potential	J
Ω	Unit cell volume	m^3
$\Phi_{M,\mu,i}^{N,\nu,j}$	Force constant matrix	Jm^{-2}

Physical constants

μ_B	Bohr Magneton	$9.27 \times 10^{-24} \text{ JT}^{-1}$
g	Gyromagnetic ratio	2.0023
h	Planck constant	$6.626 \times 10^{-34} \text{ J s}$
\hbar	Reduced Planck constant	$1.054 \times 10^{-34} \text{ J s}$
e	Elementary charge	$1.602 \times 10^{-19} \text{ C}$
c	Speed of light	$299\,792\,458 \text{ ms}^{-1}$
m_e	Electron rest mass	$9.109 \times 10^{-31} \text{ kg}$
m_p	Proton rest mass	$1.672 \times 10^{-27} \text{ kg}$
k_B	Boltzmann constant	1.38 JK^{-1}
Å	Ångström	$1 \times 10^{-10} \text{ m}$

Chapter 1

Introduction

This work is concerned with the *ab initio* calculation of the spin-dynamics in the nitrogen vacancy center (NV center), which is a very interesting defect, behaving like a molecule embedded in a diamond lattice with a lot of applications. This color center consists of a substitutional nitrogen atom adjacent to a carbon vacancy, forming a defect with C_{3v} -symmetry as illustrated in Figure 1.1. The defect occurs in two different charge states: the neutral NV^0 , consisting of the four dangling electrons and the substitutional electron from the nitrogen, and the negatively charged NV^- , where an additional electron from the surrounding is found on the defect, most probably a substitutional electron from a nitrogen impurity, forming a $S = 1$ spin state. This thesis is concerned with the negatively charged version of the defect, because, as we will see, its spin properties allow for many applications in sensing, measuring and for quantum information processing purposes. First, we deal with the history and describe the success-story of this very special defect to stress the importance of a proper understanding of the spin-dynamics in this system until we introduce the theoretical toolkit necessary for the calculation of the NV^- centers spin lattice relaxation time T_1 .

1.1 History of the NV center

The vibronic band of the 1.945 eV zero phonon line (ZPL) of the NV^- center was first analyzed by Du Preez (1965) in his Ph.D. thesis. He found out that the ZPL occurs in a diamond containing a lot of isolated nitrogen impurities (so called type Ib diamond) after irradiation and subsequent annealing. He proposed that the measured ZPL could correspond to a NV center in diamond. Clark and Norris (1971) performed polarized luminescence measurements and determined the symmetry of the defect to be either trigonal (C_{3v}) or monoclinic. That the ZPL indeed corresponds to a nitrogen vacancy center was defi-

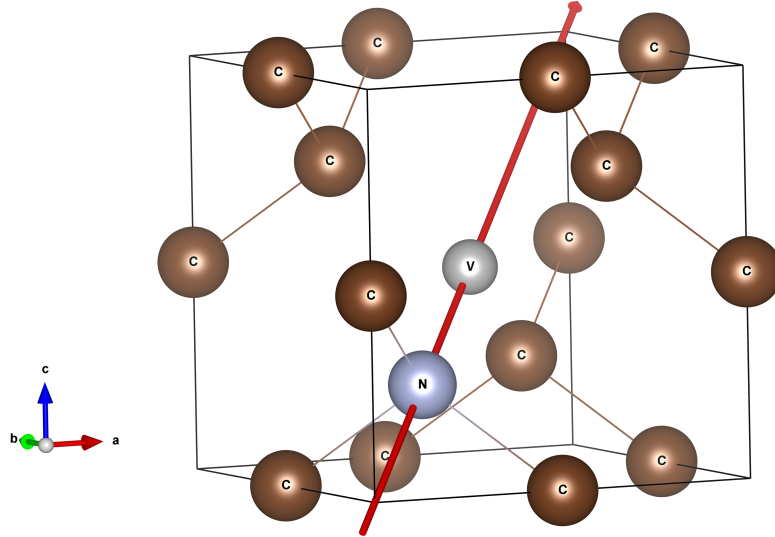


Figure 1.1: **The nitrogen vacancy center.** The local environment of the NV center is shown: In a diamond host lattice one carbon atom is replaced by the substitutional nitrogen and one adjacent carbon atom is missing. The atoms are labeled according to their type and in red the C_{3v} symmetry axis of the defect is shown.

nately answered by uniaxial stress measurements by Davies and Hamer (1976). In their electron spin resonance (ESR) studies on diamond, Loubser and Wyk (1978) provided a six electron LCAO model to explain the electronic properties of the defect, although they claimed the ground state to be a singlet. Data from spectral hole burning performed by Harley, Henderson, and Macfarlane (1984) and Reddy, Manson, and Krausz (1987) and optically detected magnetic resonance (ODMR) experiments done by Oort, Manson, and Glasbeek (1988) revealed that the 3A_2 triplet state is the ground state of the NV^- center and that the spin triplet is split due to fine-structure effects by 2.88 GHz. The complete LCAO model of the NV^- ground state is the following: two orbitals transforming according to the a_1 representation are hosting 4 electrons and the other two electrons are found in the spin polarized orbitals transforming as e , thus forming a ground state triplet transforming as 3A_2 . The qualitative influence of spin-spin and spin-orbit coupling was theoretically analyzed by Lenef and Rand (1996) using a group theoretical approach and it turns out that the diagonal components of the spin-spin interaction are responsible for the splitting of the 3A_2 ground state manifold in one lower $m_s = 0$ level and two degenerate upper levels $m_s = \pm 1$ with a zero field splitting constant D of 2.88 GHz. This zero field splitting and the pressure dependence thereof was calculated *ab initio* by Ivády et al. (2014). The spin-polarization of the center in the $m_s = 0$ ground state by means of optical cycles was measured

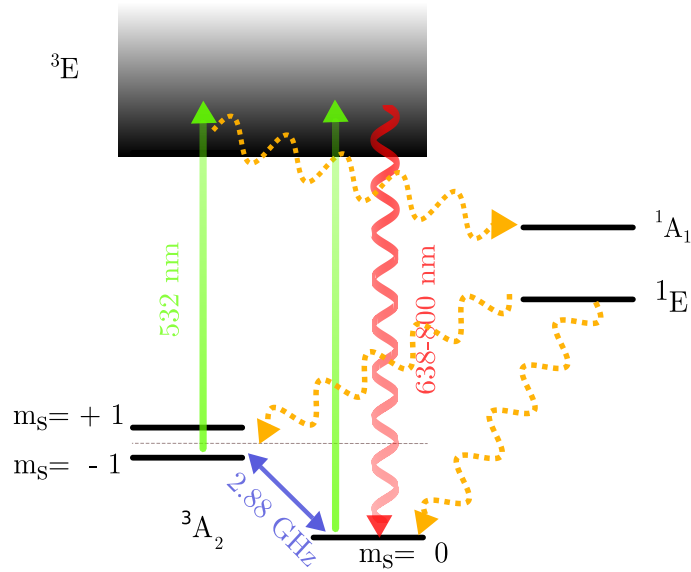


Figure 1.2: NV^- **level scheme**¹. The green lines depict excitations in vibronic levels, the wiggly red line is the red shifted zero phonon fluorescence line and the yellow lines denote non-radiative transitions in the system. The red fluorescence line is responsible for the red to pink color, that those diamonds exhibit. The $m_s \pm 1$ levels show a very strong intersystem crossing to the dark singlet states in their excited state, which is mediated by spin-orbit coupling. The singlet states decay preferentially into the $m_s = 0$ ground state, which allows for a net polarization into the $m_s = 0$ state by means of optical cycles.

by Redman, Brown, and Rand (1992) and it was theoretically explained by Goldman et al. (2015): The excited electrons in the excited 3E states with a spin projection $m_s = \pm 1$ show a strong phonon assisted intersystem crossing to the singlet states, while the $m_s = 0$ states fluoresce quickly to the ground state. The electrons in the $m_s = \pm 1$ states thus lose their energy and may either end up in the $m_s = \pm 1$ or $m_s = 0$ state. This selective intersystem crossing allows to populate the $m_s = 0$ ground state by optical means, if the electrons are excited and phonons are present. The effect is enhanced if the excitation energy is equal to a high vibrational level because of the excitation of the phonons. The initialization cycle is depicted in Figure 1.2. The possibility of the use of a single NV^- center for sensing was demonstrated by the first detection of single NV^- centers using confocal optical microscopy by Gruber (1997), which also paved the way to use the center as single photon sources (Drabenstedt et al. (1999)). From this point on, the NV^- center started to be an important workhorse to experimentally explore quantum theory. The excellent spin properties of the NV^- center were measured by Balasubramanian et al. (2008), who showed that the center exhibits spin-coherence times T_2 of

¹This illustration was redrawn in the style of Bar-Gill et al. (2012).

more than 1.8 ms at room temperature, if the interaction with nuclear spins is hindered by using a purified ^{12}C sample. These coherence times make it a very promising candidate to be used as a solid state quantum bit.

1.2 Applications of the NV^- center

Due to the quasi-molecular behaviour of the spin-polarized orbitals and the optical spin-initialization mechanism, the response of the energy levels with respect to an external field may be resolved by measuring the transition frequency between the $m_s = 0$ ground state and the $m_s = \pm 1$ states of the ground state spin triplet by taking a look at the Rabi-oscillation frequency, which is accessible via the time dependent fluorescence. The simple orbital structure of the center allows to model the response to external fields, s.t. the center may be used as an atomic sized sensor with a very high spatial resolution if single centers are employed. There is a vast number of applications arising but here we will mention only a small selection to introduce the main ideas of this field in measurement technology.

1.2.1 Sensing

A magnetic field shifts the $m_s = \pm 1$ states due to the Zeeman effect by an energy $E_Z = \frac{g\mu_B}{\hbar} (\mathbf{J} \cdot \mathbf{B})$. Therefore, a measurement of the splitting energy between the $m_s = \pm 1$ levels allows to determine a magnetic field by measuring the transition frequency. If single NV^- centers are addressed, we obtain an atomic sized sensor, with a very high spatial resolution. A typical measurement consists of an initialization of the spin state in the $m_s = 0$ state with green laser light and a microwave signal to induce transitions between the $m_s = 0$ and the $m_s = \pm 1$ states. If the microwave signal is in resonance with the energy levels, the fluorescence of the center will decrease because of the loss of the $m_s \pm 1$ electrons in the excited states due to the intersystem crossing. The high resolution and the previously mentioned excellent spin properties allow for room temperature applications: This measurement technique was already used to measure the tiny magnetic fields of ~ 100 pT, which arise due to induction if low currents are streaming through neurons when action potentials are applied, by Barry et al. (2016). The spatial resolution of ~ 10 nm enabled Le Sage et al. (2013) to locate the chains of magnetic nanoparticles produced in bacteria and thus the bacteria themselves. Another impressive example for NV^- magnetometry is a study by DeVience et al. (2015), where they resolved the spins of the ^1H , ^{19}F and ^{31}P nuclei on a diamond surface and therefore laid

the foundation for nuclear magnetic resonance (NMR) and magnetic resonance imaging (MRI).

The ground state $m_s \pm 1$ levels also split due to the Stark effect, if electric fields are applied. Dolde et al. (2011) used the interaction with electric fields of an NV^- center to measure an a.c. electric field with a sensitivity that corresponds to the field of a single elementary electric charge at a distance of ~ 150 nm (averaged over one second).

The temperature dependence of the zero field splitting constant D was measured by Acosta et al. (2010), who found a linear dependence of D with temperature with a slope $\frac{dD}{dT} = -76 \frac{\text{kHz}}{\text{K}}$, and by Chen et al. (2011), where small nonlinearities were observed. With the known temperature dependence of D , Neumann et al. (2013) constructed a NV^- nano scale sensor with a long-term temperature accuracy of 1 mK.

1.2.2 NV^- centers in quantum information technology

Another potential of the NV^- center is to use the spins of the electrons and ^{13}C nuclei as quantum bits (Qbits). The electron and nuclear spins are coupled by the hyperfine interaction, which allows for the preparation of an entangled state. The application as a Qbit creates the need to perform many gate operations which rely on a high decoherence time T_2 , which van der Sar et al. (2012) were able to prolong by the application of decoupling pulses in order to reverse the time evolution due to the interaction with the surrounding. Still, the fundamental limit for coherence times is the longitudinal relaxation due to spin-lattice interaction.

These applications show that an understanding of the spin dynamics of the center is crucial and that the insight on the fundamental mechanism of spin-phonon coupling in the NV^- center may open the doors to tailor the relaxation times by phononic bandgaps (see Safavi-Naeini et al. (2014)) or find systems with even better spin properties than the NV^- center.

1.3 Sample production

As we will derive in this thesis, the production of the diamond samples plays an important role in the spin properties of the NV^- center. Nowadays, samples are produced by taking diamond crystals with an abundance of substitutional isolated nitrogen atoms (so called type Ib diamonds, containing up to 500 ppm nitrogen atoms), irradiating them with electrons or neutrons to create vacancies and annealing them to make the vacancies mobile. Another way to create

them is by chemical vapour deposition, which favours the alignment of the NV^- centers to the growth direction (Edmonds et al. (2012)). In this thesis, we will be concerned with high pressure high temperature (HPHT) samples, which differ in initial N concentration before they are irradiated by either electrons or neutrons. The structural impact of neutron irradiation is much higher than the electron one, which can be seen in the optical properties of the samples because they lose their transparency.

The effect of the structural change on the spin-lattice relaxation time will be calculated in Chapter 5. The computational foundations thereof are laid with an introduction to density functional theory (DFT) in Chapter 2 and with the description of ionic vibrations in a solid in Chapter 3. The different spin-lattice relaxation mechanisms are presented in Chapter 4.

References

- Acosta, V. M. et al. (2010). “Temperature Dependence of the Nitrogen-Vacancy Magnetic Resonance in Diamond”. In: *Phys. Rev. Lett.* 104 (7), p. 070801.
- Balasubramanian, G. et al. (2008). “Nanoscale imaging magnetometry with diamond spins under ambient conditions”. In: *Nature* 455, pp. 648–651.
- Bar-Gill, N. et al. (2012). “Solid-state electronic spin coherence time approaching one second”. In: *Nature Communications* 4, pp. 1743–1746.
- Barry, J. F. et al. (2016). “Optical magnetic detection of single-neuron action potentials using quantum defects in diamond”. In: *Proceedings of the National Academy of Sciences* 113.49, p. 14133.
- Chen, X.-D. et al. (2011). “Temperature dependent energy level shifts of nitrogen-vacancy centers in diamond”. In: *Applied Physics Letters* 99.16, p. 161903.
- Clark, C. D. and C. A. Norris (1971). “Photoluminescence associated with the 1.673, 1.944 and 2.498 eV centres in diamond”. In: *Journal of Physics C: Solid State Physics* 4, pp. 2223–2229.
- Davies, G. and M. F. Hamer (1976). “Optical Studies of the 1.945 eV Vibronic Band in Diamond”. In: *Proceedings of the Royal Society A: Mathematical, Physical and Engineering Sciences* 348, pp. 285–298.
- DeVience, S. J. et al. (2015). “Nanoscale NMR spectroscopy and imaging of multiple nuclear species”. In: *Nature Nanotechnology* 10.2, pp. 129–134.
- Dolde, F. et al. (2011). “Electric-field sensing using single diamond spins”. In: *Nature Physics* 7, pp. 459–463.
- Drabenstedt, A. et al. (1999). “Low-temperature microscopy and spectroscopy on single defect centers in diamond”. In: *Phys. Rev. B* 60, pp. 11503–11508.
- Du Preez, L. (1965). “Electron paramagnetic resonance and optical investigations of defect centres in diamond”. PhD thesis. University of the Witwatersrand.
- Edmonds, A. M. et al. (2012). “Production of oriented nitrogen-vacancy color centers in synthetic diamond”. In: *Phys. Rev. B* 86, pp. 1–7.
- Goldman, M. L. et al. (2015). “State-selective intersystem crossing in nitrogen-vacancy centers”. In: *Phys. Rev. B* 91 (16), p. 165201.
- Gruber, A. (1997). “Scanning Confocal Optical Microscopy and Magnetic Resonance on Single Defect Centers”. In: *Science* 276, pp. 2012–2014.
- Harley, R. T., M. J. Henderson, and R. M. Macfarlane (1984). “Persistent spectral hole burning of colour centers in diamond”. In: *J. Phys. C: Solid State Phys.* 17, pp. L233–L236.

- Ivány, V. et al. (2014). “Pressure and temperature dependence of the zero-field splitting in the ground state of NV centers in diamond: A first-principles study”. In: *Phys. Rev. B* 90 (23), p. 235205.
- Le Sage, D. et al. (2013). “Optical magnetic imaging of living cells”. In: *Nature* 496.7446, pp. 486–489.
- Lenef, A. and S. C. Rand (1996). “Electronic structure of the N-V center in diamond: Theory”. In: *Phys. Rev. B* 53, pp. 13441–13455.
- Loubser, J. H. N. and J. A. van Wyk (1978). “Electron spin resonance in the study of diamond”. In: *Reports on Progress in Physics* 41, pp. 1201–1248.
- Neumann, P. et al. (2013). “High-Precision Nanoscale Temperature Sensing Using Single Defects in Diamond”. In: *Nano Letters* 13.6, pp. 2738–2742.
- Oort, E. van, N. B. Manson, and M. Glasbeek (1988). “Optically detected spin coherence of the diamond N-V centre in its triplet ground state”. In: *Journal of Physics C: Solid State Physics* 21, pp. 4385–4391.
- Reddy, N. R. S., N. B. Manson, and E. R. Krausz (1987). “Two-laser spectral hole burning in a colour centre in diamond”. In: *Journal of Luminescence* 38, pp. 46–47.
- Redman, D., S. Brown, and S. C. Rand (1992). “Origin of persistent hole burning of N–V centers in diamond”. In: *Journal of the Optical Society of America B* 9.5, p. 768.
- Safavi-Naeini, Aa H. et al. (2014). “Two-Dimensional Phononic-Photonic Band Gap Optomechanical Crystal Cavity”. In: *Phys. Rev. Lett.* 112 (15), p. 153603.
- van der Sar, T. et al. (2012). “Decoherence-protected quantum gates for a hybrid solid-state spin register”. In: *Nature* 484.7392, pp. 82–86.

Chapter 2

Introduction to density functional theory (DFT)¹

A calculation of the spin-lattice relaxation time T_1 requires the knowledge of both the electronic and ionic properties of the system of interest. Of particular interest in this thesis are the vibrational spectra of the atoms in motion and the electronic wavefunctions of the NV^- center. Both of these quantities are investigated in a quantum mechanical manner: Since the calculation of the defect center is (up to now) a very demanding task on basis of the wavefunction methods, we will take advantage of the wonderful simplification of the problem, rewritten in terms of the electronic density only (which is not too easy either as we will see in this Chapter). How this magic is justified will be shown in the subsequent sections. Starting from the general quantum mechanical treatment of a many-body system, we will recapitulate the most important foundations of density functional theory and introduce a way to obtain the relevant density functionals, which are used in this work.

2.1 The Born-Oppenheimer Approximation and the Hellmann-Feynman theorem

In order to determine the stationary properties of a solid state system consisting of N_e electrons and N_n nuclei, the time independent Schrödinger equation

$$\widehat{\mathcal{H}}\Phi(\mathbf{R}_1, \mathbf{R}_2, \dots, \mathbf{R}_{N_n}, \mathbf{x}_1, \mathbf{x}_2, \dots, \mathbf{x}_{N_e}) = E\Phi(\mathbf{R}_1, \mathbf{R}_2, \dots, \mathbf{R}_{N_n}, \mathbf{x}_1, \mathbf{x}_2, \dots, \mathbf{x}_{N_e}) \quad (2.1)$$

¹This introduction is based upon the books of Engel and Dreizler (2011) Fiolhais et al. (2003) and Parr and Yang (1989)

has to be solved with $\mathbf{x}_i = (\mathbf{r}_i, \sigma_i)$ denoting the position and the spin of the i -th electron and the Hamiltonian $\widehat{\mathcal{H}}$ reads:

$$\begin{aligned} \widehat{\mathcal{H}} = & \underbrace{-\sum_{I=1}^{N_n} \frac{\hbar^2}{2M_I} \vec{\nabla}_I^2}_{\widehat{T}_n} - \underbrace{\sum_{i=1}^{N_e} \frac{\hbar^2}{2m_e} \vec{\nabla}_i^2}_{\widehat{T}_e} + \underbrace{\frac{e^2}{2} \sum_{I=1}^{N_n} \sum_{J \neq I}^{N_n} \frac{Z_I Z_J}{|\widehat{\mathbf{R}}_I - \widehat{\mathbf{R}}_J|}}_{\widehat{v}_{nn}} + \\ & + \underbrace{\frac{e^2}{2} \sum_{i=1}^{N_e} \sum_{j \neq i}^{N_e} \frac{1}{|\widehat{\mathbf{r}}_i - \widehat{\mathbf{r}}_j|}}_{\widehat{v}_{ee}} - \underbrace{e^2 \sum_{I=1}^{N_n} \sum_{i=1}^{N_e} \frac{Z_I}{|\widehat{\mathbf{R}}_I - \widehat{\mathbf{r}}_i|}}_{\widehat{v}_{en}}. \end{aligned} \quad (2.2)$$

The terms \widehat{T}_n and \widehat{T}_e are the kinetic energies of the nuclei and the electrons, \widehat{v}_{nn} , \widehat{v}_{ee} and \widehat{v}_{en} are the Coulomb interactions between the nuclei, the electrons, the nuclei with the electrons, respectively. Atomic units have been used to simplify the occurring prefactors. The factor $\frac{1}{2}$ accounts for the double counting of the interactions. Even though this is the most simple form of a Hamiltonian, where only the electrostatical contributions are taken into account (there are no spin-dependent interactions or external fields present), solving this Hamiltonian exactly is very cumbersome, even for simple molecules because it leads to a system of coupled partial differential equations. As Born and Oppenheimer (1927) showed, the problem simplifies, if we assume the electrons to move in a potential, where the nuclei are kept frozen and their positions $\{\mathbf{R}\}$ are to be taken as a parameter for the solution of a purely electronic problem. The aim is to decouple the Hamiltonian in 2.2 into two parts, one accounting for the electronic problem and the other for the nuclei:

$$\widehat{H} = \underbrace{\widehat{T}_e + \widehat{v}_{ee} + \widehat{v}_{en}}_{\widehat{h}_e} + \widehat{T}_n + \widehat{v}_{nn} \quad . \quad (2.3)$$

We assume the electronic wavefunction Ψ to depend parametrically on the positions of all the nuclei, denoted by $\{\mathbf{R}\}$, s.t. $\Psi = \Psi(\{\mathbf{R}\}, \{\mathbf{x}\})$. Then we can solve

$$\begin{aligned} \widehat{h}_e \Psi^k(\{\mathbf{R}\}, \{\mathbf{x}\}) &= \epsilon^k(\{\mathbf{R}\}) \Psi^k(\{\mathbf{R}\}, \{\mathbf{x}\}) \\ \rightarrow \langle \Psi^{k'}(\{\mathbf{R}\}, \{\mathbf{x}\}) | \widehat{h}_e | \Psi^k(\{\mathbf{R}\}, \{\mathbf{x}\}) \rangle &= \delta_{k,k'} \epsilon^k(\{\mathbf{R}\}) \end{aligned} \quad (2.4)$$

for fixed positions of the nuclei. With this solution in our hand, the full Schrödinger equation may be tackled by an ansatz of the form

$$\Phi(\{\mathbf{R}\}, \{\mathbf{x}\}) = \sum_{k=1}^K \Psi^k(\{\mathbf{R}\}, \{\mathbf{x}\}) \chi^k(\{\mathbf{R}\}), \quad (2.5)$$

where χ denotes the wavefunction of the nuclei. This leads to

$$\left(\widehat{h}_e + \widehat{T}_n + \widehat{v}_{nn}\right) \sum_{k=1}^K \Psi^k(\{\mathbf{R}\}, \{\mathbf{x}\}) \chi^k(\{\mathbf{R}\}) = E \sum_{k=1}^K \Psi^k(\{\mathbf{R}\}, \{\mathbf{x}\}) \chi^k(\{\mathbf{R}\}). \quad (2.6)$$

Projecting on the electronic state $\Psi_e^j(\{\mathbf{R}\}, \{\mathbf{x}\})$ gives

$$\epsilon^j(\{\mathbf{R}\}) \chi^j(\{\mathbf{R}\}) + \sum_{k=1}^K \langle \Psi^j | \widehat{T}_n | \Psi^k \rangle \chi^k + \widehat{v}_{nn} \chi^j(\{\mathbf{R}\}) = E \chi^j(\{\mathbf{R}\}). \quad (2.7)$$

Now we consider the action of the kinetic energy operator of the nuclei on the total wavefunction

$$\begin{aligned} \sum_{k=1}^K \langle \Psi^j | \widehat{T}_n | \Psi^k \rangle \chi^k &= \sum_{k=1}^K \langle \Psi^j | \sum_{I=1}^{N_n} \frac{-\hbar^2}{2M_I} \Delta_I | \Psi^k \rangle \chi^k = \\ &= \sum_{k=1}^K \langle \Psi^j | \sum_{I=1}^{N_n} \frac{-\hbar^2}{2M_I} \Delta_I | \Psi^k \rangle | \chi^k \rangle + \langle \Psi^j | \sum_{I=1}^{N_n} \frac{-\hbar^2}{M_I} \vec{\nabla}_I | \Psi^k \rangle \vec{\nabla}_I | \chi^k \rangle + \\ &\quad + \underbrace{\langle \Psi^j | \Psi^k \rangle}_{=\delta_{jk}} \sum_{I=1}^{N_n} \frac{-\hbar^2}{2M_I} \Delta_I | \chi^k \rangle \end{aligned} \quad (2.8)$$

The off-diagonal terms in the kinetic energy account for electronic transitions induced due to the movement of the nuclei. In the *adiabatic approximation* these terms are neglected and obtaining the solution of the full Hamiltonian 2.2 may be reduced to finding solutions of the electronic problem for a given constellation of the nuclei followed by the task to find the lowest energy state for the positions of the nuclei:

$$\left[\widehat{T}_e + \widehat{v}_{ee}(\{\widehat{\mathbf{r}}\}) + \widehat{v}_{en}(\{\widehat{\mathbf{x}}\}, \{\mathbf{R}\})\right] \Psi^k(\{\mathbf{x}\}, \{\mathbf{R}\}) = \epsilon^k(\{\mathbf{R}\}) \Psi^k(\{\mathbf{x}\}, \{\mathbf{R}\}) \quad (2.9)$$

$$\left[\widehat{T}_n + \widehat{v}_{nn}(\{\mathbf{R}\}) + \epsilon(\{\mathbf{R}\})\right] \chi(\{\mathbf{R}\}) = E \chi(\{\mathbf{R}\}) \quad (2.10)$$

Since the wavefunction of a certain nucleus is confined to a very small region in space (≈ 1 fm), it can be treated classically because the interesting length scales in a solid are large compared to the extent thereof. Thus, their movement may be determined by solving the classical Newtonian equations of motion for the nuclei:

$$\frac{\partial^2 \vec{P}_I(t)}{\partial t^2} = -\vec{\nabla}_I V \quad (2.11)$$

with

$$V = v_{nn}(\{\mathbf{R}\}) + \epsilon(\{\mathbf{R}\}) \quad (2.12)$$

If the electronic ground state of a certain constellation is found, the forces acting on the nuclei may be calculated very effectively by applying the *Hellmann-Feynman theorem* (Feynman (1939)):

$$\frac{dE}{d\lambda} = \left\langle \frac{d}{d\lambda} \Psi | \widehat{\mathcal{H}} | \Psi \right\rangle + \left\langle \Psi | \frac{d\widehat{\mathcal{H}}}{d\lambda} | \Psi \right\rangle + \left\langle \Psi | \widehat{\mathcal{H}} | \frac{d}{d\lambda} \Psi \right\rangle \quad (2.13)$$

assume $|\Psi\rangle$ being an eigenfunction of $\widehat{\mathcal{H}}$

$$= \left\langle \frac{d}{d\lambda} \Psi | E | \Psi \right\rangle + \left\langle \Psi | \frac{d\widehat{\mathcal{H}}}{d\lambda} | \Psi \right\rangle + \left\langle \Psi | E | \frac{d}{d\lambda} \Psi \right\rangle \quad (2.14)$$

$$= \frac{d}{d\lambda} \langle \Psi | \Psi \rangle + \left\langle \Psi | \frac{d\widehat{\mathcal{H}}}{d\lambda} | \Psi \right\rangle \quad (2.15)$$

since $|\Psi\rangle$ is normalized the first term vanishes

$$= \left\langle \Psi | \frac{d\widehat{\mathcal{H}}}{d\lambda} | \Psi \right\rangle \quad (2.16)$$

$$\rightarrow \vec{\nabla}_I \epsilon = \left\langle \Psi | \vec{\nabla}_I \widehat{h}_e(\{\mathbf{R}\}) | \Psi \right\rangle \quad (2.17)$$

With the solution of the electronic problem in our hand, we can therefore propagate the ions to find their equilibrium positions (where there are no forces acting on the ions) or to perform molecular dynamics. This shows that a proper understanding of solids relies heavily on the determination of the electronic wavefunctions. Since the calculation of the electronic wavefunctions itself is a quite demanding task, the rest of this Chapter is concerned with possible ways to obtain the electronic wavefunctions.

2.2 Hartree and Hartree-Fock theory

To understand the crucial aspects of calculating electronic wavefunctions, the history of the treatment is depicted in this section: The starting point for self consistent field calculations are the Hartree equations. A quantum mechanical refinement thereof is the Hartree-Fock method and going beyond Hartree-Fock theory provides a definition for the electronic correlation, which will be of utmost importance in the application of DFT.

Finding the ground state of the wavefunction corresponding to the Hamiltonian

in equation (2.9) is done by minimizing the energy functional

$$E(|\Psi\rangle) = \frac{\langle \Psi | \widehat{\mathcal{H}} | \Psi \rangle}{\langle \Psi | \Psi \rangle} \quad (2.18)$$

with respect to the wavefunction $|\Psi\rangle$. In the Hartree approximation, the wavefunction $\Psi(\{\mathbf{x}\})$ is assumed to be a product of one-electron wavefunctions²

$$\Psi(\{\mathbf{x}\}) = \prod_{i=1}^{N_e} \phi_i(\mathbf{r}_i \sigma_i). \quad (2.19)$$

Insertion of the product wavefunction and minimization by a functional derivate with respect to $\phi_l^*(\mathbf{r}_l \sigma_l)$ with the constraint of normalized wavefunctions leads to the Hartree equations:

$$\begin{aligned} \frac{\delta}{\delta \phi_l^*(\mathbf{r} \sigma_l)} \left(E - \sum_i^{N_e} \epsilon_i \left(\int |\phi_i(\mathbf{r}_i \sigma_i)|^2 d^3 r - 1 \right) \right) = 0 \rightarrow \\ \left[\frac{-\hbar^2}{2m_e} \Delta - \sum_{k=1}^{N_n} \frac{Z_k e^2}{|\mathbf{r} - \mathbf{R}_k|} + \underbrace{\sum_{j=1, j \neq l}^{N_e} \int d^3 r' \frac{e^2 |\phi_j(\mathbf{r}' \sigma_j)|^2}{|\mathbf{r} - \mathbf{r}'|}}_{V_H} \right] \phi_l(\mathbf{r} \sigma_l) = \epsilon_l \phi_l(\mathbf{r} \sigma_l) \end{aligned} \quad (2.20)$$

The orthogonality of the wavefunctions had not to be introduced as a Lagrangian multiplier because the operator on the left side of the eigenvalue equation (2.20) is hermitian and therefore the wavefunctions are orthogonal (except for the spin degenerate subspaces, where the orthogonality is easily obtained by choosing orthogonal spin functions). Since the Hartree potential V_H in this equation depends on the ϕ 's itself, this equation has to be solved self consistently as shown in Figure 2.1. The electron-electron interaction in the Hartree theory is represented in the Coulomb term, where the wavefunction interacts with the charge density of the other electrons only. This potential, called the Hartree potential, reminds us of the classical interaction between two charge densities. Since the Hartree equations do not account for the symmetry character of the fermionic wavefunction, which should change its sign if two electrons are interchanged, the next refinement to the theory was found independently by Slater and Fock in 1930. It consists of accounting for the antisymmetry of the N_e -electron wavefunction by assuming it to be of the form

²From now on, we will stop to denote the parametrical dependence of the electronic wavefunctions and the corresponding energies on the nuclei $\Psi(\{\mathbf{x}\}) \equiv \Psi(\{\mathbf{R}\}, \{\mathbf{x}\})$ and $\epsilon \equiv \epsilon(\{\mathbf{R}\})$

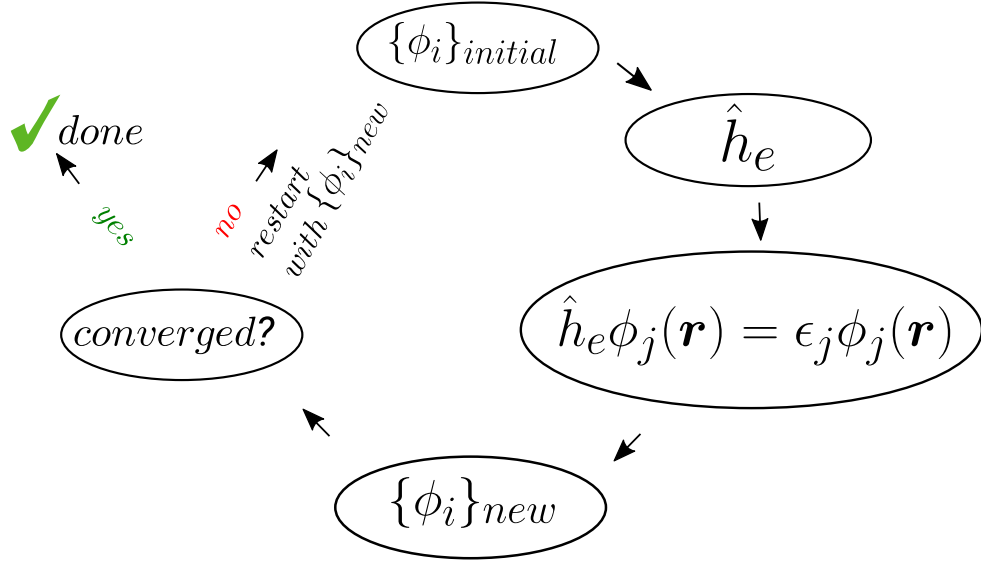


Figure 2.1: **Self consistency cycle**, Starting from initial orbitals, the Hamiltonian is set up. Using this Hamiltonian, a new set of orbitals and the corresponding energies are calculated. These orbitals may again be used to set up a new Hamiltonian. This cycle is repeated until the change in energies is below a chosen threshold, then the orbitals are assumed to be converged.

of a single Slater determinant $\Phi_{n_1, \dots, n_{N_e}}(\mathbf{r}_1 \sigma_1, \dots, \mathbf{r}_{N_e} \sigma_{N_e})$:

$$\begin{aligned} \Psi(\{\mathbf{x}\}) &= \Phi_{n_1, \dots, n_{N_e}}(\mathbf{r}_1 \sigma_1, \dots, \mathbf{r}_{N_e} \sigma_{N_e}) \\ &:= \frac{1}{\sqrt{N_e!}} \begin{vmatrix} \phi_1(\mathbf{r}_1 \sigma_1) & \dots & \phi_1(\mathbf{r}_{N_e} \sigma_{N_e}) \\ \vdots & \ddots & \vdots \\ \phi_{N_e}(\mathbf{r}_1 \sigma_1) & \dots & \phi_{N_e}(\mathbf{r}_{N_e} \sigma_{N_e}) \end{vmatrix} \end{aligned} \quad (2.21)$$

The approximation here consists of taking the N_e -electron wavefunction as a single determinant: Mathematically, each N_e -electron antisymmetric wavefunction can exactly be represented as the sum of Slater-determinants

$$\Psi(\{\mathbf{x}\}) = \sum_{n_1 < \dots < n_{N_e}} a_{n_1, \dots, n_{N_e}} \Phi_{n_1, \dots, n_{N_e}}(\mathbf{r}_1 \sigma_1, \dots, \mathbf{r}_{N_e} \sigma_{N_e}) \quad (2.22)$$

but a treatment thereof is very cumbersome even for the calculation of simple molecules.

Performing the energy minimization using the Slater determinant wavefunction

leads to the Hartree-Fock equations

$$\begin{aligned} & \left[\frac{-\hbar^2}{2m_e} \Delta - e^2 \sum_{k=1}^{N_n} \frac{Z_k}{|\mathbf{r} - \mathbf{R}_k|} + \sum_{\substack{j=1 \\ j \neq i}}^{N_e} \int \phi_j^*(\mathbf{r}'\sigma_j) w(\mathbf{r}, \mathbf{r}') \phi_j(\mathbf{r}'\sigma_j) d^3r' \right] \phi_i(\mathbf{r}\sigma_i) - \\ & - \sum_{\substack{j=1 \\ j \neq i}}^{N_e} \int \phi_j^*(\mathbf{r}'\sigma_j) w(\mathbf{r}, \mathbf{r}') \phi_i(\mathbf{r}'\sigma_i) d^3r' \phi_j(\mathbf{r}\sigma_j) = \epsilon(\{\mathbf{R}\}) \phi_i(\mathbf{r}\sigma_i). \end{aligned} \quad (2.23)$$

with $w(\mathbf{r}, \mathbf{r}') = \frac{e^2}{|\mathbf{r} - \mathbf{r}'|}$ denoting the kernel of the electron-electron interaction potential \hat{v}_{ee} in real space. Taking into account the antisymmetry of the fermionic wavefunction thus gives an additional potential energy term, which is called the exchange term. The energy change caused by going beyond the single determinant representation of Ψ is called the *correlation energy*. Correlation is treated within the wavefunction methods by so called *cluster expansions*, which take into account additional orbitals and construct wavefunctions, which consist of several Slater-determinants.

The wavefunction methods are used a lot in chemistry but they scale very badly with increasing system size. That is why density methods, as discussed in the next section play a very crucial role in the theoretical treatment of real systems.

2.3 Hohenberg-Kohn theorem

The mathematical foundations of the density methods were laid by Hohenberg and Kohn (1964) in the two Hohenberg-Kohn theorems, which read:

1st Hohenberg-Kohn theorem:

There is a one-to-one mapping between an additive external potential $v_{ext}(\mathbf{r})$ and the electronic ground state density $n_0(\mathbf{r})$ for a non-degenerate system.³

Proof by *reductio ad absurdum*:

Assume there are two different potentials v_{ext} and v'_{ext} , which give the same ground state electronic density. Let Ψ_0 and Ψ'_0 be the corresponding electronic wavefunctions giving the ground state energies $E_0 = \langle \Psi_0 | \widehat{\mathcal{H}} | \Psi_0 \rangle$ and $E'_0 = \langle \Psi'_0 | \widehat{\mathcal{H}}' | \Psi'_0 \rangle$ with the Hamiltonians $\widehat{\mathcal{H}} = \widehat{T} + \widehat{v}_{ee} + \widehat{v}_{ext}$ and $\widehat{\mathcal{H}}' = \widehat{T} + \widehat{v}_{ee} + \widehat{v}'_{ext}$. According to the Rayleigh-Ritz variational principle we have

$$E_0 < \langle \Psi'_0 | \widehat{\mathcal{H}} | \Psi'_0 \rangle = \langle \Psi'_0 | \widehat{\mathcal{H}}' | \Psi'_0 \rangle + \langle \Psi'_0 | \widehat{\mathcal{H}} - \widehat{\mathcal{H}}' | \Psi'_0 \rangle \quad (2.24)$$

³except for an additive constant which has no influence on the physics

$$= E'_0 + \int n_0(\mathbf{r}) [v_{ext}(\mathbf{r}) - v'_{ext}(\mathbf{r})] d^3r. \quad (2.25)$$

Interchanging Ψ and Ψ' gives

$$E'_0 < \langle \Psi_0 | \widehat{\mathcal{H}}' | \Psi_0 \rangle = \langle \Psi_0 | \widehat{\mathcal{H}} | \Psi_0 \rangle + \langle \Psi_0 | \widehat{\mathcal{H}}' - \widehat{\mathcal{H}} | \Psi_0 \rangle \quad (2.26)$$

$$= E_0 - \int n_0(\mathbf{r}) [v_{ext}(\mathbf{r}) - v'_{ext}(\mathbf{r})] d^3r. \quad (2.27)$$

Adding up these two equations gives the contradiction $E_0 + E'_0 < E'_0 + E_0$. Therefore, there can not exist two different external potentials which give the same electronic ground state density. So the mapping between the external potential and the density is unique (up to a constant in the potential). For degenerate ground states there exists a mapping between the external potentials and classes of degenerate ground states, which lead to disjunct ground state densities, keeping the mapping between the density and the external potential unique. Using this potential we can solve the Schrödinger equation and therefore map the potential and the density to the wavefunction Ψ . The calculation principle for obtaining the ground state electronic density is given by the second Hohenberg-Kohn theorem:

2nd Hohenberg-Kohn theorem:

The electronic ground state density $n_0(\mathbf{r})$ minimizes the energy of the electronic system for a given Hamiltonian

Proof: Let $\tilde{n}(\mathbf{r})$ be any density. According to the Rayleigh-Ritz principle we have:

$$E[\tilde{n}] = \langle \Psi[\tilde{n}] | \widehat{\mathcal{H}} | \Psi[\tilde{n}] \rangle \geq \langle \Psi[n_0] | \widehat{\mathcal{H}} | \Psi[n_0] \rangle = E[n_0]. \quad (2.28)$$

Using this inequality, we can solve for the electronic ground state density by minimizing the energy variationally by using a Lagrangian multiplier, which accounts for a proper normalized density

$$\delta \left\{ E[n] - \mu \left(\int n(\mathbf{r}) d^3r - N \right) \right\} = 0 \quad . \quad (2.29)$$

2.4 Thomas-Fermi theory

The first density approach for solving quantum theoretical problems was a theory derived by Thomas (1927) and Fermi (1928) long before the theoretical justification thereof was given by the Hohenberg-Kohn theorem. They took the electronic density as the central variable to calculate atomic fields. In the *Thomas-Fermi theory* a pure density approach is taken, where the kinetic

energy is derived from a non-interacting electron gas. This leads to the total energy expression

$$E_{TF}[n(\mathbf{r})] = \frac{3\hbar^2}{10m_e}(3\pi^2)^{2/3} \int n(\mathbf{r})^{5/3} d^3r + e \int n(\mathbf{r})v_{ext}(\mathbf{r})d^3r + \frac{e^2}{2} \iint \frac{n(\mathbf{r})n(\mathbf{r}')}{|\mathbf{r} - \mathbf{r}'|} d^3r d^3r' \quad (2.30)$$

which has to be minimized under the constraint that the integrated density gives the number of electrons in the system. Unfortunately this theory agrees very badly with experiments but the advantage of a pure density approach is obvious: we have to deal with a quantity that depends on three coordinates only instead of the wavefunction which gives 3 degrees of freedom for each particle. A further step will be taken in the next section, where the density is parametrized by a set of orbitals.

2.5 Kohn-Sham theory

In their famous paper Kohn and Sham (1965) developed a theory, where the interacting system is mapped to a system of non-interacting electrons which gives the same density as the interacting one. They introduce an auxiliary system of non-interacting electrons (the Kohn-Sham system), which are moving in the presence of an external potential $\hat{v}_s(\mathbf{r})$

$$\hat{H}_s = \hat{T} + \int d^3r \hat{n}(\mathbf{r}) \hat{v}_s(\mathbf{r}). \quad (2.31)$$

The ground state wavefunction is parametrized by a single Slater determinant built up by a set of orbitals ϕ_i , which gives rise to the definition of the kinetic energy of the non-interacting system $\hat{T}_s = \sum_i \phi_i^*(\mathbf{r}) \frac{-\hbar^2}{2m} \Delta \phi_i(\mathbf{r})$. This system should give the same density as the interacting system with the Hamiltonian

$$E[n] = T_s[n] + V_H[n] + V_{ext}[n] + E_{xc}[n]. \quad (2.32)$$

Here the energy is split up in the exactly known contributions for the kinetic energy of the non-interacting system, the Hartree-energy E_H , the energy associated with the external potential V_{ext} and all the not exactly known contributions are included in the term E_{xc} , which has to be approximated in a suitable manner. In order for (2.31) and (2.32) to be equal, the potential of the Kohn-Sham system must read

$$\hat{v}_s = \hat{v}_{ext} + \hat{v}_H + \hat{v}_{xc} \quad . \quad (2.33)$$

If the energy is minimized with respect to the electronic orbitals, one ends up with the Kohn-Sham equations:

$$\left[\frac{-\hbar^2}{2m} \Delta + \hat{v}_{ext}(\mathbf{r}) + \hat{v}_H(\mathbf{r}) + \hat{v}_{xc}(\mathbf{r}) \right] \phi_i(\mathbf{r}\sigma_i) = \epsilon_i \phi_i(\mathbf{r}\sigma_i) \quad (2.34)$$

with $v_{xc}(\mathbf{r}) = \frac{\delta E_{xc}}{\delta n(\mathbf{r})}$ accounting for the many-body effects. The nuisance to deal with antisymmetric wavefunctions has been removed by putting all the exchange and correlation effects in the Hamiltonian. The structure of the Kohn-Sham equations resembles the structure of the Hartree-Fock equations in a way that the quantity we want to calculate is needed in order to set up the Hamiltonian. These equations therefore also have to be solved in a self-consistent manner as depicted in Figure 2.1. The only (quite important!) question is, how we can get an expression for the unknown quantity E_{xc} . This will be answered in the next section.

2.6 The exchange and correlation Energy E_{xc}

Since the exchange and correlation energy is universal (independent of the external potential v_{ext}), a knowledge thereof would enable us to solve whichever system we want (that is the dream). As a consequence of the *Hohenberg-Kohn theorem* E_{xc} should depend on the density only. Before we dive into the calculus of E_{xc} , let us spend one paragraph to consider what exchange and correlation effects do with the distribution of electrons in general:

For this purpose it is advantageous to introduce the one- and two-particle density matrices for a system containing N electrons

$$\begin{aligned} \gamma_1(\mathbf{r}'_1\sigma'_1, \mathbf{r}_1\sigma_1) = \\ N \sum_{\sigma_2 \dots \sigma_N} \int d^3r_2 \dots \int d^3r_N \Psi^*(\mathbf{r}'_1\sigma'_1, \mathbf{r}_2\sigma_2, \dots, \mathbf{r}_N\sigma_N) \Psi(\mathbf{r}_1\sigma_1, \mathbf{r}_2\sigma_2, \dots, \mathbf{r}_N\sigma_N) \end{aligned} \quad (2.35)$$

$$\begin{aligned} \gamma_2(\mathbf{r}'_1\sigma'_1\mathbf{r}'_2\sigma'_2, \mathbf{r}_1\sigma_1\mathbf{r}_2\sigma_2) = \\ \frac{N(N-1)}{2} \sum_{\sigma_3 \dots \sigma_N} \int d^3r_3 \dots \int d^3r_N \cdot \\ \Psi^*(\mathbf{r}'_1\sigma'_1, \mathbf{r}'_2\sigma'_2, \mathbf{r}_3\sigma_3, \dots, \mathbf{r}_N\sigma_N) \Psi(\mathbf{r}_1\sigma_1, \mathbf{r}_2\sigma_2, \mathbf{r}_3\sigma_3, \dots, \mathbf{r}_N\sigma_N) \end{aligned} \quad (2.36)$$

and their spin-free relatives

$$\rho_1(\mathbf{r}', \mathbf{r}) = \sum_{\sigma_1} \gamma_1(\mathbf{r}'\sigma_1, \mathbf{r}\sigma_1) =$$

$$N \sum_{\sigma_1 \dots \sigma_N} \int d^3 r_2 \dots \int d^3 r_N \Psi^*(\mathbf{r}'_1 \sigma_1, \mathbf{r}_2 \sigma_2, \dots, \mathbf{r}_N \sigma_N) \Psi(\mathbf{r}_1 \sigma_1, \mathbf{r}_2 \sigma_2, \dots, \mathbf{r}_N \sigma_N) \quad (2.37)$$

$$\begin{aligned} \rho_2(\mathbf{r}'_1 \mathbf{r}'_2, \mathbf{r}_1 \mathbf{r}_2) &= \sum_{\sigma_1, \sigma_2} \gamma_2(\mathbf{r}'_1 \sigma_1 \mathbf{r}'_2 \sigma_2, \mathbf{r}_1 \sigma_1 \mathbf{r}_2 \sigma_2) = \\ &= \frac{N(N-1)}{2} \sum_{\sigma_1 \dots \sigma_N} \int d^3 r_3 \dots \int d^3 r_N \cdot \\ &= \Psi^*(\mathbf{r}'_1 \sigma_1, \mathbf{r}'_2 \sigma_2, \dots, \mathbf{r}_N \sigma_N) \Psi(\mathbf{r}_1 \sigma_1, \mathbf{r}_2 \sigma_2, \dots, \mathbf{r}_N \sigma_N). \end{aligned} \quad (2.38)$$

We note here, that the diagonal of the spin-free one particle density matrix is just the density

$$\rho_1(\mathbf{r}, \mathbf{r}) = n(\mathbf{r}). \quad (2.39)$$

With those density matrices in our hand, we can rewrite the expectation value for general spin-independent one-particle and two-particle operators as

$$\langle \hat{O}_1 \rangle = \int d^3 r_1 [O_1(\mathbf{r}_1) \rho_1(\mathbf{r}'_1, \mathbf{r}_1)]_{\mathbf{r}'_1 = \mathbf{r}_1} \quad (2.40)$$

$$\langle \hat{O}_2 \rangle = \int d^3 r_1 d^3 r_2 [O_2(\mathbf{r}_1, \mathbf{r}_2) \rho_2(\mathbf{r}'_1 \mathbf{r}'_2, \mathbf{r}_1 \mathbf{r}_2)]_{\mathbf{r}'_1 = \mathbf{r}_1, \mathbf{r}'_2 = \mathbf{r}_2}. \quad (2.41)$$

Denoting the diagonal of $\rho_2(\mathbf{r}'_1 \mathbf{r}'_2, \mathbf{r}_1 \mathbf{r}_2)$ by $\rho_2(\mathbf{r}_1, \mathbf{r}_2)$ allows to express the electron-electron interaction as

$$V_{ee} = \int \int d^3 r_1 d^3 r_2 \underbrace{\frac{e^2}{|\mathbf{r}_1 - \mathbf{r}_2|}}_{=w(\mathbf{r}_1, \mathbf{r}_2)} \rho_2(\mathbf{r}_1, \mathbf{r}_2) \quad (2.42)$$

Express the joint probability $\rho_2(\mathbf{r}_1, \mathbf{r}_2)$ by the correlation function $h(\mathbf{r}_1, \mathbf{r}_2)$

$$= \int \int d^3 r_1 d^3 r_2 w(\mathbf{r}_1, \mathbf{r}_2) (n(\mathbf{r}_1) n(\mathbf{r}_2) [1 + h(\mathbf{r}_1, \mathbf{r}_2)]) / 2 \quad (2.43)$$

Define the exchange correlation hole $n_{xc}(\mathbf{r}_1, \mathbf{r}_2) = n(\mathbf{r}_2) h(\mathbf{r}_1, \mathbf{r}_2)$

$$= V_H + \underbrace{\frac{1}{2} \int \int d^3 r_1 d^3 r_2 w(\mathbf{r}_1, \mathbf{r}_2) n(\mathbf{r}_1) n_{xc}(\mathbf{r}_1, \mathbf{r}_2)}_{E_{xc}}. \quad (2.44)$$

From the normalization of the density matrices we can deduce the normalization of the exchange correlation hole n_{xc}

$$\begin{aligned} \int d^3r_2 \rho_2(\mathbf{r}_1, \mathbf{r}_2) &\stackrel{2.37,2.38}{=} \frac{N-1}{2} n(\mathbf{r}_1) \stackrel{2.43,2.44}{=} \frac{1}{2} n(\mathbf{r}_1) \left(N + \int d^3r_2 n_{xc}(\mathbf{r}_1, \mathbf{r}_2) \right) \\ &\rightarrow \int d^3r_2 n_{xc}(\mathbf{r}_1, \mathbf{r}_2) = -1. \end{aligned} \quad (2.45)$$

Comparing V_{ee} with the Hartree-Fock results (2.23) we see, that the exchange correlation hole i) has to correct for the self-interaction of the particle, ii) is responsible for the compliance with the Pauli-exclusion principle, and iii) takes into account screening processes which go beyond Hartree-Fock theory.

The calculation of the exchange and correlation energy E_{xc} may be established on a quantum mechanical footing by performing a coupling constant integration: We consider the non-interacting Kohn-Sham system (2.31) and switch to the fully interacting electron system by turning on the electron-electron interaction potential \hat{v}_{ee} . The interaction is turned on by introducing the coupling parameter λ , which interpolates between the Kohn-Sham system and the fully interacting system. This is done either by keeping the external potential unaffected and allowing the density to change or by introducing a different external potential for every strength of \hat{v}_{ee} which leads to the same density as the non-interacting and the fully interacting system (which should give the same density by the construction of the Kohn-Sham system). Here we will take the second approach and use the potential

$$u_\lambda(\mathbf{r}) = \begin{cases} \hat{v}_s(\mathbf{r}) & \text{for } \lambda = 0 \\ \text{unknown} & \text{for } 0 < \lambda < 1 \\ \hat{v}_{ext}(\mathbf{r}) & \text{for } \lambda = 1 \end{cases} \quad (2.46)$$

and a resulting Hamiltonian for every value of λ :

$$\widehat{\mathcal{H}}(\lambda) = \widehat{T} + \int d^3r u_\lambda(\mathbf{r}) \hat{n}(\mathbf{r}) + \lambda \underbrace{(\hat{v}_{ee} - \hat{v}_s + \hat{v}_{ext})}_{\widehat{\mathcal{H}}_1} \quad (2.47)$$

The energy difference between the fully interacting and the non-interacting system can now be derived by using the *Hellman-Feynman theorem* (2.13):

$$\frac{dE}{d\lambda} = \langle \Psi | \frac{d\widehat{\mathcal{H}}}{d\lambda} | \Psi \rangle = \int d^3r (u_{\lambda=1} - u_{\lambda=0}) n(\mathbf{r}) + \int_0^1 d\lambda \langle \Psi_0(\lambda) | \widehat{\mathcal{H}}_1 | \Psi_0(\lambda) \rangle \quad (2.48)$$

$$\rightarrow E_0^{\lambda=1} - E_0^{\lambda=0} = V_{ext} - V_s + \int_0^1 d\lambda \langle \Psi_0(\lambda) | \hat{v}_{ee} - \hat{v}_s + \hat{v}_{ext} | \Psi_0(\lambda) \rangle \quad (2.49)$$

Considering that the energy $E_0^{\lambda=1}$ of the fully interacting system is given by (2.34) and the energy $E_0^{\lambda=0}$ of the non-interacting system is the Kohn-Sham systems energy and thus given by $E_s = T_s + V_s$ we end up with

$$E_{xc}[n] = \int_0^1 d\lambda \langle \Psi_0(\lambda) | \hat{v}_{ee} | \Psi_0(\lambda) \rangle - V_H[n]. \quad (2.50)$$

For a systematic perturbative approach to the exchange and correlation energies it is also instructive to introduce the time ordered density-density response function

$$\chi(\mathbf{r}t, \mathbf{r}'t') = \frac{-i}{\hbar} \langle \Psi_0 | \hat{T} \delta \hat{n}(\mathbf{r}t) \delta \hat{n}(\mathbf{r}'t') | \Psi_0 \rangle, \quad (2.51)$$

where \hat{T} is the time ordering operator, which puts the operators at later times to the left of operators acting at earlier times and δn is the difference of the density $n(\mathbf{r})$ with respect the ground state density $n_0(\mathbf{r})$ (a more rigorous introduction to response functions is given in Appendix A.1).

With the help of this response function, we can rewrite equation (2.50):

$$E_{xc} = \frac{1}{2} \int d^3r \int d^3r' w(\mathbf{r}, \mathbf{r}') \int_0^1 d\lambda [i\hbar \chi(\mathbf{r}0, \mathbf{r}'0) - n(\mathbf{r}) \delta(\mathbf{r} - \mathbf{r}')] \quad (2.52)$$

Now we have seen how to extract the exchange and correlation energy in principle. The calculation thereof is a whole branch of physics and many physicists are looking for a universal E_{xc} functional, describing the physics of many different systems. The chase of this holy grail of DFT turned out to be a very demanding and cumbersome task and the next sections will give a short introduction to the history of the development fo the functional and the current state of research.

2.6.1 The local density approximation (LDA)

Historically the first investigation on E_{xc} was the local density approximation (LDA), where an additive energy-particle-density $\epsilon_{xc}(n(\mathbf{r})) = \epsilon_x(n(\mathbf{r})) + \epsilon_c(n(\mathbf{r}))$ is assumed and the exchange-correlation energy reads

$$E_{xc} = \int d^3r \epsilon_{xc}(n(\mathbf{r})) n(\mathbf{r}). \quad (2.53)$$

In the local spin density approximation (LSDA), two densities with opposite spin are considered. They sum up to the total density $n_{\uparrow}(\mathbf{r}) + n_{\downarrow}(\mathbf{r}) = n(\mathbf{r})$ and their interaction is represented in the exchange and correlation energy

$$E_{xc}^{LSDA}[n_{\uparrow}(\mathbf{r}), n_{\downarrow}(\mathbf{r})] = \int d^3r \epsilon_{xc}(n_{\uparrow}(\mathbf{r}), n_{\downarrow}(\mathbf{r})) n(\mathbf{r}). \quad (2.54)$$

For the calculation of ϵ_x and ϵ_c , jellium is taken as a reference system. The jellium system consists of a gas of electrons moving in a potential given by a uniform positive background charge n^+ . The positive background is necessary to create a stable system because due to the long range of the Coulomb interaction, the energy of the system would diverge. This system is convenient for the study of exchange and correlation energies because there exist analytical expressions for the cases of very low and high densities (derivations thereof can be found in Carr (1961) and Macke (1950)). The exchange energy density, which was derived by Dirac (1930) and Slater (1951) has the form $-\frac{3}{4} \left(\frac{3}{\pi}\right)^{1/3} n(\mathbf{r})^{1/3}$. The correlation energy densities were extracted from quantum Monte Carlo simulations and parametrized by a function, which fulfills the low and high density limits and shows enough flexibility to closely match the intermediate region. The first Monte Carlo simulations were performed by Ceperley and Alder (1980) for a non-spin-polarized homogeneous electron gas. Simulations for the spin-polarized case were performed by many authors, the most prominent being Vosko, Wilk, and Nusair (1980) and Perdew and Wang (1992). In general, the LDA underestimates the exchange energy and overestimates the correlation energy. The LDA is simple and for this level of simplicity the agreement with experiment in is remarkable in many cases, although it tends to overbind and gives too small band gaps.

2.6.2 Gradient expansion approximation (GEA)

In their famous paper on the inhomogeneous electron gas, where the *Hohenberg-Kohn theorem* was derived, Hohenberg and Kohn (1964) refined the LDA and parametrized the exchange and correlation energy for the case of a slowly varying inhomogeneous electron gas. In this gradient expansion approximation an inhomogeneity in the positive background density

$$\delta v(\mathbf{r}) = - \int d^3r' w(\mathbf{r} - \mathbf{r}') \delta n^+(\mathbf{r}') \quad (2.55)$$

with

$$\int d^3r \delta n^+(\mathbf{r}) = 0 \quad (2.56)$$

is considered and the response of the system is analyzed in Fourier space, where the slow variation of the density corresponds to a long wavelength expansion in the Fourier coefficients. Transformation of the result back to real space, results in an exchange and correlation energy, which depends not only on the density but also on the gradients thereof

$$E_{xc} = \int f(n(\mathbf{r}), \nabla n(\mathbf{r})) d^3r. \quad (2.57)$$

If the perturbation series in Fourier space is performed to the order of q^2 , the change in the energy contributions is given by

$$\Delta E_x^{[2]} = -C_x \int d^3r e_x^{LDA}(n) \left[\eta - \frac{4}{3}\xi \right] \quad (2.58)$$

$$\Delta E_{xc}^{[2]} = \int d^3r e_x^{LDA}(n) \xi C_{xc}(n) \quad (2.59)$$

with the two gradient functions

$$\xi = \left(\frac{\nabla n(\mathbf{r})}{2[3\pi^2 n(\mathbf{r})]^{1/3} n(\mathbf{r})} \right)^2 \quad \text{and} \quad \eta = \frac{\Delta n(\mathbf{r})}{4[3\pi^2 n(\mathbf{r})]^{2/3} n(\mathbf{r})}. \quad (2.60)$$

These are diverging at large distances for exponentially decaying densities. Even if higher orders of the gradients are considered, this divergence is present. This makes the use of the GEA impossible in the case of finite systems. While the gradient expansion to second order improves the exchange energy of the LDA, it has the wrong sign for the correlation energy (Ma and Brueckner (1968)) and gives in general no improvement over LDA results. This is the reason, why the GEA has to be refined to obtain a precise semi-local theory, which is done in the generalized gradient approximation (GGA).

2.6.3 Generalized gradient approximations (GGA)

The failure of the GEA was explained by performing a wavevector analysis of the kernel of ΔE_{xc} by Langreth and Mehl (1983). They found out that the GEA showed a wrong behaviour for small wavevectors and were able to correct for this by introducing a cutoff for small wavevectors in this kernel. Perdew (1985) analyzed the failure of the GEA in real space. Starting from the exchange correlation hole formalism in equation (2.44), he considered the real space formulation of the GEA and forced the exchange energy to fulfill theoretical constraints by introducing cutoff functions for the real space behaviour of the exchange and correlation hole, resulting in the exchange energy

expression

$$E_x^{GGA} [n] = \int d^3r e_x^{HEG} (n) f (R_c(\xi)), \quad (2.61)$$

where R_c is a cutoff parameter, chosen to obtain the proper normalization of the exchange hole, depending on the density gradient function ξ from equation (2.60). Based on these considerations, Perdew, Burke, and Ernzerhof (1996) described a way to construct GGA functionals in a simpler way by considering limits of high and low density gradients and scaling relations and ended up with the PBE functional, which will be the GGA of choice in this work and is parametrized by the enhancement factor F_{xc}

$$E_{xc}^{GGA} [n_\uparrow, n_\downarrow] = \int d^3r n \epsilon_x^{LDA}(n) F_{xc} (n_\uparrow, n_\downarrow, \nabla n_\uparrow, \nabla n_\downarrow) \quad . \quad (2.62)$$

Later Perdew et al. (2008) revised this functional for the application in solids, calling the resulting functional PBEsol.

PBE generally improves the performance of LDA for many physical and chemical properties, even though its success is still based on an error cancellation in exchange and correlation energies. For the present purpose, the main failures of PBE include too big lattice constants and still too small band gaps, as can be seen in the bandstructure of different functionals in the case of diamond in Figure 2.4.

2.6.4 MetaGGAs

The next reasonable step to improve the functional, would of course be to include higher order gradients of the density. Since this computation is rather difficult to implement numerically, the way to go is to parametrize the exchange and correlation energy by including the kinetic energy density

$$t_s = \frac{\hbar^2}{2m_e} \sum_k \Theta_k |\nabla \phi_k(\mathbf{r})|^2. \quad (2.63)$$

Functionals of this type are called Meta-GGAs and are given by the expression

$$E_{xc}^{MGGA} = \int d^3r n \epsilon_{xc}^{MGGA} (n_\uparrow, n_\downarrow, \nabla n_\uparrow, \nabla n_\downarrow, t_{s,\uparrow}, t_{s,\downarrow}). \quad (2.64)$$

With the introduction of a new quantity, the number of possible parametrizations increases dramatically. In this work, we will only make use of a very recent Meta-GGA, developed by Sun, Ruzsinszky, and Perdew (2015). It is called SCAN (Strongly Constrained and Appropriately Normed Semilocal Density Functional) and is the first functional to fulfill all the theoretically known constraints on a density functional (6 for exchange, 6 for correlation, and five

for the sum of the two).

2.6.5 Hybrid functionals

Becke (1993) had another idea to obtain proper exchange energies by coupling DFT and Hartree-Fock theory. He proposed to add a certain amount of exact exchange, obtained with the Kohn-Sham orbitals and ended up with an exchange and correlation energy

$$E_x^{hyb} = a_0 E_x^{exact} + a_1 E_x^{GGA} + (1 - a_0 - a_1) E_x^{LDA} \quad (2.65)$$

$$E_c^{hyb} = b_1 E_c^{GGA} + (1 - b_0) E_c^{LDA} \quad (2.66)$$

Functionals of this type are called *hybrids* for obvious reasons. Becke motivated this ansatz theoretically by starting from the coupling constant integration in equation (2.50) and assuming a linear interpolation between the non-interacting and the fully interacting system, resulting in the crude approximation

$$E_{xc} \approx \frac{1}{2} E_{xc}^{\lambda=0} + \frac{1}{2} E_{xc}^{\lambda=1}, \quad (2.67)$$

and taking into account that $E_{xc}^{\lambda=0}$ of the non-interacting Kohn-Sham system is given by the Hartree-Fock like exchange, calculated with the Kohn-Sham orbitals. Becke obtained the coefficients in equation (2.65) by fitting the energies to a thermochemical database. A theoretical justification was given by Perdew, Ernzerhof, and Burke (1996) and resulted in the PBE0 functional. The evaluation of the Hartree-Fock kernel is computationally expensive, which led Heyd, Scuseria, and Ernzerhof (2003) to develop a functional, which uses a screened Coulomb kernel for the evaluation of the exchange energy. In their scheme they split the Coulomb interaction into a short-range (SR) and a long-range part (LR)

$$\frac{1}{r} = \underbrace{\frac{1 - \text{erf}(\omega)}{r}}_{SR} + \underbrace{\frac{\text{erf}(\omega)}{r}}_{LR}, \quad (2.68)$$

where erf is the Gaussian error function and ω a screening parameter. In their paper, they prove that the evaluation of the exact exchange for the small range interaction may be sufficient and that the long range part may be treated at PBE level, resulting in their HSE-functional.

$$E_{xc}^{HSE} = a E_x^{HF,SR}(\omega) + (1 - a) E_x^{PBE,SR}(\omega) + E_x^{PBE,LR}(\omega) + E_c^{PBE}. \quad (2.69)$$

This expression gives the PBE0 functional in the unscreened limit $\omega \rightarrow 0$. In their original HSE03 functional, they chose different screening parameters

ω_{HF} and ω_{PBE} for the evaluation of the exchange Coulomb kernel, which was inconsistent with the uniform electron gas limit. A revised version of the functional with $\omega_{HF} = \omega_{PBE} = 0.11 a_0^{-1}$ called HSE06 was proposed by Krukau et al. (2006) and yields improved band gaps for solids. Due to this reason, this will often be the functional of choice in this work.

2.6.6 Semi-empirical functionals

As mentioned in the previous paragraph, it is possible to obtain density functionals by fitting some parameters of known theoretically derived functionals to experimental data. This approach contradicts the demand of an *ab initio* theory and it is impossible to systematically improve such functionals by theoretical means. Becke himself, one of the founders of the semi-empirical functionals, noted on the fitting to molecular data that "many wish this door had never been opened" (Becke (2014)). Due to this lack of theoretical foundation, functionals of this type will not be used in this thesis, even though there is valuable applicability in chemistry.

2.7 Solid state systems

2.7.1 Periodic systems - crystals structures and Bloch's theorem ⁴

Up to now we dealt with a simplification of the quantum theoretical problem in equations (2.1) and (2.2) by trying to map a system of many interacting electrons, described as a sum of Slater-determinants, to the non-interacting Kohn-Sham system, where all the exchange and correlation effects were taken into account in the potential. This simplification paves the way to deal with up to thousand atoms. However, the system we deal with in this thesis, consists of a much larger number of atoms ($\approx 10^{23}$), and is therefore not manageable by modern computer clusters without any further simplification. The most fascinating tool to reduce the amount of necessary calculations is symmetry, expressed by the mathematics of group theory and representation theory. In this Chapter, the translational symmetry of solids is exploited to obtain basis functions that diagonalize the underlying Hamiltonian, resulting in the concept of a bandstructure. As an example, diamond as the host material of the NV^- center will be considered. Group theory allows us to find basis functions, which diagonalize the Hamiltonian and find the degeneracies of the system. All that

⁴The derivation of Bloch's theorem in this section follows the treatment of Marder (2000)

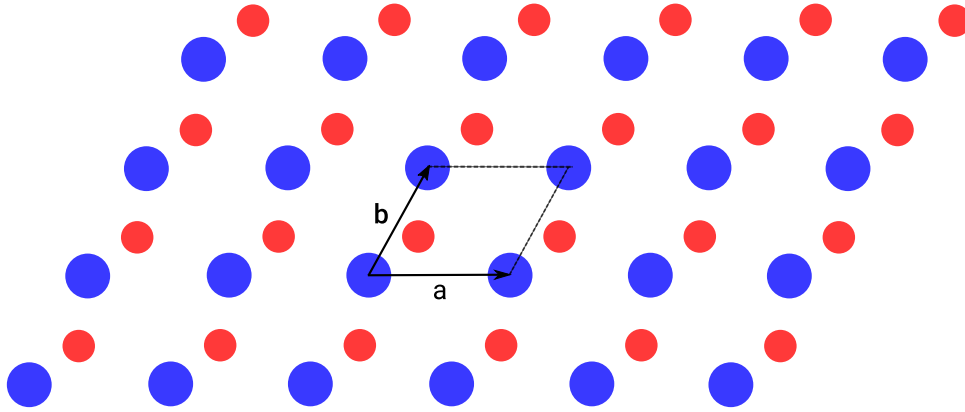


Figure 2.2: **2d Bravais lattice.** This Figure illustrates one example of a Bravais lattice, where the building blocks consist of a basis with two atoms, shown as red and blue circles.

needs to be done, is to find the irreducible representations of the underlying group and a wavefunction representation, which transforms according to those. A small systematic introduction to the group theoretical tools used is given in Appendix B. Due to the long range order of a solid, we expect the system to be invariant under translations, s.t. the underlying atomic structure is described by repetitions of the smallest basic constituents, the unit cells. These cells form a grid, called the *Bravais*-lattice, where each gridpoint fulfills the equation

$$\mathbf{R} = n_1 \mathbf{a}_1 + n_2 \mathbf{a}_2 + n_3 \mathbf{a}_3 \quad \text{with } n_i \in \mathbb{Z}, \quad (2.70)$$

with \mathbf{a}_i being the basis vectors of the unit cell. A two dimensional example of a *Bravais* lattice is depicted in Figure 2.2.

A group theoretical classification of all the possible Bravais lattices by symmetry considerations in 3-dimensional crystals yields 14 different possible Bravais lattices and, if point symmetries are also taken into account, 230 different possible symmetry groups, called *space groups* (for a more detailed discussion see Marder (2000)). This thesis deals with diamond, as the host of the NV^- center, where two common choices of unit cells exist, the *primitive* and the *conventional* cell. As shown in Figure 2.3, the diamond structure consists of a face centered cubic structure with a basis of two carbon atoms, which are separated by the vector $(\frac{1}{4}, \frac{1}{4}, \frac{1}{4})$ and according to the symmetry operations it belongs to the space group $Fd\bar{3}m$. In describing a periodic system, a very useful concept is the reciprocal lattice, which consists of all points, fulfilling

$$\mathbf{G} = n_1 \mathbf{b}_1 + n_2 \mathbf{b}_2 + n_3 \mathbf{b}_3 \quad \text{with } n_i \in \mathbb{Z}, \quad (2.71)$$

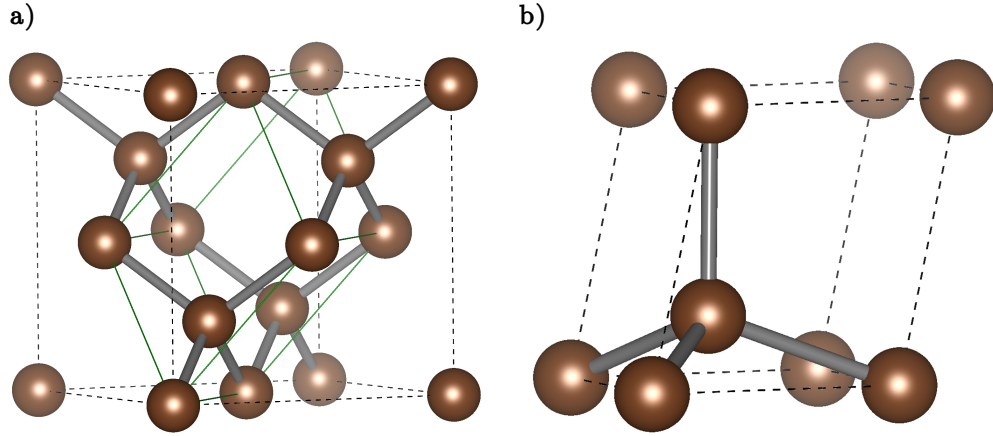


Figure 2.3: **a)** The conventional unit cell of diamond. The grey lines denote the bonds and the green box is the smallest translational unit cell, the primitive cell, which is shown enlarged in **b)**

where the basis vectors \mathbf{b}_i are dual to the basis vectors of the real-space grid

$$\mathbf{a}_i \mathbf{b}_j = 2\pi \delta_{ij} \quad (2.72)$$

and may be constructed according to

$$\mathbf{b}_i = \frac{2\pi}{\Omega} \epsilon_{ijk} \mathbf{a}_j \mathbf{a}_k, \quad (2.73)$$

where Ω is the volume of the unit cell in real space and ϵ_{ijk} the *Levi-Civita* symbol. These wave vectors reflect the periodicity of the *Bravais*-lattice because

$$e^{i\mathbf{G}\mathbf{R}} = 1. \quad (2.74)$$

As already mentioned, we need to find the representations for translations of the system. Since the translations commute, each symmetry operation is a class itself, the irreducible representations are 1-dimensional and there are N classes, where N is the number of total translations ($N = N_1 \cdot N_2 \cdot N_3$). An idea for the structure of the representations is obtained by considering the 1-dimensional case, with a basis vector a . Since we have N_1 translations in the system, we label each translation by some index k_1 . To extract the representation, we consider the composite action of two translations

$${}_{k_1} \mathcal{T}(ma_1) {}_{k_1} \mathcal{T}(na_1) = {}_{k_1} \mathcal{T}((m+n)a_1) \quad (2.75)$$

which allows to write the representation as an exponential, which we choose for convenience to be parametrized by k_1 as

$${}_{k_1}\mathcal{T}(ma_1) = e^{-i2\pi mk_1}. \quad (2.76)$$

This choice of phase allows to use the reciprocal basis vectors to write the representation of a general translation as

$${}_{\mathbf{k}}\mathcal{T}(l\mathbf{a}_1 + m\mathbf{a}_2 + n\mathbf{a}_3) = e^{-i\mathbf{k}\mathbf{R}} \quad (2.77)$$

$$\text{with } \mathbf{k} = k_1\mathbf{b}_1 + k_2\mathbf{b}_2 + k_3\mathbf{b}_3 \quad k_1, k_2, k_3 \in \mathbb{R} \quad . \quad (2.78)$$

The translation of a wavefunction, which transforms according to a certain irreducible representation must therefore read

$${}_{\mathbf{k}}\mathcal{T}(\mathbf{R})\psi_{n\mathbf{k}}(\mathbf{r}) = e^{-i\mathbf{k}\mathbf{R}}\psi_{n\mathbf{k}}(\mathbf{r}). \quad (2.79)$$

From now on we will label the wavefunctions by the irreducible representation, according which they transform according to, and the quantum numbers n . The translational transformation may be separated off, by rewriting the wavefunction as ⁵

$$\psi_{n\mathbf{k}}(\mathbf{r}) = e^{i\mathbf{k}\mathbf{r}}u_{n\mathbf{k}}(\mathbf{r}) \quad (2.80)$$

\Rightarrow

$${}_{\mathbf{k}}\mathcal{T}(\mathbf{R})\psi_{n\mathbf{k}}(\mathbf{r}) = \psi_{n\mathbf{k}}(\mathbf{r} - \mathbf{R}) = e^{i\mathbf{k}(\mathbf{r}-\mathbf{R})}u_{n\mathbf{k}}(\mathbf{r}) = e^{-i\mathbf{k}\mathbf{R}}\psi_{n\mathbf{k}}(\mathbf{r}) \quad (2.81)$$

where $u_{n\mathbf{k}}$ is a cell periodic function $u_{n\mathbf{k}}(\mathbf{r}) = u_{n\mathbf{k}}(\mathbf{r} + \mathbf{R})$. In solid state physics *Born-von Karman* periodic boundary conditions are usually assumed, where a translation ${}_{k_i}\mathcal{T}$ by N_i basis vectors is equivalent to no translation. In analogy to a particle in a box, this results in a quantization of the allowed \mathbf{k} vectors

$$\mathcal{T}(N_i a_i) = \mathcal{T}(0a_i) \quad i \in \{1, 2, 3\} \quad (2.82)$$

$$\Rightarrow e^{-i2\pi k_i N_i} = 1 \Rightarrow k_i N_i = n_i \quad n_i \in 1, 2, \dots, N_i. \quad (2.83)$$

Due to equation (2.74), if two \mathbf{k} vectors differ by a reciprocal lattice vector, they label the same representation ${}_{\mathbf{k}}\mathcal{T} = {}_{\mathbf{k}+\mathbf{G}}\mathcal{T}$. Thus, we can restrict the allowed \mathbf{k} vectors to a region around the origin in reciprocal space, where each

⁵The transformation of a function under some symmetry operation \mathcal{O} is derived by considering that the transformed function at the transformed point should equal the old function at the old point:

$$\mathcal{O}_f f(\mathcal{O}_r \mathbf{r}') \stackrel{!}{=} f(\mathbf{r}') \quad \mathbf{r}' \stackrel{\mathcal{O}_r^{-1}}{\longmapsto} \mathbf{r} \quad \mathcal{O}_f f(\mathbf{r}) = f(\mathcal{O}_r^{-1} \mathbf{r}),$$

where \mathcal{O}_f and \mathcal{O}_r are the transformation operators in function and real space respectively.

point is supposed to be closer to the origin, than to some neighbour point. This region is called the first *Brillouin zone* and it contains all the information about the crystal because of the periodicity in reciprocal space. Due to the large number of unit cells, the \mathbf{k} vectors form a quasi-continuum, where the number of available states is the same as the number of unit cells in the crystal. The additional label n is called the band index and according to the previous considerations, each band can hold 1 electron per unit cell (2, if spin is not taken into account). The energy dispersion and the filling of the bands inside the zone are determining the scattering characteristics of a material: If energy levels above the highest occupied levels are accessible, the electrons are easily scattered and thus charge is transported. This is related to the conduction mechanism in metals. In our case of the NV^- center, the induced energy levels of the center should not interact with the host material in order to allow for a simple molecular system, where the interactions with external fields are modeled in a simple way. In order to make the defect states not to interact with the surrounding, a substantial separation in energy of the relevant orbitals is needed. Thus, diamond is a brilliant host material, because it is an insulator and the highest occupied bands are separated by the lowest unoccupied bands by a band gap of 5.47 eV ⁶. This allows for well separated defect states (in energy), which do not hybridize strongly with the surrounding.

	LDA	PBE	SCAN	HSE06	HF	Exp
E_{gap}^{global}	4.164	4.204	3.404	5.435	10.862	5.47
E_{gap}^{direct}	5.53	5.590	4.927	7.004	11.031	-

Table 2.1: The global and direct band gaps for Diamond for four different exchange correlation functionals. The hybrid functional HSE06 performs best for predicting the gap value.

2.8 Wannier functions

Since the NV^- centers break the translation symmetry of the crystal, Bloch's theorem is strictly speaking not valid. Neglecting other defects or NV^- centers, the dispersion relation due to the strong localization of the orbitals should resemble the molecular orbital states and be flat in \mathbf{k} -space. This is not the case for the Bloch-functions, since the calculation programs use periodic boundary conditions and the NV^- center will have some interaction with the one in the neighbouring cell. However, as Wannier (1937) pointed out, there exists a

⁶This value was taken from Wort and Balmer (2008)

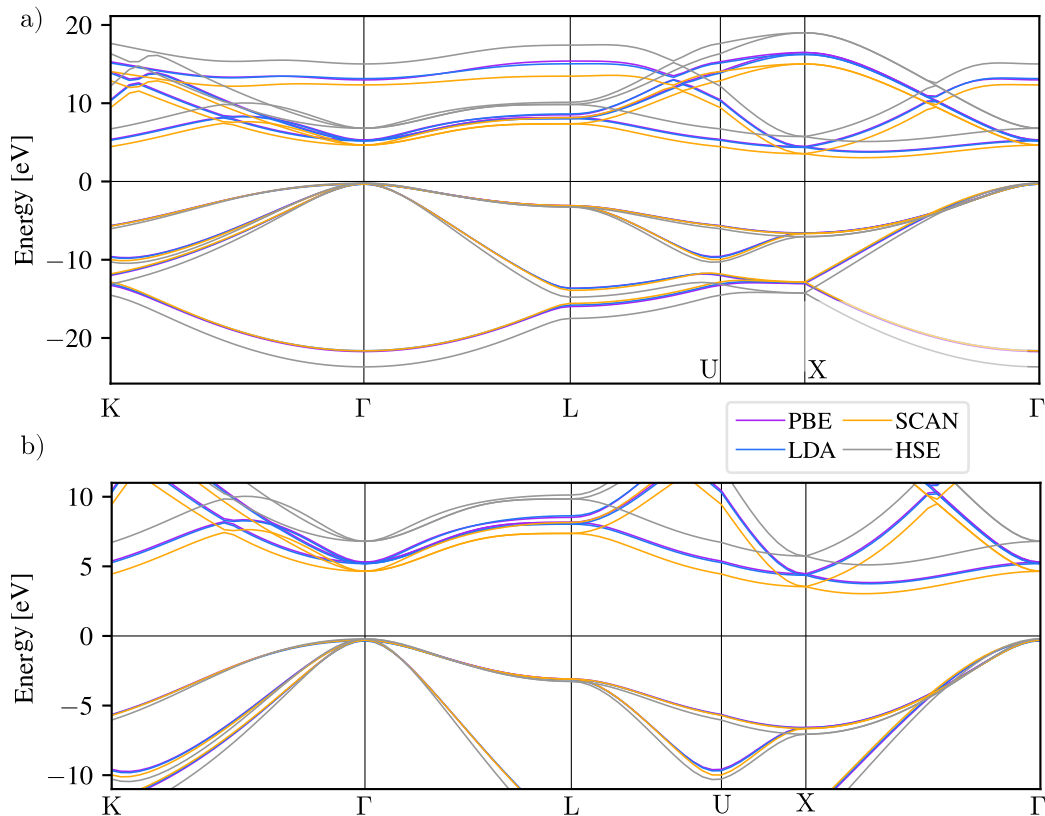


Figure 2.4: **Bandstructure of diamond**, The bandstructure of diamond calculated *ab initio* using 4 different exchange-correlation functionals. a) The total band structure. b) A zoomed view to highlight the gap properties of the different functionals. As mentioned previously, the most accurate band gap compared to the experimental value is obtained using the hybrid functional HSE06.

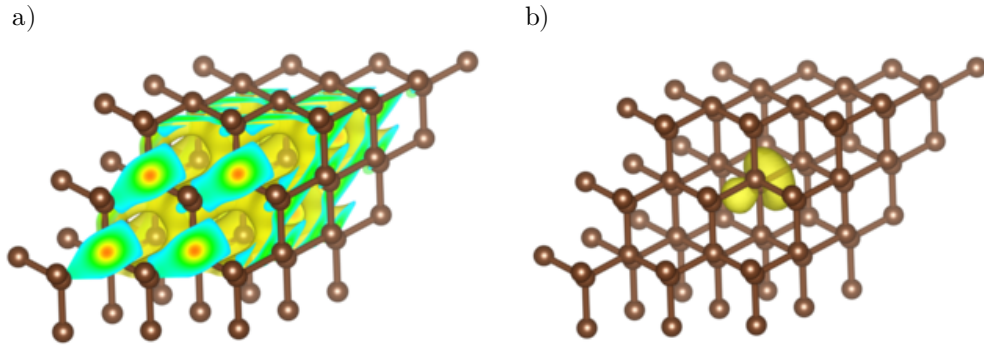


Figure 2.5: **Bloch and Wannier functions in diamond**, the absolute values of a Bloch wavefunction [a)] and the maximally localized Wannier function [b)] in diamond are shown. The level of the isosurfaces correspond to the same value of Ψ/Ψ_{max} .

set of localized orthogonal wavefunctions, which are the solid state analogue of atomic wavefunctions, which are located at certain positions in space \mathbf{R} . These orbitals $w_{n\mathbf{R}}$ are called *Wannier-orbitals* and are obtained by a unitary transformation of the Bloch functions

$$w_{n\mathbf{R}} = \frac{\Omega}{(2\pi)^3} \int_{BZ} \left[\sum_m U_{mn}^{(\mathbf{k})} \psi_{m\mathbf{k}}(\mathbf{r}) \right] e^{-i\mathbf{r}\mathbf{k}} d\mathbf{k}. \quad (2.84)$$

This transformation is not unique, since there is a "gauge freedom" in choosing the unitary transformation, which changes the individual centers of the Wannier orbital but keeps the sum of the Wannier centers, modulo a lattice vector. This allows to use these phases (Marzari and Vanderbilt, 1997) to minimize the spread Ω_W of the resulting Wannier orbitals, defined as

$$\Omega_W = \sum_n \left[\langle w_{n\mathbf{0}(\mathbf{r})} | \mathbf{r}^2 | w_{n\mathbf{0}(\mathbf{r})} \rangle - \left| \langle w_{n\mathbf{0}(\mathbf{r})} | \mathbf{r} | w_{n\mathbf{0}(\mathbf{r})} \rangle \right|^2 \right]. \quad (2.85)$$

The spread may be decomposed in a gauge independent and gauge dependent contribution:

$$\Omega_W = \Omega_W^I + \tilde{\Omega}_W. \quad (2.86)$$

The method of Marzari and Vanderbilt minimizes the gauge dependent spread with respect to the $U_{mn}^{(\mathbf{k})}$ to obtain maximally localized Wannier functions (MLWFs). In this thesis all the Wannier functions are calculated using the program Wannier90(Mostofi et al. (2014)). For a comparison between MLWF and Bloch wavefunctions in diamond, see Figure 2.5. MLWFs provide a way to operate in a much smaller basis set than the Bloch functions and are therefore often used to map a system to a model tight-binding Hamiltonian. In our

case we use the MLWFs to obtain a localized basis, in order to get rid of the interactions with the repetitions of the defect states in the calculated cells and to average out the effects of the bandstructure on a non-periodic system.

2.9 Software package

The density functional theory calculations in this work are all performed using the Vienna *ab initio* simulation package (VASP), a code using plane wave basis functions to describe the orbitals with an implementation of the projector augmented wave method (Blöchl (1994), Kresse and Joubert (1999)). All the previously mentioned functionals are included and there exist interfaces between this code and the software packages we use to obtain maximally localized Wannier functions and phonon properties.

References

- Becke, A. D. (1993). “A new mixing of Hartree-Fock and local density-functional theories”. In: *The Journal of Chemical Physics* 98, pp. 1372–1377.
- (2014). “Perspective: Fifty years of density-functional theory in chemical physics”. In: *Journal of Chemical Physics* 140.
- Blöchl, P. E. (1994). “Projector augmented-wave method”. In: *Phys. Rev. B* 50 (24), pp. 17953–17979.
- Born, M. and R. Oppenheimer (1927). “Zur Quantentheorie der Molekeln”. In: *Annalen der Physik* 389, pp. 457–484.
- Carr, W. J. (1961). “Energy, Specific Heat, and Magnetic Properties of the Low-Density Electron Gas”. In: *Phys. Rev.* 122 (5), pp. 1437–1446.
- Ceperley, D. M. and B. J. Alder (1980). “Ground state of the electron gas by a stochastic method”. In: *Phys. Rev. Lett.* 45, pp. 566–569.
- Dirac, P. A. M. (1930). “Note on Exchange Phenomena in the Thomas Atom”. In: *Mathematical Proceedings of the Cambridge Philosophical Society* 26, p. 376.
- Fermi, E. (1928). “Eine statistische Methode zur Bestimmung einiger Eigenschaften des Atoms und ihre Anwendung auf die Theorie des periodischen Systems der Elemente”. In: *Zeitschrift für Physik* 48, pp. 73–79.
- Feynman, R. P. (1939). “Forces in molecules”. In: *Phys. Rev.* 56, pp. 340–343.
- Heyd, J., G. E. Scuseria, and M. Ernzerhof (2003). “Hybrid functionals based on a screened Coulomb potential”. In: *Journal of Chemical Physics* 118, pp. 8207–8215.
- Hohenberg, P. and W. Kohn (1964). “Inhomogeneous Electron Gas”. In: *Phys. Rev.* 136, B864–B871.
- Kohn, W. and L. J. Sham (1965). “Self-consistent equations including exchange and correlation effects”. In: *Phys. Rev.* 140.
- Kresse, G. and D. Joubert (1999). “From ultrasoft pseudopotentials to the projector augmented-wave method”. In: *Physical Review B* 59.3, pp. 1758–1775.
- Krukau, A. V. et al. (2006). “Influence of the exchange screening parameter on the performance of screened hybrid functionals”. In: *Journal of Chemical Physics* 125, p. 224106.
- Langreth, D. C. and M. J. Mehl (1983). “Beyond the local-density approximation in calculations of ground-state electronic properties”. In: *Phys. Rev. B* 28, pp. 1809–1834.
- Ma, S.-K. and K. A. Brueckner (1968). “Correlation Energy of an Electron Gas with a Slowly Varying High Density”. In: *Phys. Rev.* 165, pp. 18–31.

- Macke, W. (1950). “Über die Wechselwirkungen im Fermi-Gas.” In: *Zeitschrift für Naturforschung A*, 192.
- Marder, M. (2000). *Condensed Matter Physics*. Wiley-interscience.
- Marzari, N. and D. Vanderbilt (1997). “Maximally localized generalized Wannier functions for composite energy bands”. In: *Phys. Rev. B* 56, pp. 12847–12865.
- Mostofi, A. A. et al. (2014). “An updated version of wannier90: A tool for obtaining maximally-localised Wannier functions”. In: *Computer Physics Communications* 185, pp. 2309–2310.
- Perdew, J. P. (1985). “Accurate Density Functional for the Energy: Real-Space Cutoff of the Gradient Expansion for the Exchange Hole”. In: *Phys. Rev. Lett.* 55, pp. 1665–1668.
- Perdew, J. P., K. Burke, and M. Ernzerhof (1996). “Generalized Gradient Approximation Made Simple”. In: *Phys. Rev. Lett.* 77 (18), pp. 3865–3868.
- Perdew, J. P., M. Ernzerhof, and K. Burke (1996). “Rationale for mixing exact exchange with density functional approximations”. In: *Journal of Chemical Physics* 105, pp. 9982–9985.
- Perdew, J. P. and Y. Wang (1992). “Accurate and simple analytic representation of the electron-gas correlation energy”. In: *Phys. Rev. B* 45, pp. 13244–13249.
- Perdew, J. P. et al. (2008). “Restoring the Density-Gradient Expansion for Exchange in Solids and Surfaces”. In: *Phys. Rev. Lett.* 100 (13), p. 136406.
- Slater, J. C. (1951). “A Simplification of the Hartree-Fock Method”. In: *Phys. Rev.* 81 (3), pp. 385–390.
- Sun, Jianwei, Adrienn Ruzsinszky, and John P. Perdew (2015). “Strongly Constrained and Appropriately Normed Semilocal Density Functional”. In: *Phys. Rev. Lett.* 115 (3), p. 036402.
- Thomas, L. H. (1927). “The calculation of atomic fields”. In: *Mathematical Proceedings of the Cambridge Philosophical Society* 23, p. 542.
- Vosko, S. H., L. Wilk, and M. Nusair (1980). “Accurate spin-dependent electron liquid correlation energies for local spin density calculations: a critical analysis”. In: *Canadian Journal of Physics* 58, pp. 1200–1211.
- Wannier, G. H. (1937). “The Structure of Electronic Excitation Levels in Insulating Crystals”. In: *Phys. Rev.* 52, pp. 191–197.
- Wort, C. J. H. and R. S. Balmer (2008). “Diamond as an electronic material”. In: *Materials Today* 11, pp. 22–28.

Chapter 3

The theory of lattice vibrations

The tools we derived in the previous Chapter will enable us to calculate the electronic properties of the NV^- center. To understand Spin-lattice relaxation in solids, a proper understanding of lattice vibrations is of utmost importance. This chapter will introduce the theory of lattice vibrations and build the foundation that is necessary to understand the Spin-lattice relaxation processes, described in the next Chapter. In order to get insight into the dynamics of a crystal lattice, the easiest approach to be taken is to use Hook's law and assume that the ions are coupled by spring forces as shown in Figure 3.1. This assumption is valid for small forces, i.e. ions which are only displaced by a small amount from their equilibrium positions where the net force acting on them is zero. In the first section, the theory of lattice vibrations within this harmonic approximation is presented. A quantum mechanical treatment of the coupled harmonic oscillators moving the ions in second quantized form will show that the vibrational excitations can be treated as quasiparticles which are called phonons. This section follows the treatment of Wallace (1998) because in this thesis the program PHONOPY (see Togo and Tanaka (2015)) was used to diagonalize the dynamical matrix, where the same conventions as in Wallace's book are used.

The second section is concerned with the computational details of the calculation of phonon properties on the example of diamond.

3.1 The harmonic approximation

Given the equilibrium positions of all the ions in a structure $\{\mathbf{R}_{M,\mu}^{(0)}\}^1$, we may calculate the lattice vibrations by considering the displacements around

¹The index M denotes the unit cell and μ is the index of the ion inside this cell, so we are also considering lattices with a basis. The exact position of a single ion is therefore given by the sum of the position vectors $\mathbf{R}_{M,\mu}^{(0)} = \mathbf{R}_M^{(0)} + \mathbf{R}_\mu^{(0)}$.

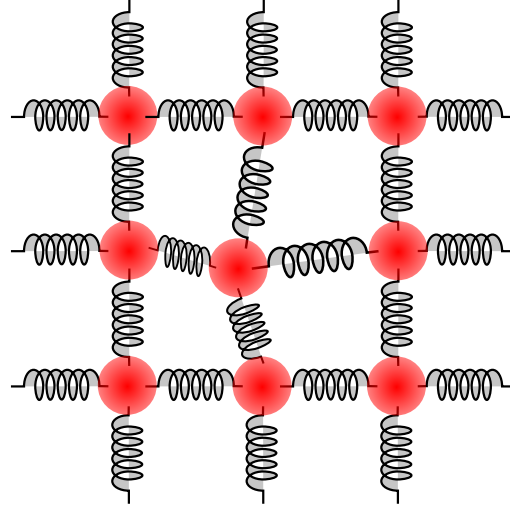


Figure 3.1: The presented model of the lattice vibrations in the harmonic approximation may be thought of as coupled harmonic oscillators. In this picture only the nearest neighbour interactions are depicted by springs. This does not fully resemble the theory presented below, since there is a coupling to all ions taken into account.

the equilibrium position $\mathbf{Q}_{M,\mu} = \mathbf{R}_{M,\mu} - \mathbf{R}_{M,\mu}^{(0)}$ and perform a Taylor-expansion of the ion-ion potential V for small displacements around the equilibrium position:

$$\begin{aligned}
 V(\mathbf{Q}_{M,\mu}) = & V(\mathbf{Q}_{M,\mu} = \mathbf{0}) + \sum_{M,\mu} \underbrace{\frac{\partial V}{\partial \mathbf{R}_{M,\mu}}}_{=\mathbf{F}_{M,\mu}} \bigg|_{\mathbf{R}_{M,\mu}^{(0)}} \mathbf{Q}_{M,\mu} \\
 & + \frac{1}{2} \sum_{M,\mu} \sum_{N,\nu} \frac{\partial^2 V}{\partial \mathbf{R}_{M,\mu} \partial \mathbf{R}_{N,\nu}} \bigg|_{\mathbf{R}_{M,\mu}^{(0)}, \mathbf{R}_{N,\nu}^{(0)}} \mathbf{Q}_{M,\mu} \otimes \mathbf{Q}_{N,\nu} + \mathcal{O}(\mathbf{Q}^3) \quad .
 \end{aligned} \tag{3.1}$$

Since the forces $\mathbf{F}_{n,l}$ are supposed to be zero in the equilibrium position, we can neglect the first order term and obtain a Hamiltonian of coupled harmonic oscillators with the ionic masses M_μ

$$\widehat{\mathcal{H}} = \sum_{M,\mu} \frac{\widehat{P}_{M,\mu}^2}{2M_\mu} + \frac{1}{2} \sum_{M\mu i, N\nu j} \widehat{Q}_{M,\mu}^i \Phi_{N,\nu,j}^{M,\mu,i} \widehat{Q}_{N,\nu}^j \tag{3.2}$$

where we introduced the force constant matrix $\Phi_{N,\nu,j}^{M,\mu,i} = \frac{\partial^2 V}{\partial R_{M,\mu}^i \partial R_{N,\nu}^j} \bigg|_{\mathbf{R}_{M,\mu}^{(0)}, \mathbf{R}_{N,\nu}^{(0)}}$. In order to diagonalize this Hamiltonian, we first note that it describes a set of coupled harmonic oscillators, so we may try to expand it in the second quantized form in raising and lowering operators in analogy to the single harmonic

oscillator

$$\widehat{\mathbf{Q}}_{M,\mu} = \sum_{\mathbf{q},\lambda} \sqrt{\frac{\hbar}{2M_\mu N_u \omega_{\mathbf{q},\lambda}}} \left(\widehat{a}_{\mathbf{q},\lambda} + \widehat{a}_{-\mathbf{q},\lambda}^\dagger \right) \boldsymbol{\epsilon}_{\mathbf{q},\lambda}^\mu e^{i\mathbf{q}\mathbf{R}_{M,\mu}^{(0)}} \quad (3.3)$$

$$\widehat{\mathbf{P}}_{M,\mu} = \sum_{\mathbf{q},\lambda} \sqrt{\frac{\hbar M_\mu \omega_{\mathbf{q},\lambda}}{2N_u}} \left(-i\widehat{a}_{\mathbf{q},\lambda} + i\widehat{a}_{-\mathbf{q},\lambda}^\dagger \right) \boldsymbol{\epsilon}_{\mathbf{q},\lambda}^\mu e^{i\mathbf{q}\mathbf{R}_{M,\mu}^{(0)}} \quad (3.4)$$

with \widehat{a} and \widehat{a}^\dagger being the creation and annihilation operators for the phonons, N_u denotes the number of unit cells in the crystal and $\boldsymbol{\epsilon}_{\mathbf{q},\lambda}$ is the polarization vector of ion b in the particular mode. As we will see later, it is reasonable to choose the polarization vectors as being the eigenvectors of the dynamical matrix.

With this Ansatz in our hand we are able to diagonalize the Hamiltonian in equation (3.2). To keep things simple we first consider only the potential part of the Hamiltonian.

$$\begin{aligned} \frac{1}{2} \sum_{nli,abj} \widehat{Q}_{M,\mu}^i \Phi_{M,\mu,i}^{N,\nu,j} \widehat{Q}_{N,\nu}^j &= \frac{1}{2} \sum_{M\mu i, N\nu j} \sum_{\mathbf{q},\lambda} \sqrt{\frac{\hbar}{2M_\mu N_u \omega_{\mathbf{q},\lambda}}} \underbrace{\left(\widehat{a}_{\mathbf{q},\lambda} + \widehat{a}_{-\mathbf{q},\lambda}^\dagger \right)}_{:=A_{\mathbf{q},\lambda}} \boldsymbol{\epsilon}_{\mathbf{q},\lambda}^{\mu,i} e^{i\mathbf{q}\mathbf{R}_{M,\mu}^{(0)}} \\ &\quad \Phi_{M,\mu,i}^{N,\nu,j} \sum_{\mathbf{k},\rho} \sqrt{\frac{\hbar}{2M_\nu N \omega_{\mathbf{k},\rho}}} \underbrace{\left(\widehat{a}_{\mathbf{k},\rho} + \widehat{a}_{-\mathbf{k},\rho}^\dagger \right)}_{:=A_{\mathbf{k},\rho}} \boldsymbol{\epsilon}_{\mathbf{k},\rho}^{\nu,j} e^{i\mathbf{k}\mathbf{R}_{N,\nu}^{(0)}} \end{aligned} \quad (3.5)$$

This can be simplified by considering the following sum

$$\frac{1}{N_u} \sum_{M,N} \Phi_{M,\mu,i}^{N,\nu,j} e^{i\left(\mathbf{q}\mathbf{R}_{M,\mu}^{(0)} + \mathbf{k}\mathbf{R}_{N,\nu}^{(0)}\right)} = \quad (3.6)$$

$$= \frac{1}{N_u} \sum_M e^{i(\mathbf{q}+\mathbf{k})\mathbf{R}_M^{(0)}} \sum_N \Phi_{M,\mu,i}^{N,\nu,j} e^{i\mathbf{R}_\mu^{(0)}(\mathbf{q}+\mathbf{k})} e^{i\mathbf{k}\left(\mathbf{R}_{N,\nu}^{(0)} - \mathbf{R}_{M,\mu}^{(0)}\right)} \quad (3.7)$$

The second sum is over all reciprocal lattice vectors and will be independent of the index M , if we neglect boundary effects and assume all points in the interior of the crystal. Thus, we can as well evaluate the second sum at $M = 0$, resulting in the expression

$$\frac{1}{N_u} \underbrace{\sum_M e^{i(\mathbf{q}+\mathbf{k})\mathbf{R}_M^{(0)}}}_{=\delta_{\mathbf{q},-\mathbf{k}}} \sum_N \Phi_{0,\mu,i}^{N,\nu,j} e^{i\mathbf{R}_\mu^{(0)}(\mathbf{q}+\mathbf{k})} e^{i\mathbf{k}\left(\mathbf{R}_{N,\nu}^{(0)} - \mathbf{R}_{0,\mu}^{(0)}\right)} \quad (3.8)$$

$$= \delta_{\mathbf{q},-\mathbf{k}} \sum_N \Phi_{0,\mu,i}^{N,\nu,j} e^{i\mathbf{k}\left(\mathbf{R}_{N,\nu}^{(0)} - \mathbf{R}_{0,\mu}^{(0)}\right)}. \quad (3.9)$$

These simplifications allow for a much nicer expression of the potential term in the Hamiltonian and make the occurring sums computationally feasible. If we plug equation (3.9) into equation (3.5), we can evaluate the Kronecker delta and remove the sum over all \mathbf{k} -vectors to end up with

$$\begin{aligned} & \frac{1}{2} \sum_{nli,abj} \widehat{Q}_{M,\mu}^i \Phi_{M,\mu,i}^{N,\nu,j} \widehat{Q}_{N,\nu}^j = \\ & \frac{\hbar}{4} \sum_{\mu i, \nu j} \sum_{\mathbf{q}, \lambda, \rho} \frac{1}{\sqrt{\omega_{\mathbf{q},\lambda} \omega_{-\mathbf{q},\rho}}} A_{\mathbf{q},\lambda} A_{-\mathbf{q},\rho} \epsilon_{\mathbf{q},\lambda}^{\mu,i} \epsilon_{-\mathbf{q},\rho}^{\nu,j} \underbrace{\frac{1}{\sqrt{M_\mu M_\nu}} \sum_N \Phi_{0,\mu,i}^{N,\nu,j} e^{iq(\mathbf{R}_{0,\mu}^{(0)} - \mathbf{R}_{N,\nu}^{(0)})}}_{:= D_{\mathbf{q}}^{\mu\nu,ij}}. \end{aligned} \quad (3.10)$$

The underbraced quantity in this equation is known as the dynamical matrix $D_{\mathbf{q}}^{\mu\nu,ij}$ which is supposed to be diagonalized by the polarization vectors ϵ . Exchanging $\mu \leftrightarrow \nu$ and $i \leftrightarrow j$ and taking the complex conjugate we end up with the same matrix, which proves the hermiticity of $D_{\mathbf{q}}^{\mu\nu,ij}$

$$D_{\mathbf{q}}^{\mu\nu,ij} = D_{-\mathbf{q}}^{\nu\mu,ji} = \left(D_{\mathbf{q}}^{\mu\nu,ij} \right)^\dagger. \quad (3.11)$$

The real eigenvalues of the dynamical matrix are the angular frequencies $\omega_{\mathbf{q},\lambda}^2$ and the eigenvectors of different eigenvalues are orthogonal and span the entire space, mathematically speaking

$$\sum_{\mu i} \left(\epsilon_{\mathbf{q},\lambda}^{\mu,i} \right)^* \epsilon_{\mathbf{q},\rho}^{\mu,i} = \delta_{\rho,\lambda} \quad \textit{orthonormality} \quad (3.12)$$

$$\sum_{\lambda} \left(\epsilon_{\mathbf{q},\lambda}^{\mu,i} \right)^* \epsilon_{\mathbf{q},\lambda}^{\nu,j} = \delta_{\mu,\nu} \delta_{i,j} \quad \textit{completeness} \quad (3.13)$$

Additionally we may take the complex conjugate eigenvalue equation

$$\sum_{\mu i} D_{\mathbf{q}}^{\mu\nu,ij} \epsilon_{\mathbf{q},\rho}^{\mu,i} = \omega_{\mathbf{q},\lambda}^2 \epsilon_{\mathbf{q},\rho}^{\nu,j} \quad \textit{take the complex conjugate}^* \quad (3.14)$$

$$\Rightarrow \sum_{\mu i} D_{-\mathbf{q}}^{\mu\nu,ij} \left(\epsilon_{\mathbf{q},\rho}^{\mu,i} \right)^* = \omega_{\mathbf{q},\lambda}^2 \left(\epsilon_{\mathbf{q},\rho}^{\nu,j} \right)^* \quad (3.15)$$

$$\sum_{\mu i} D_{-\mathbf{q}}^{\mu\nu,ij} \epsilon_{-\mathbf{q},\rho}^{\mu,i} = \omega_{-\mathbf{q},\lambda}^2 \epsilon_{-\mathbf{q},\rho}^{\nu,j} \quad \textit{and compare it with the eigenvalue equation for } -\mathbf{q} \quad (3.16)$$

$$\Rightarrow \left(\epsilon_{\mathbf{q},\rho}^{\mu,i} \right)^* = \epsilon_{-\mathbf{q},\rho}^{\mu,i} \text{ and } \omega_{\mathbf{q},\lambda}^2 = \omega_{-\mathbf{q},\lambda}^2 \quad (3.17)$$

These properties guarantee that $\widehat{\mathbf{Q}}_{M,\mu}$ and $\widehat{\mathbf{P}}_{M,\mu}$ in equations (3.3) and (3.4) are hermitian and fulfill the fundamental canonic commutation relation

$$\left[\widehat{\mathbf{P}}_{M,\mu}, \widehat{\mathbf{Q}}_{M,\mu} \right] = -i\hbar \quad (3.18)$$

and allow for a drastic simplification of equation (3.10)

$$\frac{1}{2} \sum_{nli,abj} \widehat{Q}_{M,\mu}^i \Phi_{M,\mu,i}^{N,\nu,j} \widehat{Q}_{N,\nu}^j = \quad (3.19)$$

$$= \frac{\hbar}{4} \sum_{q,\lambda,\rho} \frac{1}{\sqrt{\omega_{q,\lambda}\omega_{-q,\rho}}} A_{q,\lambda} A_{-q,\rho} \underbrace{\sum_{\mu i,\nu j} \epsilon_{-q,\rho}^{\nu,j} D_{\mathbf{q}}^{\mu\nu,ij} \epsilon_{q,\lambda}^{\mu,i}}_{=\delta_{\lambda,\rho}\omega_{q,\lambda}^2} = \frac{\hbar}{4} \sum_{q,\lambda} \omega_{q,\lambda} A_{q,\lambda} A_{-q,\lambda} \quad (3.20)$$

which could not look any nicer. To diagonalize the Hamiltonian, we have to consider the kinetic energy term

$$\sum_{M,\mu} \frac{\widehat{P}_{M,\mu}^2}{2M_{\mu}} = \quad \begin{array}{l} \text{first we insert the second quantized form} \\ \text{of } \widehat{P}_{M,\mu}^2 \text{ (see equation (3.4)) with} \\ B_{q,\lambda} := -i\widehat{a}_{q,\lambda} + i\widehat{a}_{-q,\lambda}^\dagger \end{array} \quad (3.21)$$

$$= \sum_{M,\mu} \frac{\hbar}{4N_u} \sum_{q,\lambda} \sqrt{\omega_{q,\lambda}\omega_{k,\rho}} B_{q,\lambda} B_{k,\rho} \epsilon_{q,\lambda}^{\mu} \epsilon_{k,\rho}^{\mu} e^{i\mathbf{R}_{M,\mu}^{(0)}(\mathbf{q}+\mathbf{k})} \quad (3.21)$$

$$= \frac{\hbar}{4} \sum_{q,\lambda} \sqrt{\omega_{q,\lambda}\omega_{k,\rho}} B_{q,\lambda} B_{k,\rho} \sum_{\mu} \epsilon_{q,\lambda}^{\mu} \epsilon_{k,\rho}^{\mu} e^{i\mathbf{R}_{\mu}^{(0)}(\mathbf{q}+\mathbf{k})} \underbrace{\frac{1}{N_u} \sum_M e^{i\mathbf{R}_M^{(0)}(\mathbf{q}+\mathbf{k})}}_{=\delta_{q,-k}} \quad (3.22)$$

$$= \frac{\hbar}{4} \sum_{q,\lambda,\rho} \sqrt{\omega_{q,\lambda}\omega_{-q,\rho}} B_{q,\lambda} B_{-q,\rho} \underbrace{\sum_{\mu} \epsilon_{q,\lambda}^{\mu} \epsilon_{-q,\rho}^{\mu}}_{=\delta_{\rho,\lambda}} \quad (3.23)$$

$$= \frac{\hbar}{4} \sum_{q,\lambda} \omega_{q,\lambda} B_{q,\lambda} B_{-q,\lambda}. \quad (3.24)$$

Adding up the kinetic and the potential energy we obtain the diagonalized form of the phonon Hamiltonian in the harmonic approximation

$$\widehat{\mathcal{H}} = \sum_{q,\lambda} \frac{\hbar\omega_{q,\lambda}}{4} A_{q,\lambda} A_{-q,\lambda} + B_{q,\lambda} B_{-q,\lambda} \quad (3.25)$$

$$= \sum_{q,\lambda} \frac{\hbar\omega_{q,\lambda}}{4} \left(\widehat{a}_{q,\lambda} + \widehat{a}_{-q,\lambda}^\dagger \right) \left(\widehat{a}_{-q,\lambda} + \widehat{a}_{q,\lambda}^\dagger \right) + \left(-i\widehat{a}_{q,\lambda} + i\widehat{a}_{-q,\lambda}^\dagger \right) \left(-i\widehat{a}_{-q,\lambda} + i\widehat{a}_{q,\lambda}^\dagger \right) \quad (3.26)$$

$$= \sum_{q,\lambda} \frac{\hbar\omega_{q,\lambda}}{4} \left(\widehat{a}_{q,\lambda} \widehat{a}_{q,\lambda}^\dagger + \widehat{a}_{-q,\lambda}^\dagger \widehat{a}_{-q,\lambda} \right) \cdot 2 \quad \begin{array}{l} \text{use the commutation relation} \\ \left[\widehat{a}_{q,\lambda}, \widehat{a}_{q,\lambda}^\dagger \right] = 1 \text{ and the fact that} \\ \text{we sum over all } \mathbf{q} \end{array} \quad (3.27)$$

$$= \sum_{q,\lambda} \hbar\omega_{q,\lambda} \left(\widehat{a}_{q,\lambda}^\dagger \widehat{a}_{q,\lambda} + \frac{1}{2} \right) \quad (3.28)$$

Thus, our Ansatz was suitable to diagonalize the Hamiltonian. All that has to be calculated in practice is the dynamical Matrix $D_{\mathbf{q}}^{\mu\nu,ij}$, which has to be diagonalized in order to obtain the polarization vectors. If we get those, we can calculate the dispersion relation, the phononic density of states and the displacements of all the modes of interest.

3.2 Calculating the phonon dispersion

Now we are in the situation where we can model the phonons completely, given the dynamical matrix of the system of interest. In our case we will deal with the pure diamond structure for illustrational purposes since this structure is the host for the NV^- center. In this section we will follow two different approaches to calculate the dynamical matrix: The first will be the small displacement method, where we calculate the equilibrium position of the ions and then displace some by a small amount, s.t. the $\mathcal{O}(Q^3)$ contribution to equation (3.1) is negligible. Of course the number of necessary displacements may be diminished by applying symmetry considerations. The necessary displacements are obtained by the PHONOPY program, the forces are calculated with VASP. With the calculated forces, PHONOPY sets up the dynamical matrix and performs the diagonalization thereof.

3.2.1 Diamond phonons

Diamond is a possible form in which carbon can crystallize. The diamond structure consists of a face centered cubic structure with a basis of two carbon atoms, which are separated by the vector $(\frac{1}{4}, \frac{1}{4}, \frac{1}{4})$ and thus has the space group symmetry $Fd\bar{3}m$ (227). The primitive and the conventional cells are shown in Figure 2.3. Since the atomic positions are completely determined by the symmetry, no relaxation has to be performed to obtain the equilibrium positions of the atoms. The only parameter to be determined is the equilibrium lattice constant, whose experimental value is 3.567 Å at room temperature. The calculated values for 4 different functionals are depicted in Figure 3.2 and we see that we achieve a very close agreement with the experimental value. With the equilibrium configuration in our hand, we can displace the atoms by a very small amount to stay in a regime where the harmonic approximation is valid in order to extract the dynamical matrix of the system. The calculations are performed for the primitive cell and since the cell is periodically continued, we can not simulate the force on the second next neighboring atom properly with just 2 atoms in the cell. To circumvent this problem, supercells have to

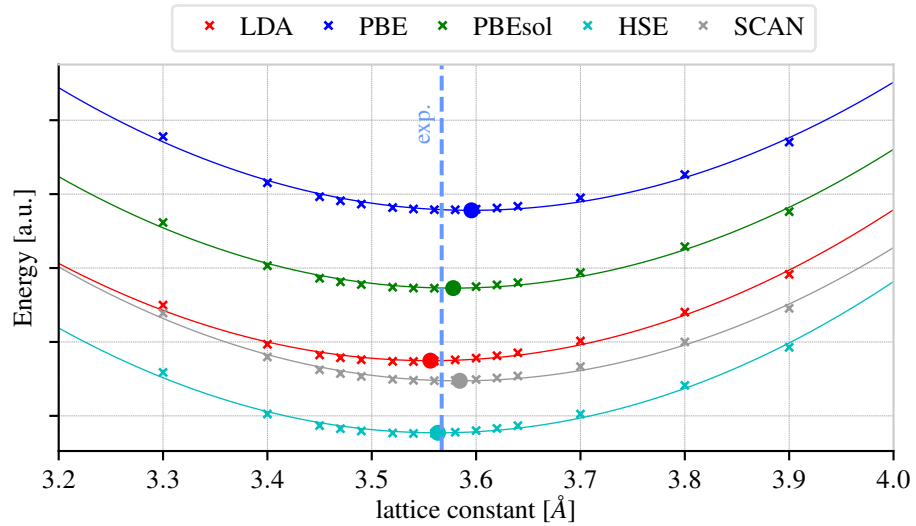


Figure 3.2: **Determining the lattice constant** The energy dependence of the lattice constant is shown in this Figure for 4 different functionals. Since we are close to the minimum, a first order Taylor-expansion of the forces around the minimum position is a reasonable fit. The fitted parabolas resulting from Hooke's law match the calculated values very well. With the fitted parabolas, we determine the value of the minimal energy for each functional. We see that the HSE06-functional gets closest to the experimental value, which is shown as the dashed line.

be used with a size as big as making the forces between the farthest separated atoms negligible. In the present case, due to symmetry, a general displacement of one atom is sufficient to obtain all entries of the dynamical matrix. We calculate the forces on the atoms using VASP and diagonalize the dynamical matrix, to obtain the dispersion relation for the phonons. Counting the number of possible states for a given energy allows to plot the density of states, which describes how many vibrational states are available in a given energy interval. The density of states (DOS) is normalized to contain all possible vibrations, $3N_a$ in number, since each of the N_a atoms has 3 degrees of freedom. For the diagonalization of the dynamical matrix the program PHONOPY is used. To extract the physics of the system, a convergence study with respect to the supercell size has to be performed. This will also give important insight on the decay of forces in the diamond system, since convergence will be obtained, if the forces acting on atoms, which are separated by a certain distance from the displaced atoms, are negligible. This distance will also be of importance in the case of the NV^- center and the investigations thereof are depicted in Figure 3.3. It turns out that the forces decay very fast with increasing distance in a diamond lattice due to very strong bonds (which corresponds to very stiff springs). Atoms, which are separated by more than 4.4 \AA exhibit forces of less

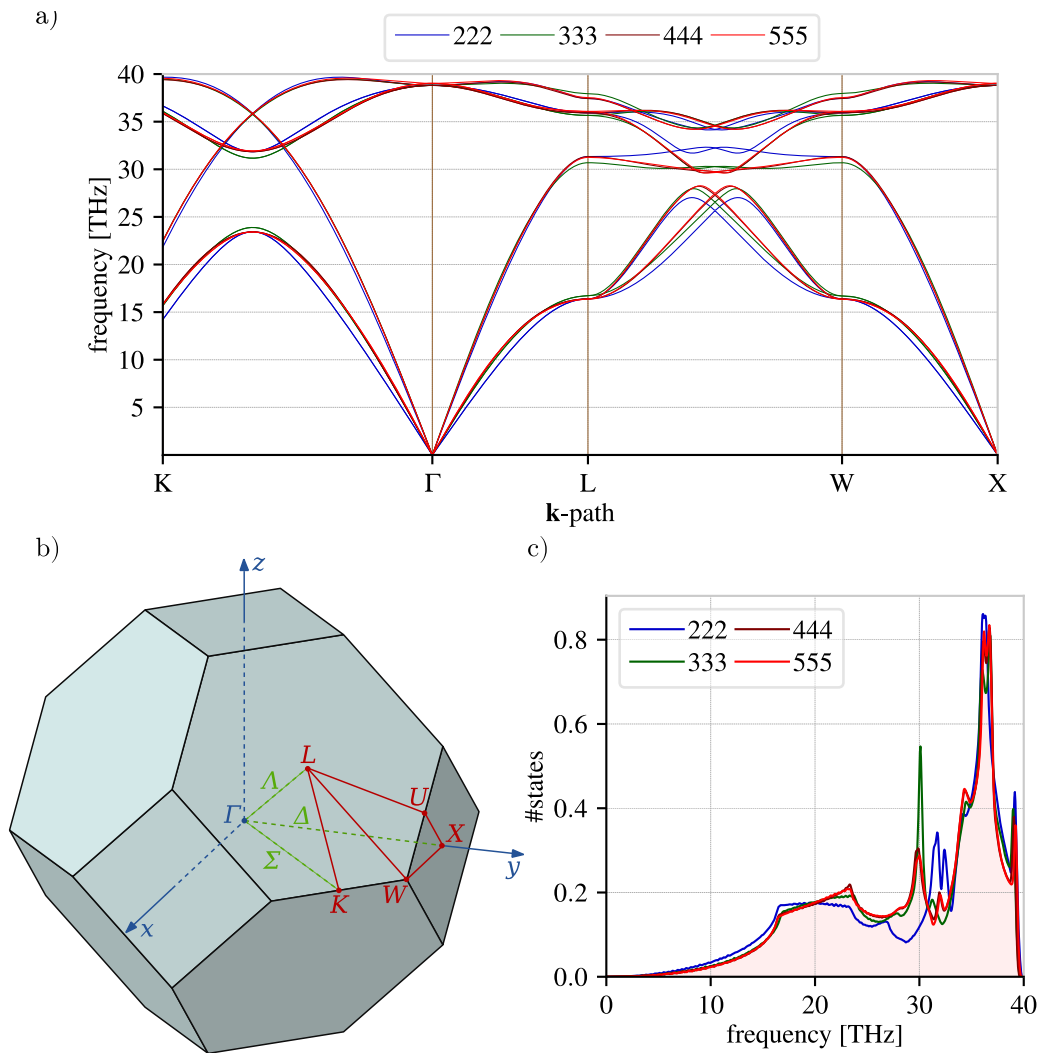


Figure 3.3: **Band and DOS convergence** a) Here we see the bandstructure of the phonons in the diamond lattice dependent on the size of the calculated supercell. The eigenvalues along high symmetry paths were calculated for different sizes of the simulated supercells. As we see in this plot, the bandstructure is converged, if a $4 \times 4 \times 4$ supercell is chosen, since there is nearly no difference between the $4 \times 4 \times 4$ (brown line) and the $5 \times 5 \times 5$ (red line) supercells. The $4 \times 4 \times 4$ supercell includes 128 atoms and this guarantees negligible forces on atoms which are several \AA separated from the displaced atom (less than $10^{-5} \text{ meV \AA}^{-1}$). b) The 1st Brillouin zone of the primitive unit cell is shown and provides the high symmetry points for the path in Figure a). c) The calculated density of states is shown in this plot. As the bandstructure of the $4 \times 4 \times 4$ cell was converged, so is of course the DOS, since it depicts a projection of the eigenvalues on the energy scale.

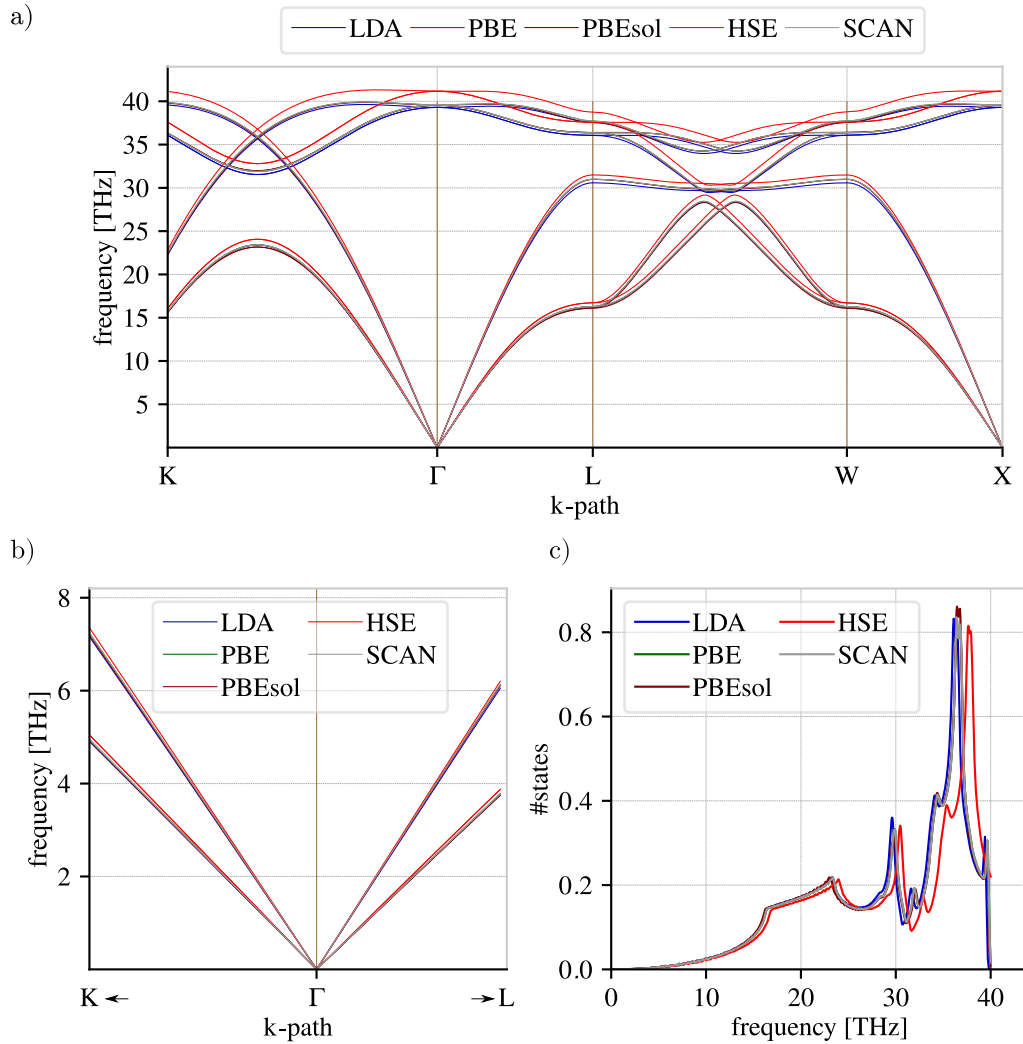


Figure 3.4: **Functional dependence of Bands and DOS** a) The dependence of the bandstructure on the functional. b) Since the long wavelength phonons will play an important role in this work, we see a zoom on the Γ point and can extract, that the dependence on the functional for these phonons is negligible. c) The resulting DOS for different functionals.

than 1 meV \AA^{-1} .

Of course the resulting properties are dependent on the exchange-correlation functional in use and therefore this dependence is also investigated in Figure 3.4. The eigenvectors of the dynamical matrix are also given as an output of the PHONOPY calculation and will play a crucial role in the calculation of the spin-lattice relaxation time T_1 . The behaviour of the eigenvectors along a non-symmetry line² starting from Γ is shown in Figure 3.5, where we see, that the polarizations do not change for a wide range of frequencies.

²The plot of the polarization vectors along a symmetry line would result in a random number output due to the fact that any superposition of two degenerate eigenvectors will also yield an eigenvector of the dynamical matrix.

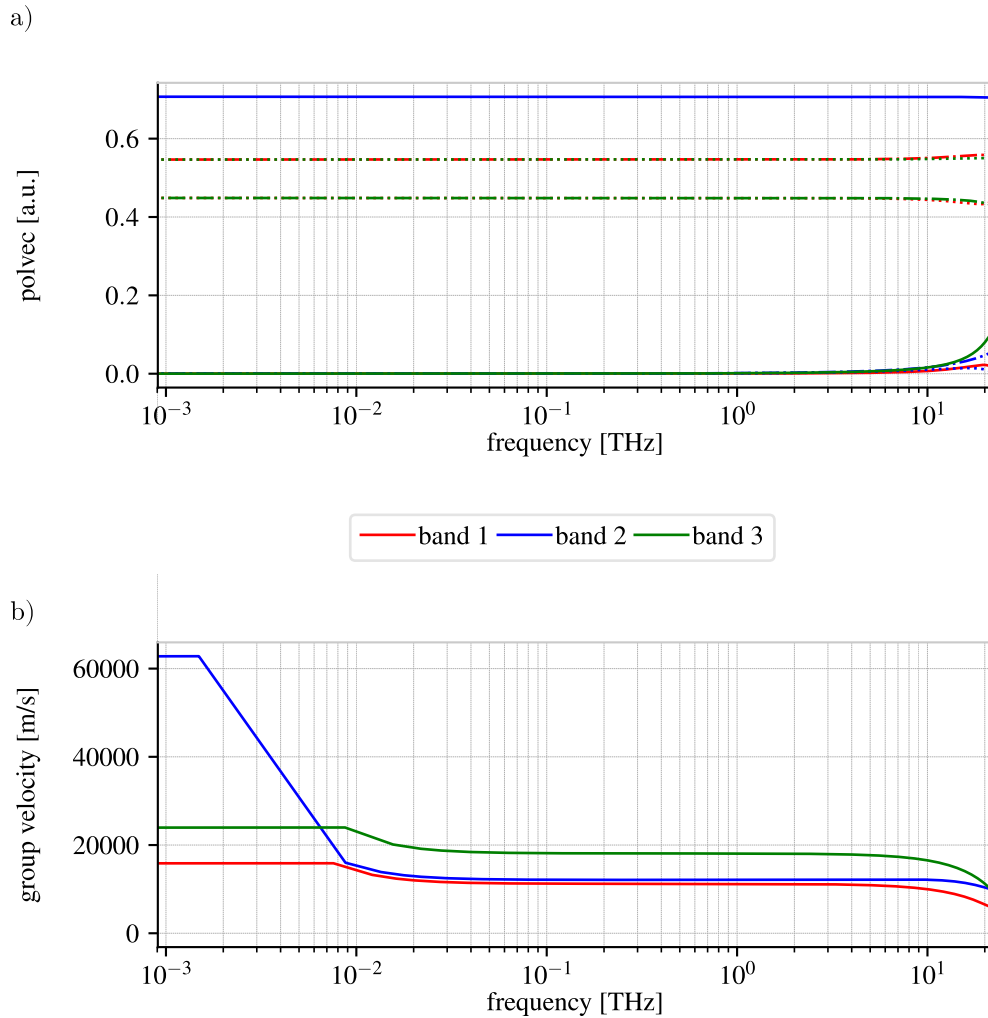


Figure 3.5: **Diamond phonons** a) the absolute values of the x - (solid), y - (dotted) and z - (dashed-dotted) components of the polarization vectors along a non-symmetry line starting from Γ . It is evident, that the polarization vectors are constant for a wide range of frequencies. b) The calculated group velocity along the same line. We find that it approaches zero at the Brillouin-zone boundary (not exactly shown) and that we get unphysically high group velocities at low frequencies.

Now that we are familiar with the treatment of electrons and phonons, we are able to couple these particles in the next chapter in order to arrive at an expression for the spin-lattice relaxation rate Γ .

References

- Togo, A. and I. Tanaka (2015). “First principles phonon calculations in materials science”. In: *Scr. Mater.* 108, pp. 1–5.
- Wallace, D. (1998). *Thermodynamics of crystals*. Mineola, N.Y: Dover Publications.

Chapter 4

Spin-lattice relaxation theory

4.1 Introduction

In the previous Chapters, we introduced how electrons in solids may be modeled and how the dynamics of the ionic lattice may be calculated. In this Chapter, we will merge the descriptions to deal with the interactions between electron spins and the lattice vibrations, in particular we will be concerned with the (longitudinal) relaxation time T_1 of the NV^- center in diamond. T_1 is the time it takes a non-equilibrium spin distribution to decay to its equilibrium state. If the occupation difference between the spins is given by $D = N_\uparrow - N_\downarrow$, T_1 is defined via

$$\frac{dD}{dt} = -\frac{D - D_0}{T_1}, \quad (4.1)$$

where D_0 is the thermal equilibrium value of D . Usually spin polarization is obtained by applying magnetic fields, but due to the level-structure of the NV^- center, the spins may also be polarized without any external magnetic field, only due to the strong intersystem crossing and the preferential decay of the 1A_1 singlet to the $m_s = 0$ ground state. To couple spins with phonons, some position dependent spin-interaction has to be taken into account and the change thereof, induced by phonons, may be responsible for a spin-flip as we will see. This Chapter gives a historical overview and a theoretical introduction to the treatment of T_1 .

4.2 The first investigation on spin-lattice relaxation - Ivar Waller

The first investigation on spin-lattice relaxation was done by Ivar Waller (1932). Waller assumed a paramagnetic crystal, where each atomic site is

occupied by one electron, whose location equals exactly the position of the ion. The interaction, which is responsible for spin-flip s is, according to his model, the dipolar spin-spin interaction between the electrons

$$\mathcal{H}_{ss} = \underbrace{-\frac{\mu_0 g_e^2 \mu_B^2}{4\pi}}_{:-\alpha} \sum_{i,j} \frac{3(\mathbf{r}_{ij} \mathbf{S}_i)(\mathbf{r}_{ij} \mathbf{S}_j) - (\mathbf{S}_i \mathbf{S}_j) r_{ij}^2}{|\mathbf{r}_{ij}|^5}. \quad (4.2)$$

In this formula μ_0, g_e, μ_B denote the vacuum permeability, the g -factor of the electron and the Bohr magneton respectively and the \mathbf{S} and \mathbf{r}_{ij} are the spin vector and the distance vector between two electrons or in the case of Waller's model, between two ions. Coupling between the spins and the phonons is achieved by a Taylor-expansion of \mathcal{H}_{ss} with respect to the ionic positions, where Waller took the linear and quadratic terms into account and got an effective spin-phonon interaction Hamiltonian

$$\mathcal{H}_{s-p} = \sum_i \frac{\partial \mathcal{H}_{ss}}{\partial \mathbf{Q}_i} \mathbf{Q}_i + \frac{1}{2} \sum_{ij} \mathbf{Q}_i \frac{\partial^2 \mathcal{H}_{ss}}{\partial \mathbf{Q}_i \partial \mathbf{Q}_j} \mathbf{Q}_j. \quad (4.3)$$

Since the displacements of the ions are usually very small, a second order Taylor-expansion is sufficient in order to extract the physical relaxation processes. He plugged the resulting \mathcal{H}_{s-p} in Fermis Golden rule and obtained relaxation rates Γ for a spin-flip and a subsequent absorption [emission] of a single phonon¹

$$\Gamma_1 = \frac{5}{2\pi^2 \hbar} \left(\frac{\mu_0 g_e^2 \mu_B^2}{r_{ij}^3} \right)^2 \omega^3 \frac{1}{\rho c^5} (f_{BE}(\omega, T)[+1]), \quad \begin{array}{l} [+1] \text{ for emission} \\ \text{of a phonon} \end{array} \quad (4.4)$$

where ω denotes the transition frequency, ρ is the density of the material, c the speed of sound and f_{BE} is the Bose-Einstein distribution, given by

$$f_{BE}(\omega, T) = \frac{1}{e^{\frac{\hbar\omega}{k_B T}} - 1}. \quad (4.5)$$

with k_B being Boltzmann's constant. In addition to single spin-flip s, Waller also considered second order perturbations, which he used to calculate transitions with $\Delta m_s = 2$. He neglected single spin-flip s induced by second order Raman-processes, which we will treat later. Waller's work was the first attempt on spin-lattice relaxation and the resulting rates are usually many orders of

¹We will denote the single phonon relaxation rates by Γ_1 and higher order processes by the number of phonons involved Γ_n . Single phonon processes are usually referred as *direct* processes and two phonon processes are called *Raman* processes, in analogy to electron photon interactions in optics.

magnitude too small. If we would naively apply this formula to the case of the NV^- center, this would result in a spin-lattice relaxation rate $\Gamma_1 \approx 10^{-6} \text{ s}^{-1}$ for $T \rightarrow 0$. However, there are two assumptions included in the model, which are not fulfilled in the case of the NV^- center:

- the spatial extension of the electronic wavefunction was completely neglected in Waller's model.
- the phonons were modeled by taking displacements for a simple cubic lattice, which has a different symmetry than the NV^- center.

As we will see later, our DFT toolkit allows us to drop these assumptions and calculate relaxation rates for the case of the NV^- center *ab initio*. Before we dive into the details of the computation, we will introduce other spin-lattice relaxation mechanisms.

4.3 Putting spin-orbit coupling in the game - Gorter, Kronig and Van Vleck

In three experimental papers², Gorter investigated the behaviour of T_1 in alums³ and found out that diluted paramagnetic crystals did not show a longer T_1 as would be expected, when the distance of the interacting dipoles is enlarged. He suggested that there is another mechanism responsible for spin-flips, which should be of a more local nature. Fierz (1938) mentioned that the origin of the interaction of spins with elastic waves could stem from internal electric fields of the ions. Kronig (1939) realized that the lattice vibrations change the electric field of the crystal, which influences the orbital motion of the electrons and via spin-orbit coupling also the spin. He carried out a calculation and ended up with an expression for first order processes, which looks quite similar to Waller's expression but shows a stronger dependence on the external magnetic field H , with

$$\Gamma_1 \propto H^4 T \quad . \quad (4.6)$$

He also considered the case analogous to *Raman*-scattering in optics, where the flip of a single spin changes the frequency of a phonon in second order

²Gorter, 1936; Gorter and Brons, 1937; Gorter, Teunissen, and Dijkstra, 1938.

³Wikipedia: "Alums are hydrated double sulfate salts of aluminum with the general formula $XAl(SO_4)_2 \cdot 12H_2O$, where X is a monovalent cation. The term is also used for salts, where aluminum is replaced by another trivalent metal ion." The alums used in Gorter's studies were *Ti*-, *Fe*-, *V*- and *Cr*-alums.

perturbation theory, giving rise to a relaxation rate

$$\Gamma_2 \propto H^2 T^7 \quad . \quad (4.7)$$

The first theoretical calculations to yield the right order of magnitude for relaxation times of chromium alums were carried out by Van Vleck (1940), considering the Hamiltonian

$$\mathcal{H} = \mathcal{H}_0 + \mathcal{H}_L + \mathcal{H}_{SO} + \mathcal{H}_{OL} + \mathcal{H}_{SS}, \quad (4.8)$$

where \mathcal{H}_0 is the crystal field, \mathcal{H}_L the vibrational energy due to phonons, \mathcal{H}_{SO} the spin-orbit interaction, \mathcal{H}_{OL} the interaction of the orbit with the lattice and \mathcal{H}_{SS} the spin-spin interaction, which he considered only in an averaged sense. As his predecessors, he performed a perturbative expansion of the Hamiltonian and treated the temporal perturbation up to first order to arrive at Fermi's Golden rule. The quantum mechanical treatment was then merged with the thermodynamical treatment of the subject by Casimir⁴, who introduced a spin temperature and specific heat and considered the exchange between the spin and phonon bath. Van Vleck's very detailed calculations give temperature and magnetic field dependencies for the direct- and Raman-processes

$$T_1 \propto \frac{H^2 + 0.5K^2}{T(C_1 H^6 + C_2 H^4 K^2 + C_3 K^6)} \quad (4.9)$$

$$T_2 \propto \frac{H^2 + 0.5K^2}{I_8(H^2 + K^2)}, \quad (4.10)$$

with H being the external magnetic field, K the mean square spin-spin field. The C_i s are material constants and

$$I_8 = \int_0^{\theta_D k_B / h} \left[\omega^8 e^{\hbar\omega/k_B T} / (e^{\hbar\omega/k_B T} - 1)^2 \right] d\omega$$

accounts for the scattering phonons and thus the temperature dependence (θ_D is the Debye temperature). For temperatures much smaller than θ_D the upper limit of the integral may be expanded to ∞ , yielding a temperature dependence of $\Gamma_2 \propto T^9$. The numerical evaluation of the prefactors agreed within orders of magnitude with the measured data in the best cases but due to the high exponents, resulting from second order processes, the estimates can only be quite inaccurate. Using the Hamiltonian in equation (4.8) opened the field for numerical calculations in general. In a subsequent paper Van Vleck

⁴Casimir and du Pré, 1938; Casimir, 1939; Casimir, de Haas, and Klerk, 1939b.

(1941) realized that in the low temperature regime, where only direct processes at a single phonon frequency occur, the phonons may obey non-equilibrium statistics: If the heat conductivity of the material is low, the phonon bath will be populated at the transition frequency and the phonons will not transport the energy out of the sample, resulting in longer relaxation times. This process limiting the relaxation rate is referred to as *phonon-bottleneck*.

4.4 Spin relaxation in metals - Overhauser

The next step towards understanding spin relaxation was taken by Overhauser (1953), who considered the spin-relaxation in paramagnetic metals and listed a whole bunch of relaxation mechanisms, which he treated at the level of a free electron gas. In his theory spin relaxation is caused by:

- a) The coupling of the spins to magnetic fields, which are induced by the movement of the ions for the case of transversal polarized phonons.
- b) Spin-orbit interaction, when the crystal field changes due to longitudinal phonons. This process is similar to the one Van Vleck proposed.
- c) The hyperfine interaction of the electron spins with the nuclear spins.
- d) The change in dipolar spin-spin interaction \mathcal{H}_{ss} due to phonons.
- e) The interaction of the electron spin with magnetic fields, induced by electronic currents.
- f) The interaction with impurities.

In his paper, he calculated the relaxation rates, using only first order processes and concluded that the most important relaxation mechanism at room temperature is due to interaction e). Of course, diamond as the host of the NV^- center is an insulator, but the above list of spin interactions still contains some interactions that could be considered for the calculation of the relaxation rate in the NV^- center. Due to the fact, that the amount of ^{13}C in the measured samples is very low, we assume that the hyperfine coupling is negligible and we will try to estimate the relaxation rates due to interactions a), b), d) and f) in this work.

4.5 Elliott and Yafet's theories of spin relaxation

Since the calculations of Van Vleck, spin-orbit coupling was considered to play an important role in the problem of the relaxing spins. In this section, we will see, that the effect of spin-orbit coupling is actually twofold: The first contribution comes from the fact, that the presence of spin-orbit coupling allows the wavefunctions of different spin-states to mix. This provides a scattering channel between two spinors, which was considered by Elliott. The second effect is due to the off-diagonal nature of the spin-orbit interaction in spin-space, which allows for a coupling of pure spin up and spin down states. Relaxation processes due to these contributions are called Yafet processes.

The first examination of spin-lattice relaxation times in semiconductors goes back to Elliott (1954). He used a scattering approach and band-theory to calculate effective g -factors and spin-lattice relaxation times. He pointed out, that in the presence of spin-orbit coupling, the former pure spin states $|\uparrow\rangle$ and $|\downarrow\rangle$ will not be eigenstates of the underlying Hamiltonian, but the spin-orbit perturbed Bloch functions will be in a superposition of spin eigenstates

$$\Psi_{\mathbf{k}} = (a_{\mathbf{k}} |\uparrow\rangle + b_{\mathbf{k}} |\downarrow\rangle) e^{i\mathbf{k}r}. \quad (4.11)$$

According to his theory, every interaction that was diagonal in spin-space may cause a spin-flip. The recipe for the quantification of T_1 is to consider the matrix elements for the pure spin-states

$$\int a_{\mathbf{k}'}^* \mathcal{H}_{int} a_{\mathbf{k}} e^{i(\mathbf{k}-\mathbf{k}')r} d^3r, \quad (4.12)$$

and insert the perturbed Bloch wave function from equation (4.11). The matrix-elements responsible for a spin-flip are now given by

$$\int (a_{\mathbf{k}'}^* \mathcal{H}_{int} b_{\mathbf{k}} + b_{\mathbf{k}'}^* \mathcal{H}_{int} a_{\mathbf{k}}) e^{i(\mathbf{k}-\mathbf{k}')r} d^3r. \quad (4.13)$$

The size of these matrix elements depends on the spin-polarization $c = b_{\mathbf{k}}/a_{\mathbf{k}}$. Since the diagonal matrix elements enter in the calculation of the electron relaxation time T_R for the electrical resistivity, Elliott deduced that the relaxation times should obey

$$T_1 = \frac{T_R}{(g-2)^2}. \quad (4.14)$$

His theory is based on first order processes, where spin-orbit coupling is assumed to be a small perturbation.

The second important contribution was given by Yafet (1963). Starting from the probability per unit time $W_{\downarrow,\uparrow}$ for a spin transition from \uparrow to \downarrow , Equation (4.1) may be rewritten as

$$\frac{dD}{dt} = 2(W_{\downarrow,\uparrow} - W_{\uparrow,\downarrow}). \quad (4.15)$$

In his paper, he used a band structure scattering approach to calculate the transition probabilities via

$$W_{\uparrow,\downarrow} = \frac{1}{(2\pi)^6} \int \int d\mathbf{k} d\mathbf{k}' \times \left\{ n_{\downarrow}(\mathbf{k}) [1 - n_{\uparrow}(\mathbf{k}')] W_{\mathbf{k},\downarrow;\mathbf{k}',\uparrow} - n_{\uparrow}(\mathbf{k}') [1 - n_{\downarrow}(\mathbf{k})] W_{\mathbf{k}',\uparrow;\mathbf{k},\downarrow} \right\}, \quad (4.16)$$

where n denotes the Fermi-Dirac distribution and the $W_{\mathbf{k}',a;\mathbf{k},b}$ are the \mathbf{k} dependent transition probabilities for a spin-flip from state b to state a . He realized that the whole effect of spin-orbit coupling on the relaxation rate is actually the sum of the processes described by Overhauser and Elliott. He considered mechanisms due to the spinor-nature of the wavefunction (Elliott) and the explicit spin-dependent contributions arising from the spin-orbit interaction (Overhauser or Yafet contribution)

$$\mathcal{H}_{e-ph} = \sum_n \int \Psi^\dagger(\mathbf{r}) \left[\mathbf{Q}_n \cdot \frac{\partial \hat{v}_{e-n}(\mathbf{r} - \mathbf{R}_n)}{\partial \mathbf{R}_n} \Big|_{\mathbf{R}_n^{(0)}} \right] \Psi(\mathbf{r}) d^3r \quad (4.17)$$

with

$$\hat{v}_{e-n}(\mathbf{x}) = \hat{v}_{en} + \xi [\nabla \hat{v}_{en} \times \hat{\mathbf{p}}] \cdot \hat{\mathbf{s}} \quad (4.18)$$

consisting of the Coulomb- and spin-orbit energy, with the spin-orbit coupling constant $\xi = \hbar/4m_e^2c^2$. The Elliott contribution is represented in the Coulomb-interaction, for the case of spinor wavefunctions Ψ and the Overhauser contribution arises in the spin-orbit coupling term. The transition probabilities were calculated with Fermi's golden rule

$$W_{\mathbf{k},\downarrow;\mathbf{k}',\uparrow} = \frac{2\pi}{\hbar} \left| \langle \Psi_{\mathbf{k}',\downarrow}, \mathcal{N}_f | \mathcal{H}_{s-ph} | \Psi_{\mathbf{k},\uparrow}, \mathcal{N}_i \rangle \right|^2 \delta(E_f - E_i), \quad (4.19)$$

where $\mathcal{N}_{(f,i)}$ denotes the quantum state of the lattice vibrations. Using the phononic displacements as given in Equation (3.3), Yafet performed a calculation for the rates for the case of small momentum transfers \mathbf{q} and obtained a relaxation rate for semiconductors, dependent on the form of the bandstructure

$$\Gamma_2 \propto T^{7/2} \quad \text{and} \quad \Gamma_2 \propto T^{5/2} \quad . \quad (4.20)$$

4.6 Dyakonov-Perel

Another relaxation mechanism driven by spin-orbit coupling was investigated by D'yakonov and Perel' (1971) in semiconductors without a center of inversion: In this case, the spin splitting in the conduction bands may be interpreted as a magnetic field, which is dependent on the third power of the momentum

$$\hbar\boldsymbol{\Omega} \propto m_c^{-3/2} E_g^{-1/2} \boldsymbol{\kappa} \quad , \quad (4.21)$$

where m_c is the effective mass of the electron in the conduction band, E_g the size of the bandgap and $\boldsymbol{\kappa} = (p_x(p_y^2 - p_z^2), p_y(p_z^2 - p_x^2), p_z(p_x^2 - p_y^2))$ is dependent on the position in \mathbf{k} space. The electrons in the conduction band will therefore precess around the magnetic field $\boldsymbol{\Omega}$, whose direction is given by the quantity $\boldsymbol{\kappa}$. If the electrons scatter, the axis of spin precession may change and therefore the direction of the electron spin is altered. This relaxation mechanism depends crucially on the momentum scattering time τ_p of the electrons. If $|\boldsymbol{\Omega}| \tau_p \gg 1$ the spins have enough time for precession, s.t. the spin perpendicular to \mathbf{k} is changing continuously. If, on the other hand $|\boldsymbol{\Omega}| \tau_p \ll 1$, then the spin axis will change so fast, that the spin relaxation may be suppressed. This relaxation mechanism therefore shows the counterintuitive behaviour: The faster the momentum relaxation, the longer the spin relaxation time.

4.7 The Bir-Aronov-Pikus mechanism - relaxation by hole scattering

The last fundamental mechanism is only mentioned for the sake of completeness: This mechanism is due to an electron-hole scattering with a subsequent spin-flip of the electron. In their paper, Bir, G., and Pikus (1975) considered a contact interaction between electrons and holes in p -doped semiconductors with axial symmetry of the form

$$\mathcal{H} = \pi a_B \hat{D} \delta(\mathbf{r}) \delta_{\mathbf{K}, \mathbf{K}'} \quad , \quad (4.22)$$

where \mathbf{r} is the distance between the electron and the hole, a_B the exciton Bohr radius and \hat{D} is a spin dependent interaction between the electron and the hole, which have a total momentum $\mathbf{K} = \mathbf{k}_e + \mathbf{p}_h$. Bir considered two couplings: The first is similar to Wallers dipole-dipole interaction, which he called the exchange interaction due to the fact that the hole and the electron change their spins in a double spin-flip event. The formula for the interaction is given

by

$$\hat{D} = \Delta_{\parallel} \sigma_z s_z + 2\Delta_{\perp} (\sigma_+ s_- + \sigma_- s_+), \quad (4.23)$$

where Δ_i denotes the coupling strength. The second interaction mediates between different spin states via the spin-mixing of the orbitals due to spin orbit coupling, as in the case of the Elliott mechanism. This annihilation interaction is given by momentum scattering

$$\hat{D}(\mathbf{K}) = \frac{4\pi e^2}{m_e^2 \epsilon_{\infty} E_g^2 \pi a_B^3} \frac{(\hat{\mathbf{p}}\mathbf{K})(\hat{\mathbf{p}}^{\dagger}\mathbf{K})}{\mathbf{K}^2}, \quad (4.24)$$

with e , m_e being the charge and the mass of the electron, ϵ_{∞} the dielectric constant at the exciton excitation frequency, E_g the band gap of the semiconductor and \mathbf{p} the momentum operator. Using these two interactions in Fermi's golden rule, they obtain relaxation times for the cases of heavy holes, light holes and bound holes.

Since the number of holes in the measured diamond samples is negligible, the Bir-Aronov-Pikus spin relaxation mechanism is not considered to be important in this study.

4.8 Higher order processes I: Raman processes

The previous sections put a focus on the history of the investigation on the fundamental coupling mechanisms of the electron spins to the phonons. As we saw, the coupling of spins to the phonons was always established by using a spin- and position dependent Hamiltonian and performing a perturbation in the phononic displacements up to first or second order. In this and the next section we will deal more profoundly with the derivation of temperature dependences of T_1 if a generalized coupling of the form

$$\mathcal{H}_{s-ph} = \sum_{m_1} \cdots \sum_{m_n} g_{m_1 \dots m_n} S^{(+/-/z)} (a_{m_1} + a_{m_1}^{\dagger}) \cdots (a_{m_n} + a_{m_n}^{\dagger}) \quad (4.25)$$

is assumed. The order of the coupling n is arising from the order of the Taylor expansion in the ionic displacements. All the information of the fundamental coupling mechanism is contained in the coupling constants $g_{m_1 \dots m_n}$. Due to the fact that most of the practical applications of NV^- centers should operate at room temperature, higher order processes will be of importance, if spin-lattice relaxation times of NV^- centers should be tailored. For this reason, we will consider this temperature regime more explicitly, where phonons are present and higher order processes are thus more likely and due to the huge phase space

more active than single phonon processes. In order to deal with higher order processes, Fermi's Golden rule has to be replaced by a higher order expansion of the perturbation in the treatment of time dependent perturbation theory. The respective Taylor expansion of the electron-phonon interaction has to be carried out to the order of interest because these processes will interfere. Two-phonon processes are calculated using the transition rate formula up to second order in the perturbation series⁵

$$\Gamma_{f \leftarrow i} = \frac{2\pi}{\hbar^2} \left| V_{fi} + \sum_m \frac{V_{fm} V_{mi}}{(E_i - E_m)} \right|^2 \delta(\omega_f - \omega_i) \quad , \quad (4.26)$$

where we can either expand the interaction to second order and use it as V_{fi} or we use the first order Taylor expansion of the interaction and second order perturbation theory with intermediate states involved. A quantitative treatment of second order processes seems to be very tough because there are a lot of divergences to be circumvented⁶ The reason for that is most probably that a term by term evaluation of the perturbation series produces divergences, which would be canceled by not considered terms. In Green's function theory it is shown rigorously, that the non-connected Green's functions, which contain divergent terms are not to be considered. Since we do not use Green's function theory for the description of the system, we will only give the phenomenological results here.

To arrive at the Raman temperature dependencies that were given in the previous sections of this Chapter, we first consider a second order expansion of the spin-phonon interaction in first order time dependent perturbation theory in subsection 4.8.1 and then a first order interaction expansion in second order perturbation theory in subsection 4.8.2

4.8.1 Raman processes in first order perturbation theory

The starting point for the description of a Raman process in first order perturbation theory is the relaxation rate between a single initial i and final state f :

$$\Gamma_{f \leftarrow i} = \frac{2\pi}{\hbar^2} |V_{fi}|^2 \delta(\omega_f - \omega_i) \quad (4.27)$$

⁵the formula is derived in Appendix C

⁶The diagrams to be calculated within second order time dependent perturbation theory are depicted in Appendix D. There we see the difficulty of a quantitative evaluation of matrix elements.

with

$$V_{fi} \propto \sum_{m_1, m_2} (a^\dagger + a)_{m_1} (a^\dagger + a)_{m_2} \frac{e^{ik_1 \mathbf{R}}}{\sqrt{\omega_1}} \frac{e^{ik_2 \mathbf{R}}}{\sqrt{\omega_2}} . \quad (4.28)$$

As Shrivastava (1983) has pointed out, the exponential factors play an important role in the observed relaxation times:⁷ In tightly bound systems, phonons are excited at high energies, in the THz regime, which means that we are usually investigating the temperature regime, where only long wavelength phonons are excited, s.t. the exponentials may be Taylor-expanded $e^{ik\mathbf{R}} \approx 1 + ik\mathbf{R}$. In addition, he states that for systems with inversion symmetry, the first term gives no contribution. Since the NV^- center lacks inversion symmetry, we have to be careful in the treatment of our system. In our numerical simulations, we will use the full exponential for the actual calculations. For the sake of completeness, we give the temperature dependence arising for conventional systems, where a scattering from state a to b is described:⁸ To extract the relaxation rate, excitations and de-excitations of the spin system have to be considered: If there are two electron levels (a and b) with occupations N_a and N_b , the system follows the equations

$$\begin{aligned} \dot{N}_a &= -\Gamma_{b \leftarrow a} N_a + \Gamma_{a \leftarrow b} N_b \\ \dot{N}_b &= -\dot{N}_a \\ \Rightarrow \dot{N}_b - \dot{N}_a &= -(\Gamma_{b \leftarrow a} + \Gamma_{a \leftarrow b}) ((N_b - N_a) - (N_b - N_a)_{th}) , \end{aligned} \quad (4.29)$$

which give an exponential decay law of population difference towards its thermal equilibrium value $(N_b - N_a)_{th}$, with a relaxation rate $\Gamma = \Gamma_{b \leftarrow a} + \Gamma_{a \leftarrow b}$. The complete rate $\Gamma_{f_e \leftarrow i_e}$ for any given final electronic state f_e is calculated by summing over all intermediate phonon states. For a given final phononic state, only certain combinations inside the absolute value of equation (4.27) will connect the initial to the final state, s.t. the sum inside the absolute value vanishes and a sum over all phonon modes has to be performed outside the absolute value. If the phonons are assumed to be thermally populated, the eigenvalues of the raising and lowering operators give Bose-Einstein distributions (+1 for raising operators). Using an isotropic Debye-model and transforming the sums into integrals, we end up with

$$\Gamma_{f_e \leftarrow i_e} \propto \int_0^{\nu_D} d\nu_1 \int_0^{\nu_D} d\nu_2 \nu_1^2 \nu_2^2 (f_{BE}(\nu_1, T)) (f_{BE}(\nu_2, T) + 1) .$$

⁷The rest of this section follows the treatment of the review paper Shrivastava (1983)

⁸This model will later be revised for the case of a degenerate excited state, when the relaxation rate for the NV^- center is calculated.

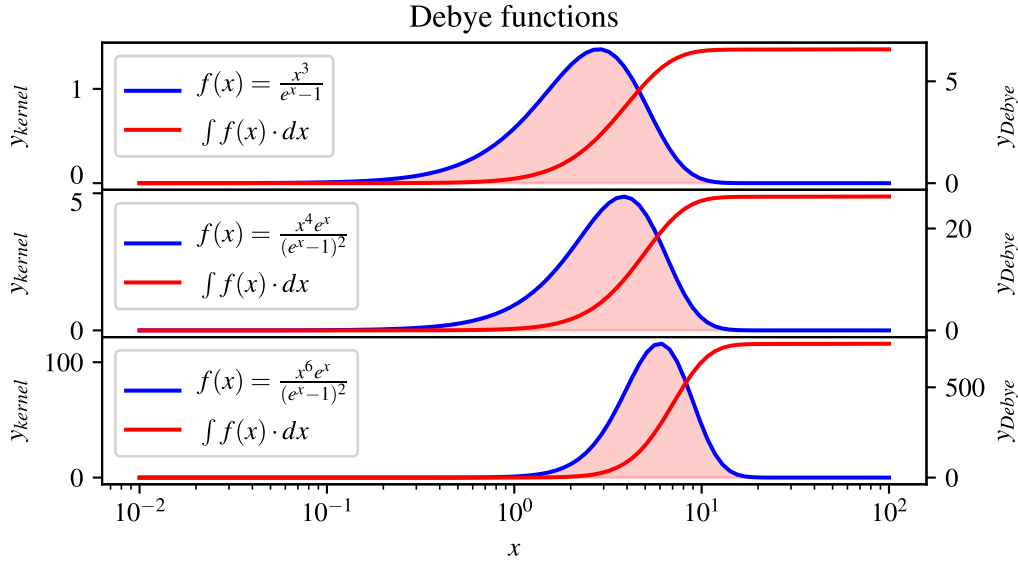


Figure 4.1: **Debye functions**, the kernels and the corresponding integrals are shown. If the upper boundary of the integration is > 20 , the value of the integrals is constant.

$$\begin{aligned}
 & \cdot \frac{\nu_1^2 \nu_2^2}{\nu_1 \nu_2} \delta(\nu_2 - \nu_1 \pm \Delta/h) \\
 & = \int_0^{\nu_D} d\nu_1 \nu_1^3 (\nu_1 \pm \Delta/h)^3 \left(\frac{1}{e^{h\nu_1/k_B T} - 1} \right) \left(\frac{1}{e^{h\nu_1 \pm \Delta/k_B T} - 1} + 1 \right) \quad ,
 \end{aligned} \tag{4.30}$$

where the splitting in the electronic levels is denoted by Δ . This expression is usually analyzed by considering two limiting cases:

a) $\Delta \gg k_B T$

In this case, the terms with Δ dominate and equation (4.30) simplifies to:

$$\Gamma_{f_e \leftarrow i_e} \propto \Delta^3 \left(\frac{k_B T}{h} \right)^4 \int_0^{h\nu_D/k_B T} dx \frac{x^3}{e^x - 1} \quad . \tag{4.31}$$

The reverse process is not accessible in this case because a thermal excitation of the system is excluded due to our assumption. As Figure 4.1 reveals, the integral is independent of temperature, as long as $h\nu_D/k_B T > 20$, s.t. the functional dependence of the transition from the initial to the final electron state is determined by the prefactor. If a Debye frequency of 10 THz is assumed, this approximation is valid up to a temperature of $T \approx 25$ K.

b) $\Delta \ll k_B T$

The other limiting case allows to omit the Δ and equation (4.30) reads

$$\Gamma_{f \leftarrow i e} \propto \int_0^{\nu_D} d\nu_1 \nu_1^6 \frac{e^{h\nu_1/k_B T}}{(e^{h\nu_1/k_B T} - 1)^2} \quad (4.32)$$

$$= \left(\frac{k_B T}{h} \right)^7 \int_0^{h\nu_D/k_B T} dx x^6 \frac{e^x}{(e^x - 1)^2} \quad (4.33)$$

The integral is again independent of temperature for values of $x > 20$ (see Figure 4.1), resulting in a temperature dependence of the relaxation rate $\propto T^7$.

4.8.2 Raman processes in second order perturbation theory

There is a second option for a Raman process, namely to use the first order Taylor expansion and second order time dependent perturbation theory:

$$\Gamma_{f \leftarrow i} = \frac{2\pi}{\hbar^2} \left| \sum_m \frac{V_{fm} V_{mi}}{(E_i - E_m)} \right|^2 \delta(\omega_f - \omega_i) \quad (4.34)$$

with

$$V_{ab} \propto \sum_{m_1} (a^\dagger + a)_{m_1} \frac{e^{i\mathbf{k}_1 \mathbf{R}}}{\sqrt{\omega_1}} \quad (4.35)$$

Starting from these equations, we can calculate the relaxation rate from level i to f via the intermediate level m . In the long wavelength expansion this relaxation rate is given by:

$$\begin{aligned} \Gamma_{f \leftarrow i} &\propto \int \int d\nu_1 d\nu_2 \nu_1^3 \nu_2^3 \frac{f_{BE}(\nu_1, T) f_{BE}(\nu_2, T)}{(\Delta_{im} - h\nu_1)^2} \delta(\Delta_{fi} + h\nu_2 - h\nu_1) \\ &= \int d\nu_1 \nu_1^3 (\nu_1 - \Delta_{fi}/h)^3 \frac{f_{BE}(\nu_1, T) f_{BE}(h\nu_1 - \Delta_{fi}, T)}{(\nu_1 - \Delta_{im}/h)^2} \\ &= \int d\nu_1 \frac{\nu_1^3 (\nu_1 - \Delta_{fi}/h)^3}{(h\nu_1 - \Delta_{im})^2} \frac{1}{e^{h\nu_1/k_B T} - 1} \cdot \frac{e^{h\nu_1 - \Delta_{fi}/k_B T}}{e^{h\nu_1 - \Delta_{fi}/k_B T} - 1} \quad (4.36) \end{aligned}$$

This expression allows for two limiting cases:

a) $\Delta_{mi} \gg h\nu_1$ and $\Delta_{fi} \ll h\nu_1$, results in a relaxation rate

$$\begin{aligned} \Gamma_{f \leftarrow i} &\propto \int d\nu_1 \frac{\nu_1^6}{\Delta_{im}^2} \frac{e^{h\nu_1/k_B T}}{(e^{h\nu_1/k_B T} - 1)^2} \\ &\propto \left(\frac{k_B T}{h} \right)^7 \int_0^{h\nu_D/k_B T} dx x^6 \frac{e^x}{(e^x - 1)^2} \quad (4.37) \end{aligned}$$

which is true for electron excitation and de-excitation, thus yielding $\Gamma_2 = 2\Gamma_{f\leftarrow i}$. In the high temperature limit, where $e^x \approx 1$ and $\frac{1}{e^x - 1} \approx \frac{1}{x}$, expression (4.37) gives

$$\Gamma_{f\leftarrow i} \propto T^2 \int d\nu_1 \nu_1^4 \quad . \quad (4.38)$$

b) $\Delta_{fi} \ll h\nu_1$, $\Delta_{mi} \ll h\nu_1$, this limiting case leads to

$$\begin{aligned} \Gamma_{f\leftarrow i} &\propto \int d\nu_1 \frac{\nu_1^4 e^{h\nu_1/k_B T}}{(e^{h\nu_1/k_B T} - 1)^2} \\ &\propto T^4 \int_0^{h\nu_D/k_B T} dx \frac{x^4 e^x}{(e^x - 1)^2} \quad . \end{aligned} \quad (4.39)$$

As Figure 4.1 reveals, the T^4 dependence is given, if the temperature fulfills $T > h\nu_D/20k_B$.

Thus, we see that Raman processes usually give polynomial dependencies of the relaxation rate on temperature, if the limiting cases are considered.

4.9 Higher order processes II: Localized phonons - the Orbach process

One special type of temperature dependence occurs, if there is one dominant intermediate level, which may also be of phononic nature. In this case, the denominator in equation (4.36) vanishes. As Orbach (1961) has noticed, the divergence of the expression may counterbalance the absence of the responsible modes in the density of states or the little thermal population of the modes. Orbach considered the case, where the resonance frequency is the most prominent contribution to the integral, and approximates the integral by this main contribution. He removes the divergence with the argument that the excited state has a finite lifetime and introduces a self-energy correction Γ_m in the denominator, which he approximates by the first order transition from the intermediate state to one of the lower states i or f . Phenomenologically, this means that the frequencies in equation (4.36) are to be replaced by the resonance frequency Δ_{im}/h and the relaxation rate turns out to be

$$\Gamma \propto \left(e^{\Delta_{im}/k_B T} - 1 \right)^{-1} \quad . \quad (4.40)$$

Therefore, the measurement of the temperature dependence of the relaxation rate allows to extract information about the excited states of the system. In

the case of the NV^- center, we will see that the localized phonon states play a crucial role in spin-lattice relaxation.

4.10 The phonon-bottleneck

The last historic mechanism to be described is about the statistics of the system. In all the previous derivations, there was the assumption that the phonons are thermalized and their occupations obey the Bose-Einstein distribution. However, as Van Vleck (1941) pointed out, the phonons which are resonant with a spin transition may be too few to carry away the heat and therefore the spin temperature is different from the surrounding. If the phonons exchange the heat via an interaction with a surrounding helium bath or via a phonon-phonon scattering event fast enough, the bottleneck will not be seen in a measurement. However, if the phonons are taking part in many further spin-flip events, the phonon distribution will be altered, similar to lasing and we end up with a non-thermal phonon distribution. In the case of the NV^- center in diamond, the velocity of the phonons is very high ($\approx 12 \times 10^3 \text{ m s}^{-1}$ transversal and $\approx 20 \times 10^3 \text{ m s}^{-1}$ for longitudinal phonons) and thus the thermal conductivity of the crystal may be sufficient to carry away the energy. In addition, the samples are rich in nitrogen, which provides an additional center for phonon scattering and may allow for a thermalization of the phonon distribution. Due to these considerations, we do not expect the bottleneck process to be important in our treatment of T_1 .

4.11 Measurements of T_1 in the NV^- center

The subject of this thesis is to understand the measured spin-lattice relaxation rate Γ at temperatures, which correspond to the spin-transition frequency. In order to measure Γ at these temperatures, the sample is to be probed without excitations of phonons which would significantly alter the local temperature. Before we deal with the difficulty of the avoidance of additional phonons, we consider a temperature regime, where there are many phonons and the fluctuation does not play a crucial role.

4.11.1 Elevated temperature measurements

A convenient method to measure T_1 in the NV^- center was applied by Jarmola et al. (2012) using laser irradiation and microwave pulses. As already mentioned, there is the possibility to obtain a spin-polarization into the $m_s = 0$

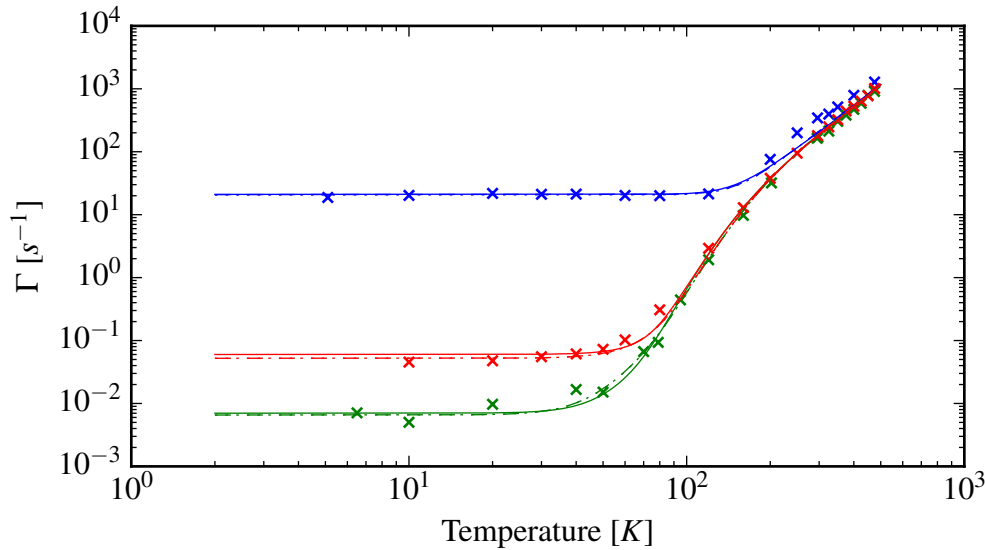


Figure 4.2: **Elevated temperature T_1 measurements for the NV^- center for 3 different samples**, the crosses denote the measured data, the solid line is the plot from Jarmola et al., 2012, and the dashed-dotted line is a fit with a variable exponent for the Raman-processes with T^n , yielding a value of $n = 4.7$.

level of the 3A_2 ground state due to the strong intersystem-crossing. The excitation of the center in the vibronic bands of the 3E levels ensures the presence of many phonons and therefore enhances the intersystem-crossing rates, and after some time of irradiation, the spins end up in the $m_s = 0$ ground state. A subsequent microwave π -pulse creates an excited spin ensemble and after a time τ , the population of the spin-ensemble may be read out by taking a look at the fluorescence of the sample, if the spins are excited into the 3E levels. With this protocol T_1 was measured for temperatures between 2 K and 500 K, where the relaxation rates were well described by Raman and Orbach processes. The results of the experiment are shown in Figure 4.2 and the authors refer to Walker (1968), who calculated the spin-lattice relaxation rates for non-Kramers systems, when there is a big separation between the ground state multiplet and the excited states. This situation is present in the case of the NV^- center. However, there are a number of polynomial temperature dependencies for Raman-processes and our fits showed, that there may as well be a T^7 contribution process participating in the relaxation. A proper quantification of the second order processes is very demanding and beyond the scope of our current *ab initio* approach, where we only consider a single phonon energy to participate in the process. Due to the limited number of phonon modes we that can be considered, we are more interested in the temperature dependence in the low temperature regime, which corresponds to the spin-transition

frequency.

4.11.2 Low temperature measurements

Low temperature measurements were performed at the Technical University of Vienna by the group of Jörg Schmiedmayr using a cavity quantum electrodynamics protocol: If a diamond sample containing an ensemble of NV^- centers is put into a cavity, the interaction of spins with photons allows to extract knowledge about the spin state of the ensemble: In Astner et al. (2018) the interaction of a spin-ensemble with the electromagnetic field inside a cavity is described by a Tavis-Cummings Hamiltonian adjusted to contain the interaction of the cavity photons with the probe field

$$\mathcal{H}/\hbar = \underbrace{\omega_c a^\dagger a + \omega_s S_z^2 + ig_N(a^\dagger S^- - aS^+)}_{\mathcal{H}_{TC}} + \underbrace{i(\eta a^\dagger e^{-i\omega_p t} - \eta^* a e^{i\omega_p t})}_{H_p}, \quad (4.41)$$

where ω_c is the resonance frequency of the cavity, ω_s the spin transition frequency, g_N the total coupling of the spins with the phonons and ω_p the frequency of the probe field. Using this Hamiltonian, the response of the cavity due to the presence of the spins and the probe field, which consists of a shift χ of the resonator eigenfrequency may be calculated as

$$\chi = \frac{Ng_0^2}{(\omega_c - \omega_s)}(2 - 3\langle S_z^2 \rangle), \quad (4.42)$$

where g_0 is the single spin coupling strength. Knowing the dependence of the cavity shift on the state of spins in the sample allows to monitor the spin state by means of photons. The measurement cycle is the following: The spin ensemble in this experiment is initialized by heating the sample until the $m_s \pm 1$ levels are populated significantly. Since the spin-lattice relaxation time in the measured temperature regime turns out to be very long, subsequent cooling of the sample may happen without the loss of the excited spins, which allows to create a non-equilibrium spin-ensemble at the target temperature. Taking a look at the resonance frequency allows to deduce the spin state of the ensemble via equation (4.42) and therefore to monitor the spin-relaxation of the ensemble. The procedure to measure the spin state, without the need of an optical excitation of the spins allows for an excellent temperature control during the measurement cycle, because no non-thermal energy has to be absorbed in the sample. The results of the measurements will be shown after a theoretical detour in the next section in Figure 4.4.

4.12 Spin-lattice relaxation in the Nitrogen-Vacancy center

In this thesis, we will consider two processes, which seem to be appropriate for the case of the NV^- -center. Since the effect of spin-orbit coupling in the ground state is of second order (Lenef and Rand (1996)), the ordering of the m_s sublevels is governed by the effect of spin-spin relaxation. In addition the present elements have a low charge Z , resulting in a small spin-orbit coupling. These considerations suggest to investigate on a spin-lattice relaxation caused by the dipolar spin-spin interaction as Waller suggested. A derivation of a formula for the relaxation rate, which is feasible to solve numerically will be presented in the first subsection. The second types of processes we can deal with numerically are the Elliott-Yafet processes, which we present in the second subsection. In both approaches we assume low density samples, where the interaction between two NV^- -centers is neglected. The states of the NV^- -center are therefore localized in space, resulting in flat dispersion relations.

4.12.1 Waller's process revised

In accordance to Waller's theory, we start with Equation (4.2). As shown in Figure 4.3, the levelstructure in the ground state triplet is determined by the dipolar spin-spin interaction. In this section, we will derive, how the change of this interaction allows for spin-flip transitions between the $m_s = \pm 1$ and $m_s = 0$ states. Since \mathcal{H}_{ss} is only dependent on the positions of the electrons,

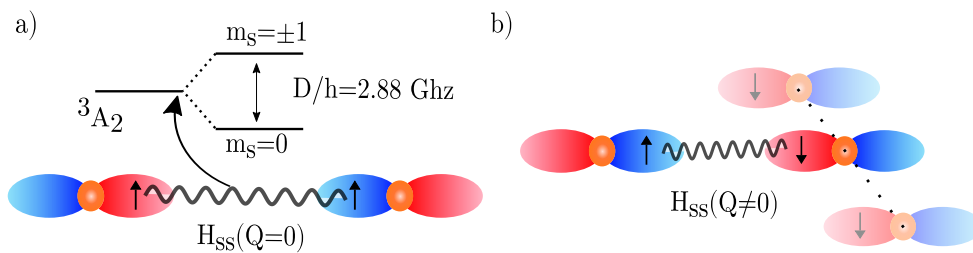


Figure 4.3: **Waller's relaxation mechanism**, a) The diagonal matrix elements of the spin-spin interaction are responsible for the zero field splitting in the NV^- center. b) If the ions start to move, we have a different spin-spin interaction between the electron spins, which allows for a spin-flip transition.

their response to the ionic motion has to be modeled to obtain electron-phonon coupling. In the temperature regime of mK the ionic displacements are very small and hence the electronic orbitals will follow the movement of the ions rigidly within a certain region around the ions. Modeling this region correctly

is crucial for the calculation of the spin lattice relaxation time T_1 and to make this theory predictable, the influence on the choice of this region has to be investigated. In this thesis two approaches for modeling this region around the n -th ion Ω_n are taken: The Wigner-Seitz cell and zero-flux surfaces of the charge density obtained by a Bader analysis. The distance vector between two electrons will behave under the displacement of the n -th ion as

$$\begin{aligned}
\mathbf{r}_{ij}(\mathbf{Q}^n) &= \mathbf{r}_{ij}(\mathbf{Q}^n = 0) + \mathbf{Q}^n \Theta(\mathbf{r}_i \in \Omega_n) - && \Omega_n \text{ is the region around the } n\text{-th} \\
& - \mathbf{Q}^n \Theta(\mathbf{r}_j \in \Omega_n) && \text{ion in which the orbitals follow} \\
& = \mathbf{r}_{ij}(\mathbf{Q}^n = 0) + \mathbf{Q}^n \Delta\Theta_{ij}^n && \Delta\Theta_{ij}^n := \Theta(\mathbf{r}_i \in \Omega_n) - \\
& \rightarrow \mathbf{r}_{ij}(\mathbf{Q}^{\{n\}}) = \mathbf{r}_{ij}(\mathbf{Q}^n = 0) + \sum_n \mathbf{Q}^n \Delta\Theta_{ij}^n && \Theta(\mathbf{r}_j \in \Omega_n) \\
& && \cdot \text{ Summation over all ions gives} \\
& && \text{the total distance vector}
\end{aligned} \tag{4.43}$$

Here Θ is a Heaviside function, whose value is 1, if the position vector of the electron \mathbf{r} is inside the volume Ω_n and 0 otherwise. The coupling between the ionic motion and the change in the potential energy between the dipoles is most easily described by a Taylor expansion of the Hamiltonian \mathcal{H}_{ss} with respect to the ionic displacements $\mathbf{Q}^{\{m\}}$ from the equilibrium position. Due to the small displacement amplitudes of the ions from their equilibrium positions at low temperatures, it is sufficient to expand the magnetic dipole-dipole interaction to first order in the ionic displacements. The summation over all ions gives the resulting spin-phonon interaction

$$\begin{aligned}
\mathcal{H}_{sp}(\mathbf{Q}) &= \sum_m \mathbf{Q}^m \frac{\partial \mathcal{H}_{ss}}{\partial \mathbf{Q}^m} \\
&= \alpha \sum_m \mathbf{Q}^m \left(\frac{3((\mathbf{S}_i \cdot (\partial \mathbf{r}_{ij} / \partial \mathbf{Q}^m)))(\mathbf{S}_j \cdot \mathbf{r}_{ij}) + (\mathbf{S}_i \cdot \mathbf{r}_{ij})(\mathbf{S}_j \cdot \partial \mathbf{r}_{ij} / \partial \mathbf{Q}^m)}{|\mathbf{r}_{ij}|^5} \right. \\
& \quad \left. - \frac{15(\mathbf{S}_i \cdot \mathbf{r}_{ij})(\mathbf{S}_j \cdot \mathbf{r}_{ij})}{|\mathbf{r}_{ij}|^7} \mathbf{r}_{ij} (\partial \mathbf{r}_{ij} / \partial \mathbf{Q}^m) + \frac{3(\mathbf{S}_i \cdot \mathbf{S}_j)}{|\mathbf{r}_{ij}|^5} \mathbf{r}_{ij} (\partial \mathbf{r}_{ij} / \partial \mathbf{Q}^m) \right) \\
& \quad \boxed{\mathbf{Q}^m \partial \mathbf{r}_{ij} / \partial \mathbf{Q}^m = \mathbf{Q}^m \Delta\Theta_{ij}^m} \\
&= \alpha \sum_m \left(\frac{3((\mathbf{S}_i \cdot \mathbf{Q}^m \Delta\Theta_{ij}^m)(\mathbf{S}_j \cdot \mathbf{r}_{ij}) + (\mathbf{S}_i \cdot \mathbf{r}_{ij})(\mathbf{S}_j \cdot \mathbf{Q}^m \Delta\Theta_{ij}^m))}{|\mathbf{r}_{ij}|^5} \right. \\
& \quad \left. - \frac{15(\mathbf{S}_i \cdot \mathbf{r}_{ij})(\mathbf{S}_j \cdot \mathbf{r}_{ij})}{|\mathbf{r}_{ij}|^7} (\mathbf{r}_{ij} \mathbf{Q}^m \Delta\Theta_{ij}^m) + \frac{3(\mathbf{S}_i \cdot \mathbf{S}_j)}{|\mathbf{r}_{ij}|^5} (\mathbf{r}_{ij} \mathbf{Q}^m \Delta\Theta_{ij}^m) \right) \quad . \tag{4.44}
\end{aligned}$$

To extract the relevant matrix elements responsible for a transition between the m_s -sublevels, the spin operators \mathbf{S} are expanded in raising and lowering operators according to the spin-algebra. The Hamiltonians in (4.2) and (4.44)

contain terms like $(\mathbf{a} \cdot \mathbf{S}_i)(\mathbf{b} \cdot \mathbf{S}_j)$ and the term $\mathbf{S}_i \mathbf{S}_j$, which can be rewritten as

$$\begin{aligned}
(\mathbf{a} \cdot \mathbf{S}_i)(\mathbf{b} \cdot \mathbf{S}_j) &= \\
&= (a^x S_i^x + a^y S_i^y + a^z S_i^z)(b^x S_j^x + b^y S_j^y + b^z S_j^z) && \begin{aligned} S^x &= 1/2(S^+ + S^-) \\ S^y &= -i/2(S^+ - S^-) \end{aligned} \\
&= \left(\frac{1}{2} (S_i^+(a^x - ia^y) + S_i^-(a^x + ia^y)) + S_i^z a^z \right) \cdot \\
&\quad \cdot \left(\frac{1}{2} (S_j^+(b^x - ib^y) + S_j^-(b^x + ib^y)) + S_j^z b^z \right) \\
&= \frac{1}{2} \left(S_i^+(a^x - ia^y) S_j^z b^z + S_i^-(a^x + ia^y) S_j^z b^z \right. \\
&\quad \left. + S_i^z a^z S_j^+(b^x - ib^y) + S_i^z a^z S_j^-(b^x + ib^y) \right) + && \text{single spin-flip events} \\
&\quad + \frac{1}{4} \left(S_i^+(a^x - ia^y) S_j^+(b^x - ib^y) + S_i^-(a^x + ia^y) S_j^-(b^x + ib^y) + \right. \\
&\quad \left. + S_i^+(a^x - ia^y) S_j^-(b^x + ib^y) + S_i^-(a^x + ia^y) S_j^+(b^x - ib^y) \right) + \\
&\quad + S_i^z a^z S_j^z b^z && (4.45)
\end{aligned}$$

and

$$\begin{aligned}
\mathbf{S}_i \mathbf{S}_j &= (S_i^x S_j^x + S_i^y S_j^y + S_i^z S_j^z) \\
&= \frac{1}{4} (S_i^+ + S_i^-)(S_j^+ + S_j^-) - \frac{1}{4} (S_i^+ - S_i^-)(S_j^+ - S_j^-) + S_i^z S_j^z \\
&= \frac{1}{2} (S_i^+ S_j^- + S_i^- S_j^+) + S_i^z S_j^z. && (4.46)
\end{aligned}$$

The only matrix elements, which can cause a transition between the $m_s = \pm 1$ and $m_s = 0$ state, are the ones, which contain only a single raising or lowering operator and are marked in (4.45), thus the last term in (4.44) can be neglected for this study⁹. Taking only the spin-flip matrix elements into account \mathcal{H}_{sp} in (4.44) can be expressed as

$$\begin{aligned}
\mathcal{H}_{sp} &= \alpha \sum_m \Delta \Theta_{ij}^m \left(\frac{3 \left((S_i^\pm S_j^z + S_i^z S_j^\pm) \left((r_{ij}^x \mp ir_{ij}^y) Q_m^z + (Q_m^x \mp Q_m^y) r_{ij}^z \right) \right)}{2 |\mathbf{r}_{ij}|^5} - \right. \\
&\quad \left. - \frac{15 \left((S_i^\pm S_j^z + S_i^z S_j^\pm) (r_{ij}^x \mp ir_{ij}^y) r_{ij}^z \right) (\mathbf{r}_{ij} \mathbf{Q}_m)}{2 |\mathbf{r}_{ij}|^7} \right). && (4.47)
\end{aligned}$$

This compact form of the Hamiltonian looks already so nice that the temptation to sandwich it between the transition states in order to calculate the

⁹The term resembles the interaction energy in the Heisenberg model, where single spin-flips do not occur.

transition rate according to Fermi's Golden rule has to be given in. The overall transition rate $\Gamma_{f \leftarrow i} = \frac{1}{T_{f \leftarrow i}}$ between an initial and final electronic state $m_i(f)$ is obtained by summing the matrix elements of all final phonon states $\tilde{\mathcal{N}}_f$ obeying energy conservation. We will denote the phonon states with the symbol \mathcal{N} and suppress the \mathbf{k} -point and band index λ .

$$\begin{aligned}
& \Gamma_{f \leftarrow i} = \\
&= \frac{2\pi}{\hbar} \sum_f \left| \langle \tilde{\mathcal{N}}_f, m_s^f | \mathcal{H}_{sp} | \mathcal{N}_i, m_s^i \rangle \right|^2 \delta(E_f - E_i - h\nu) \\
&= \frac{2\pi}{\hbar} \sum_{\mathbf{k}, \lambda} \left| \langle m_s^f | \alpha \sum_m \Delta \Theta_{ij}^m \left(\frac{3(S_i^\pm S_j^z + S_i^z S_j^\pm) \left((r_{ij}^x \mp i r_{ij}^y) \langle \tilde{\mathcal{N}}_f | Q_m^z | \mathcal{N}_i \rangle \right)}{2 |\mathbf{r}_{ij}|^5} \right. \right. \\
&+ \left. \frac{3 \langle \tilde{\mathcal{N}}_f | (Q_m^x \mp i Q_m^y) | \mathcal{N}_i \rangle r_{ij}^z}{2 |\mathbf{r}_{ij}|^5} \right. \\
&- \left. \left. \frac{15 \left((S_i^\pm S_j^z + S_i^z S_j^\pm) (r_{ij}^x \mp i r_{ij}^y) r_{ij}^z \right) \left(\mathbf{r}_{ij} \langle \tilde{\mathcal{N}}_f | \mathbf{Q}_m | \mathcal{N}_i \rangle \right)}{2 |\mathbf{r}_{ij}|^7} \right) \right|^2 \delta(E_f - E_i - h\nu)
\end{aligned} \tag{4.48}$$

To put the quantum character of the phononic displacements $\mathbf{Q}^{\{n\}}$ into play, they are expanded in second quantized form (see (3.3)). The phononic matrix elements can now be calculated using the ladder operator algebra. First we only look at one single phonon mode \mathbf{t}, μ with N_{ph} phonons in the initial state and \tilde{N}_{ph} phonons in the final state

$$\begin{aligned}
& \langle \tilde{\mathcal{N}}_f | Q_m^i | \mathcal{N}_i \rangle \\
&= \langle \tilde{\mathcal{N}}_f | i \sum_{\mathbf{q}, \rho} \sqrt{\frac{\hbar}{2M_n N \omega_{\mathbf{q}, \rho}}} (\hat{a}_{-\mathbf{q}, \rho}^\dagger + \hat{a}_{\mathbf{q}, \rho}) \epsilon_{\mathbf{q}, \rho}^i e^{i\mathbf{q}\mathbf{R}_0^n} | \mathcal{N}_i \rangle \\
&= \langle \tilde{\mathcal{N}}_f | i \sum_{\mathbf{q}, \rho} \sqrt{\frac{\hbar}{2M_n N \omega_{\mathbf{q}, \rho}}} (\hat{a}_{-\mathbf{q}, \rho}^\dagger + \hat{a}_{\mathbf{q}, \rho}) | \mathcal{N}_i \rangle \epsilon_{\mathbf{q}, \rho}^i e^{i\mathbf{q}\mathbf{R}_0^n} \\
&= \langle \tilde{\mathcal{N}}_f | i \sum_{\mathbf{q}, \rho} \sqrt{\frac{\hbar}{2M_n N \omega_{\mathbf{q}, \rho}}} (\sqrt{N_{ph} + 1} \delta_{-\mathbf{q}, \mathbf{t}} \delta_{\rho, \mu} | \mathcal{N}_i + 1 \rangle + \\
&+ \sqrt{N_{ph}} \delta_{\mathbf{q}, \mathbf{t}} \delta_{\rho, \mu} | \mathcal{N}_i - 1 \rangle) \epsilon_{\mathbf{q}, \rho}^i e^{i\mathbf{q}\mathbf{R}_0^n} \\
&= i \sqrt{\frac{\hbar}{2M_n N}} \left(\sqrt{(N_{ph} + 1)} / \omega_{-\mathbf{t}, \lambda} \delta_{\tilde{\mathcal{N}}_f = \mathcal{N}_i + 1} \epsilon_{-\mathbf{t}, \lambda}^i e^{-i\mathbf{t}\mathbf{R}_0^n} + \sqrt{N_{ph}} / \omega_{\mathbf{t}, \lambda} \delta_{\tilde{\mathcal{N}}_f = \mathcal{N}_i - 1} \epsilon_{\mathbf{t}, \lambda}^i e^{i\mathbf{t}\mathbf{R}_0^n} \right)
\end{aligned}$$

Putting all together, the transition rate is calculated as

$$\begin{aligned}
& \Gamma_{f \leftarrow i} = \\
&= \frac{\alpha^2 \hbar [N_{ph} + 1]^{emission} [N_{ph}]^{absorption}}{\hbar^2 2M_n N \omega}
\end{aligned}$$

$$\begin{aligned}
& \sum_{\mathbf{k}, \lambda} \left| \langle m_s^f | \sum_m \Delta \Theta_{ij}^m e^{i\mathbf{k}\mathbf{R}_0^m} \left(\frac{3(S_i^\pm S_j^z + S_i^z S_j^\pm) ((r^x \mp ir^y) \epsilon_{\mathbf{k}, \lambda, m}^z)}{2|\mathbf{r}_{ij}|^5} \right. \right. \\
& + \frac{3(\epsilon_{\mathbf{k}, \lambda, m}^x \mp i\epsilon_{\mathbf{k}, \lambda, m}^y) r^z}{2|\mathbf{r}_{ij}|^5} - \\
& \left. \left. - \frac{15((S_i^\pm S_j^z + S_i^z S_j^\pm) (r^x \mp ir^y) r^z) (\mathbf{r}_{ij} \epsilon_{\mathbf{k}, \lambda, m})}{2|\mathbf{r}_{ij}|^7} \right) |m_s^i \rangle \right|^2 \delta(\nu = 2.88 \text{ GHz})
\end{aligned} \tag{4.49}$$

Thus the rate is proportional to the number of phonons in the modes, which are assumed to be thermally populated. The assumption of the thermal population is, as already mentioned, not as trivial as it may seem because the direct process will inevitably populate only a single phonon mode. However, the high velocity of sound in diamond, which leads to the high thermal conductivity may overcome this bottleneck process and transfer the heat towards the end of the sample, where thermal equilibrium is established. The only thermal contribution to the relaxation rate therefore comes from the phononic matrix elements, so we can separate this off by rewriting

$$\Gamma_{f \leftarrow i} = \begin{cases} (N_{ph} + 1)\Gamma_0 & \text{for emission of a phonon} \\ N_{ph}\Gamma_0 & \text{for absorption of a phonon} \end{cases} \tag{4.50}$$

To extract the measured relaxation rate, we have to consider the populations in the m_s sub levels and account for the excitations and de-excitations in the ensemble of spins. Thus, we have to solve the following rate equations, for the spin ensemble:

$$\begin{aligned}
\dot{N}_{m_s \pm 1} &= -\Gamma_0(N_{ph} + 1)N_{m_s \pm 1} + 2\Gamma_0 N_{ph} N_{m_s=0} \\
\dot{N}_{m_s=0} &= -\dot{N}_{m_s \pm 1}
\end{aligned} \tag{4.51}$$

The quantity that is measured in the cavity in the experiment is the mean square z -component of the spin $\langle S_z^2 \rangle(t, T)$, which is related to the occupation numbers via $\langle S_z^2 \rangle(t, T) = N_{m_s \pm 1}/N$, where N is the total number of spins. Using equation (4.51), we end up with a simple differential equation

$$\frac{d}{dt} \langle S_z^2 \rangle(t, T) = - \underbrace{(3N_{ph} + 1)\Gamma_0}_{\Gamma=1/T_1} (\langle S_z^2 \rangle(t, T) - \langle S_z^2 \rangle(T)_{th}) \quad , \tag{4.52}$$

leading to an exponential decay towards its thermal equilibrium value, where we can extract the measured relaxation rate Γ . The thermal equilibrium value

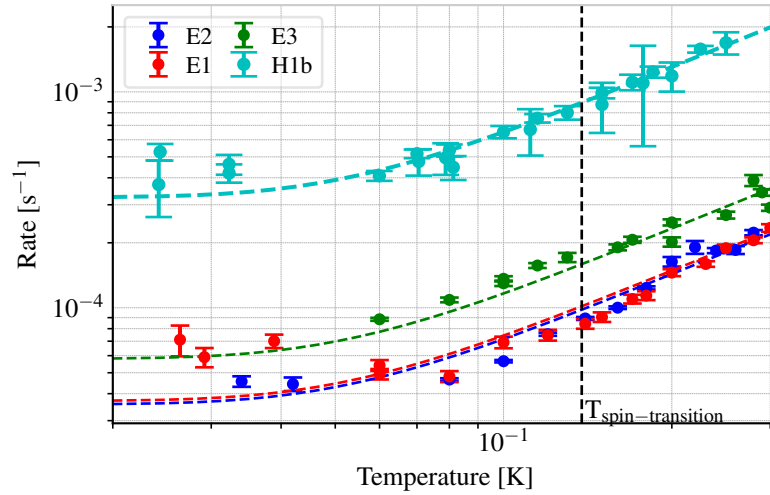


Figure 4.4: **Measured relaxation rates** Γ , we see the relaxation rates for 4 different samples, where 3 of them were created by an irradiation of electrons (samples E1, E2 and E3) and one by an irradiation with neutrons (sample H1b), which have a high impact on the crystal structure damage.

in this equation is given by

$$\langle S_z^2 \rangle (T)_{th} = \frac{2}{e^{\hbar\omega/k_B T} + 2} \quad . \quad (4.53)$$

In order to explain the measured temperature dependence, all that needs to be done is to calculate the zero temperature relaxation rate Γ_0 . The calculation of this relaxation rate will be the topic of the next Chapters of this thesis, but we can already take a look at the measured relaxation rates for different temperatures and fit our analytical formula (4.52) to the experimental data, without explicitly calculating Γ_0 . Taking a look at Figure 4.4, we see that the measured relaxation rates are fitted quite satisfactorily by our derived formula. The most interesting conclusion from our calculations is that there is a fundamental limit of the spin lattice relaxation time, given by the coupling of the spins to the zero-point fluctuations of the phonons in a regime, where no thermal phonons are present anymore. This is visible in the Figure in the measured plateau at the lowest temperatures. In a more elevated temperature regime above a temperature which corresponds to the spin-transition frequency, the direct phonon process results in a linear dependence of the relaxation rate on temperature, which is due to the high temperature limit of the Bose-Einstein distribution. We also see that the spread in measured relaxation rates is one order of magnitude for different samples: The samples used in the experiment were created by irradiating diamonds of type Ib, which naturally contain a

high amount of nitrogen, with either electrons or neutrons in order to create vacancies, followed by an annealing treatment in order to make the vacancies mobile, which supports the formation of NV^- centers. The treatment of the samples has an influence on the crystal structure and therefore via the population of the phonons at the spin-transition frequency on the spin-lattice relaxation rate. We will try to quantify this influence when the actual *ab initio* calculations are performed in Chapter 5 but take a look at spin-orbit induced relaxation mechanisms before.

4.12.2 Elliott-Yafet relaxation rate calculation

The spin-relaxation processes described by Elliott and Yafet have been revised by Baral et al. (2016) by introducing a spin-torque matrix element for a lattice with a monoatomic basis and generalized to a polyatomic basis in their subsequent paper (Vollmar, Hilton, and Schneider (2017)). In this section, we will derive an expression for the spin-lattice relaxation rate starting from Yafet's formulation and proceed in accordance with Baral to end up with a spin-phonon matrix element, which we will use to calculate transition rates in the ground state spin triplet.

First, we start with the first order Taylor expansion in the ionic coordinates of the electron-ion interaction to arrive at the electron-phonon Hamiltonian

$$\mathcal{H}_{e-ph} = \sum_n \int \Psi^\dagger(\mathbf{r}) \left[\mathbf{Q}_n \cdot \frac{\partial \hat{v}_{e-ion}(\mathbf{r} - \mathbf{R}_n)}{\partial \mathbf{R}_n} \Big|_{\mathbf{R}_n^{(0)}} \right] \Psi(\mathbf{r}) d^3r \quad (4.17)$$

Now we take Ψ to be represented in a spinor Bloch wave basis, the potential to be a screened Coulomb potential and we again expand the phonons in the second quantized form to account for the quantum nature of these particles:

$$\Psi(\mathbf{r}) = \frac{1}{\sqrt{V}} \sum_\mu \sum_{\mathbf{k}} e^{i\mathbf{k}\mathbf{r}} u_{\mu\mathbf{k}}(\mathbf{r}) c_{\mu\mathbf{k}} \quad (4.54)$$

$$\hat{v}_{e-ion}(\mathbf{x}) = v_{\text{eff}}(\mathbf{x}) + \xi [\nabla v_{\text{eff}}(\mathbf{x}) \times \hat{\mathbf{p}}] \cdot \hat{\mathbf{s}} \quad (4.55)$$

$$v_{\text{eff}}(\mathbf{x}) = -\frac{Z_{\text{eff}}}{|\mathbf{x}|} \quad (4.56)$$

$$\mathbf{Q}_n = \sum_{\mathbf{q},\lambda} l_{\mathbf{q},\lambda}^n A_{\mathbf{q},\lambda} e^{i\mathbf{q}\mathbf{R}_n^{(0)}} \boldsymbol{\epsilon}_{\mathbf{q},\lambda}^n \quad (4.57)$$

with

$$l_{\mathbf{q},\lambda}^n = \sqrt{\frac{\hbar}{2m^n N \omega_{\mathbf{q},\lambda}}} \quad \text{and} \quad A_{\mathbf{q},\lambda} = a_{-\mathbf{q},\lambda}^\dagger + a_{\mathbf{q},\lambda} \quad .$$

Splitting $v_{e\text{-ion}}$ in a spin-diagonal and the spin dependent spin orbit coupling term, we get two couplings:

$$\mathcal{H}_{e\text{-ph}}^{(1)} = - \sum_n \sum_{\mathbf{k}\mu, \mathbf{k}'\mu'} c_{\mu\mathbf{k}}^\dagger c_{\mu'\mathbf{k}'} \int \frac{d^3r}{V} u_{\mu\mathbf{k}}^* e^{-i\mathbf{r}\mathbf{k}}(\mathbf{r}) \mathbf{Q}_n \cdot \nabla v_{\text{eff}}(\mathbf{r} - \mathbf{R}_n^{(0)}) u_{\mu'\mathbf{k}'}(\mathbf{r}) e^{i\mathbf{r}\mathbf{k}'} \quad (4.58)$$

and

$$\begin{aligned} \mathcal{H}_{e\text{-ph}}^{(2)} = & -\xi \sum_n \sum_{\mathbf{k}\mu, \mathbf{k}'\mu'} c_{\mu\mathbf{k}}^\dagger c_{\mu'\mathbf{k}'} \int \frac{d^3r}{V} \\ & \cdot u_{\mu\mathbf{k}}^*(\mathbf{r}) e^{-i\mathbf{r}\mathbf{k}} \left[\nabla \left(\mathbf{Q}_n \cdot \nabla v_{\text{eff}}(\mathbf{r} - \mathbf{R}_n^{(0)}) \right) \times \hat{\mathbf{p}} \right] \cdot \hat{\mathbf{s}} u_{\mu'\mathbf{k}'}(\mathbf{r}) e^{i\mathbf{r}\mathbf{k}'} \end{aligned} \quad (4.59)$$

The first term accounts for spin-relaxation due to the spin-mixing in the wavefunctions and is associated with a pure Elliott process, whereas the second term consists of a spin-dependent operator and resembles Yafet contributions. As Baral et al. (2016) have shown with their torque-element approach, the first term vanishes, s.t. we will only treat the relaxation processes arising from the second term.

Now we split the sum over the whole crystal (n-sum) in a sum over all the unit cells (m-sum) and the atoms therein (l-sum)

$$\begin{aligned} \mathcal{H}_{e\text{-ph}}^{(2)} = & -\xi \sum_{m,l} \sum_{\mathbf{k}\mu, \mathbf{k}'\mu'} c_{\mu\mathbf{k}}^\dagger c_{\mu'\mathbf{k}'} \int \frac{d^3r}{V} u_{\mu\mathbf{k}}^*(\mathbf{r}) e^{-i\mathbf{k}\mathbf{r}} \\ & \cdot \left[\nabla \left(i \sum_{\mathbf{q},\lambda} l_{\mathbf{q},\lambda}^l A_{\mathbf{q},\lambda} e^{i\mathbf{q}(\mathbf{R}_m^{(0)} + \mathbf{R}_l^{(0)})} \boldsymbol{\epsilon}_{\mathbf{q},\lambda}^l \cdot \nabla v_{\text{eff}}(\mathbf{r} - \mathbf{R}_m^{(0)} - \mathbf{R}_l^{(0)}) \right) \times \hat{\mathbf{p}} \right] \\ & \cdot \hat{\mathbf{s}} u_{\mu'\mathbf{k}'}(\mathbf{r}) e^{i\mathbf{k}'\mathbf{r}} \end{aligned} \quad (4.60)$$

In order to treat all the terms on the same footing, we plug in the Fourier-expansion of the effective potential v_{eff} and rearrange in a convenient order

$$v_{\text{eff}}(\mathbf{r} - \mathbf{R}_m^{(0)} - \mathbf{R}_l^{(0)}) = \frac{1}{N} \sum_{\mathbf{p} \in 1^{\text{st}}\text{BZ}} \sum_{\mathbf{P}} \tilde{v}_{\text{eff}}(\mathbf{p} + \mathbf{P}) e^{i(\mathbf{r} - \mathbf{R}_m^{(0)} - \mathbf{R}_l^{(0)}) \cdot (\mathbf{p} + \mathbf{P})} \quad (4.61)$$

→

$$\begin{aligned} \mathcal{H}_{e\text{-ph}}^{(2)} = & -i\xi \sum_{m,l} \sum_{\mathbf{k}\mu, \mathbf{k}'\mu'} \sum_{\mathbf{q},\lambda} l_{\mathbf{q},\lambda}^l A_{\mathbf{q},\lambda} \sum_{\mathbf{p} \in 1^{\text{st}}\text{BZ}} \sum_{\mathbf{P}} \frac{1}{N} \tilde{v}_{\text{eff}}(\mathbf{p} + \mathbf{P}) c_{\mu\mathbf{k}}^\dagger c_{\mu'\mathbf{k}'} e^{i\mathbf{q}(\mathbf{R}_m^{(0)} + \mathbf{R}_l^{(0)})} \\ & \cdot \int \frac{d^3r}{V} u_{\mu\mathbf{k}}^*(\mathbf{r}) e^{-i\mathbf{k}\mathbf{r}} \left[\nabla \left(\boldsymbol{\epsilon}_{\mathbf{q},\lambda}^l \cdot i(\mathbf{p} + \mathbf{P}) \right) e^{i(\mathbf{r} - \mathbf{R}_m^{(0)} - \mathbf{R}_l^{(0)}) \cdot (\mathbf{p} + \mathbf{P})} \times \hat{\mathbf{p}} \right]. \end{aligned}$$

$$\cdot \hat{\mathbf{s}} u_{\mu' \mathbf{k}'}(\mathbf{r}) e^{i \mathbf{k}' \cdot \mathbf{r}} \quad (4.62)$$

→

$$\begin{aligned} \mathcal{H}_{\text{e-ph}}^{(2)} &= i\xi \sum_{m,l} \sum_{\mathbf{k}\mu, \mathbf{k}'\mu'} \sum_{\mathbf{q}, \lambda} l_{\mathbf{q}, \lambda}^l A_{\mathbf{q}, \lambda} \sum_{\mathbf{p} \in 1^{\text{st}} \text{BZ}} \sum_{\mathbf{P}} \frac{1}{N} \tilde{v}_{\text{eff}}(\mathbf{p} + \mathbf{P}) c_{\mu \mathbf{k}}^\dagger c_{\mu' \mathbf{k}'} e^{i \mathbf{q} \cdot (\mathbf{R}_m^{(0)} + \mathbf{R}_l^{(0)})} \\ &\quad \left(\boldsymbol{\epsilon}_{\mathbf{q}, \lambda}^l \cdot (\mathbf{p} + \mathbf{P}) \right) e^{i(-\mathbf{R}_m^{(0)} - \mathbf{R}_l^{(0)}) \cdot (\mathbf{p} + \mathbf{P})} \\ &\quad \cdot \int \frac{d^3 r}{V} u_{\mu \mathbf{k}}^*(\mathbf{r}) e^{i \mathbf{r} \cdot (\mathbf{k}' - \mathbf{k} + \mathbf{p} + \mathbf{P})} [(\mathbf{p} + \mathbf{P}) \times (\hat{\mathbf{p}} + \hbar \mathbf{k}')] \cdot \hat{\mathbf{s}} u_{\mu' \mathbf{k}'}(\mathbf{r}) \end{aligned} \quad (4.63)$$

Now we split the integral over the whole volume in integrals over all unit cells $\frac{1}{V} \int d^3 r f(\mathbf{r}) = \sum_i \frac{1}{N\Omega} \int_{\Omega} d^3 r f(\mathbf{r} + \mathbf{R}_i^{(0)})$ and use the fact that the cell-periodic part is the same in all of those $u(\mathbf{r} + \mathbf{R}_i^{(0)}) = u(\mathbf{r})$:

$$\begin{aligned} \mathcal{H}_{\text{e-ph}}^{(2)} &= i\xi \sum_{m,l} \sum_{\mathbf{k}\mu, \mathbf{k}'\mu'} \sum_{\mathbf{q}, \lambda} l_{\mathbf{q}, \lambda}^l A_{\mathbf{q}, \lambda} \sum_{\mathbf{p} \in 1^{\text{st}} \text{BZ}} \sum_{\mathbf{P}} \frac{1}{N} \tilde{v}_{\text{eff}}(\mathbf{p} + \mathbf{P}) c_{\mu \mathbf{k}}^\dagger c_{\mu' \mathbf{k}'} e^{i \mathbf{q} \cdot (\mathbf{R}_m^{(0)} + \mathbf{R}_l^{(0)})} \\ &\quad \left(\boldsymbol{\epsilon}_{\mathbf{q}, \lambda}^l \cdot (\mathbf{p} + \mathbf{P}) \right) e^{i(-\mathbf{R}_m^{(0)} - \mathbf{R}_l^{(0)}) \cdot (\mathbf{p} + \mathbf{P})} \\ &\quad \cdot \sum_i \frac{1}{N\Omega} \int_{\Omega} d^3 r u_{\mu \mathbf{k}}^*(\mathbf{r}) e^{i(\mathbf{r} + \mathbf{R}_i^{(0)}) \cdot (\mathbf{k}' - \mathbf{k} + \mathbf{p} + \mathbf{P})} [(\mathbf{p} + \mathbf{P}) \times (\hat{\mathbf{p}} + \hbar \mathbf{k}')] \cdot \hat{\mathbf{s}} u_{\mu' \mathbf{k}'}(\mathbf{r}) \end{aligned} \quad (4.64)$$

Here we have the pleasant situation that the sums simplify due to arising delta functions:

$$\begin{aligned} \mathcal{H}_{\text{e-ph}}^{(2)} &= i\xi \sum_l \sum_{\mathbf{k}\mu, \mathbf{k}'\mu'} \sum_{\mathbf{q}, \lambda} l_{\mathbf{q}, \lambda}^l A_{\mathbf{q}, \lambda} \sum_{\mathbf{p} \in 1^{\text{st}} \text{BZ}} \sum_{\mathbf{P}} \tilde{v}_{\text{eff}}(\mathbf{p} + \mathbf{P}) c_{\mu \mathbf{k}}^\dagger c_{\mu' \mathbf{k}'} \\ &\quad \cdot \underbrace{\sum_m \frac{1}{N} e^{i \mathbf{R}_m^{(0)} \cdot (\mathbf{q} - \mathbf{p} - \mathbf{P})} e^{i \mathbf{R}_l^{(0)} \cdot (\mathbf{q} - \mathbf{p} - \mathbf{P})}}_{\delta_{\mathbf{q}, \mathbf{p} + \mathbf{P}}} \left(\boldsymbol{\epsilon}_{\mathbf{q}, \lambda}^l \cdot (\mathbf{p} + \mathbf{P}) \right) \\ &\quad \cdot \underbrace{\frac{1}{N} \sum_i e^{i \mathbf{R}_i^{(0)} \cdot (\mathbf{k}' - \mathbf{k} + \mathbf{p} + \mathbf{P})}}_{\delta_{\mathbf{k}, \mathbf{k}' + \mathbf{p} + \mathbf{P}}} \frac{1}{\Omega} \int_{\Omega} d^3 r u_{\mu \mathbf{k}}^* e^{i \mathbf{r} \cdot (\mathbf{k}' - \mathbf{k} + \mathbf{p} + \mathbf{P})} [(\mathbf{p} + \mathbf{P}) \times (\hat{\mathbf{p}} + \hbar \mathbf{k}')] \cdot \hat{\mathbf{s}} u_{\mu' \mathbf{k}'} \end{aligned} \quad (4.65)$$

$$\begin{aligned} &= i\xi \sum_l \sum_{\mu, \mathbf{k}'\mu'} \sum_{\mathbf{q}, \lambda} l_{\mathbf{q}, \lambda}^l A_{\mathbf{q}, \lambda} \tilde{v}_{\text{eff}}(\mathbf{q}) c_{\mu \mathbf{k}' + \mathbf{q}}^\dagger c_{\mu' \mathbf{k}'} \left(\boldsymbol{\epsilon}_{\mathbf{q}, \lambda}^l \cdot \mathbf{q} \right) \\ &\quad \cdot \frac{1}{\Omega} \int_{\Omega} d^3 r u_{\mu \mathbf{k}' + \mathbf{q}}^*(\mathbf{r}) [\mathbf{q} \times (\hat{\mathbf{p}} + \hbar \mathbf{k}')] \cdot \hat{\mathbf{s}} u_{\mu' \mathbf{k}'}(\mathbf{r}) \end{aligned} \quad (4.66)$$

In order to calculate the relaxation rates in the NV^- center, we have to find

the spinor wavefunctions, corresponding to the m_s - sublevels and calculate the matrix elements of $\mathcal{H}_{\text{e-ph}}^{(2)}$ to arrive with a Fermi's Golden rule expression as was done in the previous section for the spin-spin interaction as a starting point. The rates according to the Elliott-Yafet process will be calculated *ab initio* in the next Chapter.

References

- Astner, T. et al. (2018). “Solid-state electron spin lifetime limited by phononic vacuum modes”. In: *Nature Materials* 17, pp. 313–317.
- Baral, A. et al. (2016). “Re-examination of the Elliott–Yafet spin-relaxation mechanism”. In: *New Journal of Physics* 18, p. 023012.
- Bir, G. L., Aronov A. G., and G.E. Pikus (1975). “Spin relaxation of electrons due to scattering by holes”. In: *ZhETF* 69, p. 1382.
- Casimir, H.B.G. (1939). “On the equilibrium between spin and lattice”. In: *Physica* 6, pp. 156–160.
- Casimir, H.B.G., W.J. de Haas, and D. de Klerk (1939b). “Measurements on iron ammonium alum”. In: *Physica* 6, pp. 241–254.
- Casimir, H.B.G. and F.K. du Pré (1938). “Note on the thermodynamic interpretation of paramagnetic relaxation phenomena”. In: *Physica* 5, pp. 507–511.
- D’yakonov, M.I. and V.I. Perel’ (1971). “Spin Orientation of Electrons Associated with the Interband Absorption of Light in Semiconductors”. In: *ZhETF* 60, p. 1954.
- Elliott, R. J. (1954). “Theory of the Effect of Spin-Orbit Coupling on Magnetic Resonance in Some Semiconductors”. In: *Phys. Rev.* 96, pp. 266–279.
- Fierz, M. (1938). “Zur Theorie der Suszeptibilität paramagnetischer Alaune in Wechselfeldern”. In: *Physica* 5, pp. 433–436.
- Gorter, C. J. and F. Brons (1937). “Magnetic inhibition of susceptibilities at radio frequencies”. In: *Physica* 4, pp. 579–584.
- Gorter, C.J. (1936). “Paramagnetic relaxation”. In: *Physica* 3, pp. 503–514.
- Gorter, C.J., P. Teunissen, and L.J. Dijkstra (1938). “On the apparent absence of paramagnetic dispersion and absorption in titanium caesium alum”. In: *Physica* 5, pp. 1013–1017.
- Jarmola, A. et al. (2012). “Temperature- and Magnetic-Field-Dependent Longitudinal Spin Relaxation in Nitrogen-Vacancy Ensembles in Diamond”. In: *Phys. Rev. Lett.* 108, p. 197601.
- Kronig, R. de L. (1939). “On the mechanism of paramagnetic relaxation”. In: *Physica* 6, pp. 33–43.
- Lenef, A. and S. C. Rand (1996). “Electronic structure of the N-V center in diamond: Theory”. In: *Phys. Rev. B* 53, pp. 13441–13455.
- Orbach, R. (1961). “Spin-Lattice Relaxation in Rare-Earth Salts”. In: *Proceedings of the Royal Society A: Mathematical, Physical and Engineering Sciences* 264.1319, pp. 458–484.

- Overhauser, A. W. (1953). “Paramagnetic Relaxation in Metals”. In: *Phys. Rev.* 89, pp. 689–700.
- Shrivastava, K. N. (1983). “Theory of Spin–Lattice Relaxation”. In: *Physica status solidi (b)* 117.2, pp. 437–458.
- Van Vleck, J. H. (1940). “Paramagnetic Relaxation Times for Titanium and Chrome Alum”. In: *Phys. Rev.* 57, pp. 426–447.
- (1941). “Paramagnetic Relaxation and the Equilibrium of Lattice Oscillators”. In: *Phys. Rev.* 59, pp. 724–729.
- Vollmar, S., D. J. Hilton, and H. C. Schneider (2017). “Generalized Elliott-Yafet spin-relaxation time for arbitrary spin mixing”. In: *Phys. Rev. B* 96 (7), p. 075203.
- Walker, M. B. (1968). “A T₅ spin–lattice relaxation rate for non-Kramers ions”. In: *Canadian Journal of Physics* 46.11, pp. 1347–1353.
- Waller, I. (1932). “Über die Magnetisierung von paramagnetischen Kristallen in Wechselfeldern”. In: *Zeitschrift für Physik* 79, pp. 370–388.
- Yafet, Y. (1963). “g Factors and Spin-Lattice Relaxation of Conduction Electrons”. In: *Solid State Physics* 14, pp. 1–98.

Chapter 5

Ab initio calculation of Γ_0

This Chapter deals with the calculation of the necessary figures to determine the relaxation time Γ_0 . Section 5.1 is concerned with a Waller process, where we will calculate the necessary ingredients for a quantification of the relaxation time T_1 . Section and an Elliott-Yafet process in the NV^- center.

5.1 *Ab initio* Calculation of Γ_0 for a Waller process

Taking a second look at equations (4.49), we see that for the extraction of Γ_0 we need the phononic eigenvectors and dispersion relation to calculate matrix elements for the operator

$$\sum_m \Delta \Theta_{ij}^m e^{ikR_0^m} (S_i^\pm S_j^z + S_i^z S_j^\pm) \times \left(\frac{3(r^x \mp ir^y) \epsilon_{\mathbf{k},\lambda,m}^z}{2 |\mathbf{r}_{ij}|^5} + \frac{3(\epsilon_{\mathbf{k},\lambda,m}^x \mp i \epsilon_{\mathbf{k},\lambda,m}^y) r^z}{2 |\mathbf{r}_{ij}|^5} - \frac{15(r^x \mp ir^y) r^z (\mathbf{r}_{ij} \epsilon_{\mathbf{k},\lambda,m})}{2 |\mathbf{r}_{ij}|^7} \right). \quad (5.1)$$

In order to arrive at numbers, we will calculate in this chapter

- The phonon dispersion, to extract the polarization vectors for the 2.88 GHz phonons and the velocity of sound to account for the number of phonons in a given energy interval. Since the only phonons with the target frequency are acoustic ones, a Debye model should be appropriate to model the number of accessible states.
- The relevant electronic orbitals, which are responsible for the spin-flip in the center.

- The volume around each ion, in which the electrons are supposed to follow the movement of the ions rigidly to evaluate $\Delta\Theta_{ij}^m$. We will use Bader volumes and Wigner-Seitz cells around the ions to check the sensibility of the results.

5.1.1 Accuracy of the calculations

Before we start investigating the structure and dynamic behavior of the NV^- center, we have to check how many basis functions are necessary to resolve the energy differences needed for our calculations. Also the influence of the chosen number of \mathbf{k} -points which are used to sample Brillouin-zone integrals has to be investigated. VASP uses a plane wave basis set, where the number of basis functions for a given \mathbf{k} -point is controlled by an energy cutoff parameter. Only plane waves fulfilling the condition

$$\frac{\hbar(\mathbf{k} + \mathbf{G})^2}{2m_e} < E_{cut} \quad (5.2)$$

are taken into account in the calculation. As shown in Figure 5.1a) a convergence of 1 meV is obtained by choosing an energy cutoff E_{cut} of at least 900 eV and a \mathbf{k} -points mesh with a Monkhorst-Pack sampling¹ of 3x3x3, resulting in 6 irreducible \mathbf{k} -points.

5.1.2 The phononic properties of the NV^- center

As mentioned in Chapter 3, for the harmonic approximation to work, we need a properly relaxed ground state, where the forces acting on the ions are negligible. In our case we have to proceed with great care, because we need to resolve low phonon frequencies of 2.88 GHz, whereas typical phonon frequencies are in the order of THz. The calculations in this section are performed on a cell which would correspond to 64 atoms in a pure diamond structure.

The lattice constant

If perturbations of the periodic structure are present in a crystal, the local surrounding will change accordingly. For the NV^- center this would increase the lattice constant of the crystal in the case of very high defect density as shown in Figure 5.2. The samples used in the optical cavity are of low NV^- concentration, s.t. the effect of this increased lattice constant will result in a local strain in the close vicinity of the defect. The lattice constant of the

¹Monkhorst and Pack, 1976.

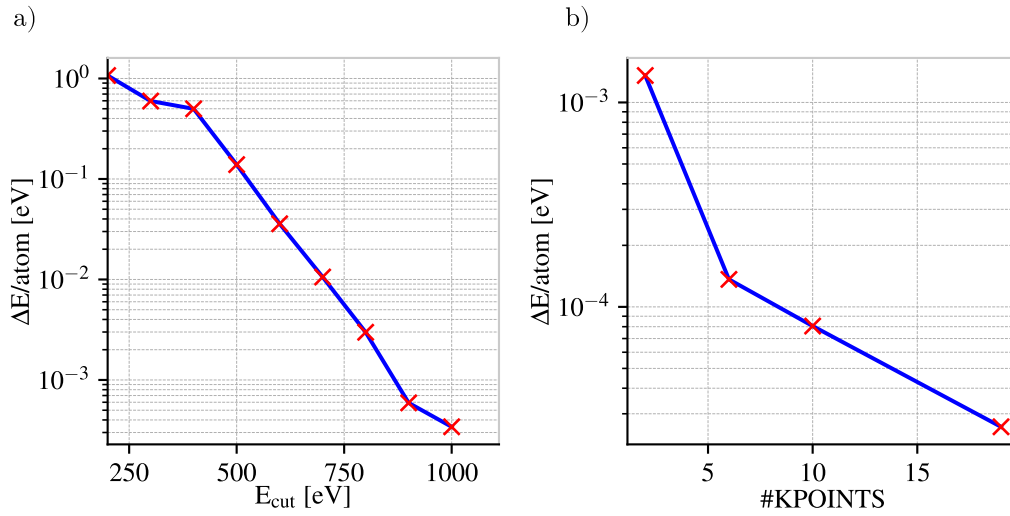


Figure 5.1: **Convergence study for a 64-atomic cell including one NV^- center**, a) The dependence of the total energy on the number of chosen basis functions is shown by plotting the difference related to a calculation with a cutoff of 1200 eV. b) The dependence on the \mathbf{k} -mesh. We used different values of a $N \times N \times N$ Monkhorst-Pack grid, resulting in the number of irreducible \mathbf{k} -points shown on the x -axis.

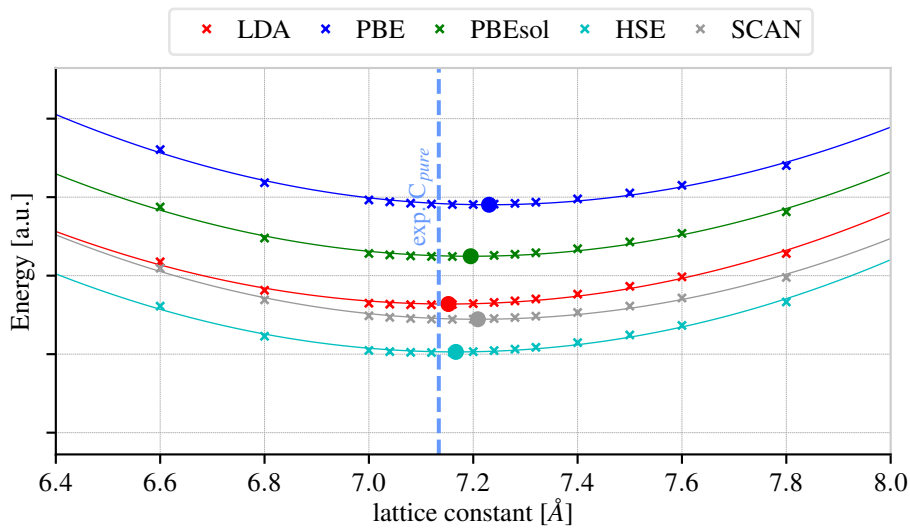


Figure 5.2: **Lattice constant with NV^- center** The energy dependence of the lattice constant is shown in this Figure for 5 different functionals. We see, that the presence of the color center favors a higher lattice constant.

functional	N		C_i	
	direction	distance [\AA]	direction	distance [\AA]
LDA	(-1,-1,-1)	0.153	(-0.62,1,1) _{cyclic}	0.105
PBE	(-1,-1,-1)	0.137	(-0.58,1,1) _{cyclic}	0.094
PBEsol	(-1,-1,-1)	0.142	(-0.58,1,1) _{cyclic}	0.0953
SCAN	(-1,-1,-1)	0.130	(-0.54,1,1) _{cyclic}	0.0886
HSE	(-1,-1,-1)	0.152	(-0.58,1,1) _{cyclic}	0.098

Table 5.1: The relaxation of the nearest neighbour ions of the vacant lattice site, obtained with a force cutoff of $1 \times 10^{-3} \text{ eV/\AA}$

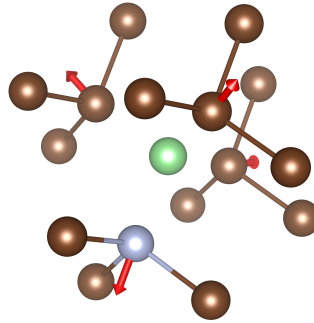


Figure 5.3: **Relaxation in the NV^- center**, The direction of the relaxation of the nearest neighbour atoms is shown in red arrows. The relaxation distance is exaggerated for illustrational purposes.

crystal will, however, be the same as in the unperturbed case. Therefore, we model the defect using the lattice constant of the pure diamond crystal.

Relaxing the structure

The next task towards a phonon dispersion is the calculation of the equilibrium positions of the ions. In order to relax the ions to their equilibrium position, we first use a conjugate gradient algorithm and double check our results with a quasi-newton algorithm. As we see in Table 5.1 and Figure 5.3, the ions relax away from the vacancy in accordance with an earlier study by Gali, Fyta, and Kaxiras (2008). The relaxation of the second nearest neighbour atoms is negligibly small with a distance of movement of $\approx 0.004 \text{ \AA}$. The resulting forces acting on the ions in the relaxed positions are less than $1 \times 10^{-3} \text{ eV/\AA}$.

Dynamical matrix and diagonalization

From the equilibrium position, we can start to displace the atoms and obtain the dynamical matrix by extracting the forces acting on the ions. Due to symmetry, we only need to calculate 78 displacements for the cell containing 64 lattice sites. A calculation of these small displacements yields the dynamical

matrix, which is diagonalized with PHONOPY, resulting in the phonon band-structure of Figure 5.4. If a NV^- center is introduced, the phonon spectrum is shifted towards lower energies and phonon branches split at high symmetry points due to the reduction in symmetry. We also see peaks arising due to presence of the NV^- center, which correspond to localized phonon modes as Gali, Simon, and Lowther (2011) have shown. These localized modes will play a crucial mode for spin-lattice relaxation at elevated temperatures, where these vibronic modes may be excited and spin-relaxation due to the Orbach process may become important. We will discuss this problem in section 5.1.2.

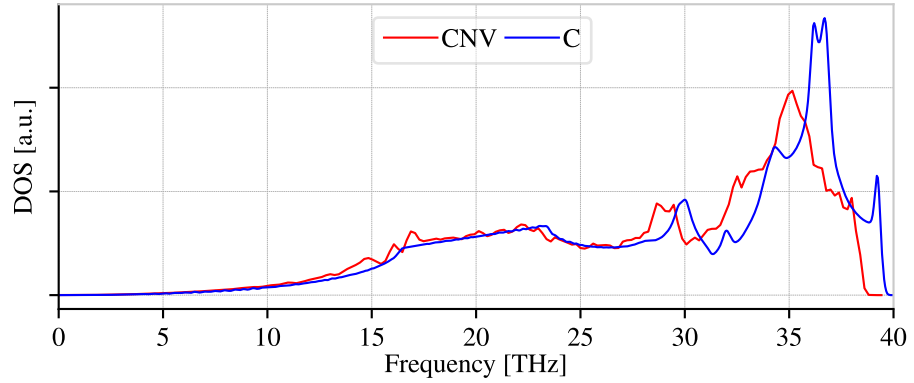
Supercell convergence

As in the case of a pure diamond structure, we will also check for convergence with respect to the supercell size, where we do not change the NV^- density of the crystals. The case of a more diluted crystal will be calculated in section 5.1.2. We double the cell in each direction and calculate the resulting forces to end up with the phononic properties shown in Figure 5.5. The calculations show that there is a significant difference between a $2 \times 2 \times 2$ cell, containing 8 NV^- centers and 512 lattice sites and the cell calculated in the previous subsection for high phonon frequencies. The low energy spectrum, where the spin-transition frequency is located, is similar for both of the cells. A comparison of the eigenvectors of the dynamical matrices which are the polarization vectors and of the resulting group velocities is shown in Appendix E.

Cell size convergence

Since the samples in the experiment are low in NV^- concentration, the phonon spectrum of a larger supercell, containing only one NV^- center is also to be calculated. The calculation of this spectrum is rather cumbersome since it requires 574 displacements with very accurate force evaluation. As we see in Figure 5.6, the vibrational properties of the NV^- center is strongly dependent on the local surrounding. For the case of a diluted sample, containing a small amount of NV^- centers, the density of states does not differ from the one of a pure diamond crystal, with the exception of the peaks arising from the localized modes, which are smeared out in Figure 5.6 due to the high number of considered phonons and the normalization of the density of states. We see, that the acoustic branches of the phonon dispersion are similar for the cases of low and high NV^- density. Taking a look at the group velocities and polarization vectors of the big and small cell in Figure 5.7, we see that they

a)



b)

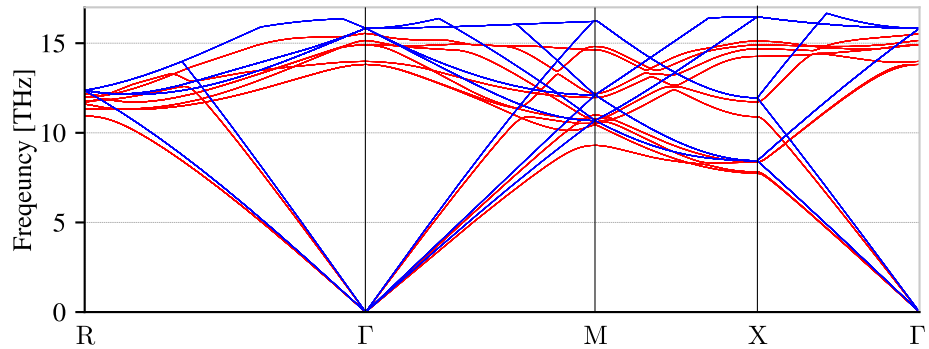
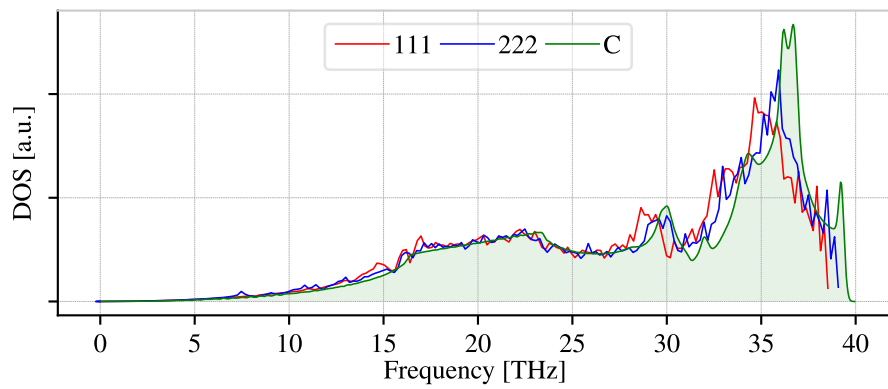


Figure 5.4: **Phonon DOS and BANDS with NV^- center**, a) the density of states reveals that the energy spectrum is shifted towards lower frequencies. Peaked structures arising at frequencies of ≈ 15 THz occur in the presence of an NV^- center. b) the lowest bands of the 64 atomic cell are shown. We see that the loss of symmetry is responsible for splitting of phonon modes at high symmetry points.

a)



b)

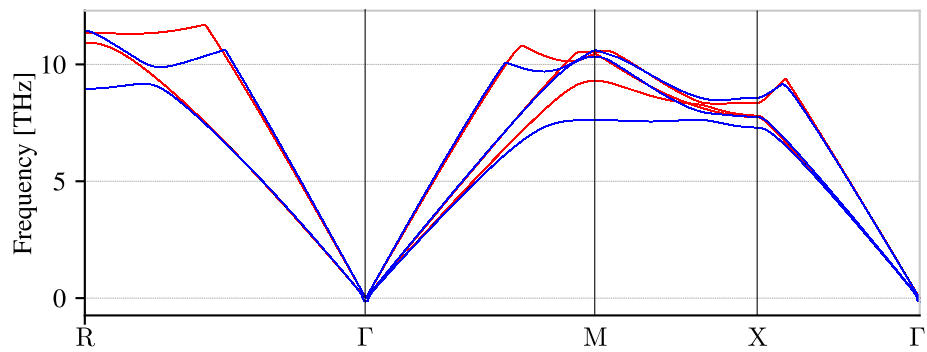
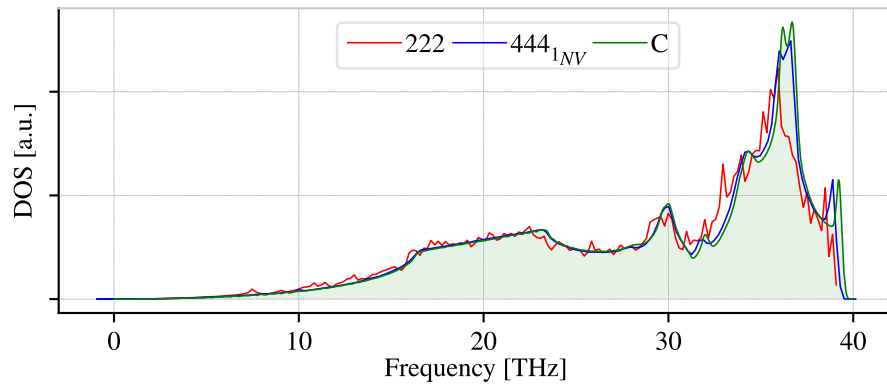


Figure 5.5: **Supercell 2x2x2 vs. 1x1x1**, a) density of states b) bandstructure

a)



b)

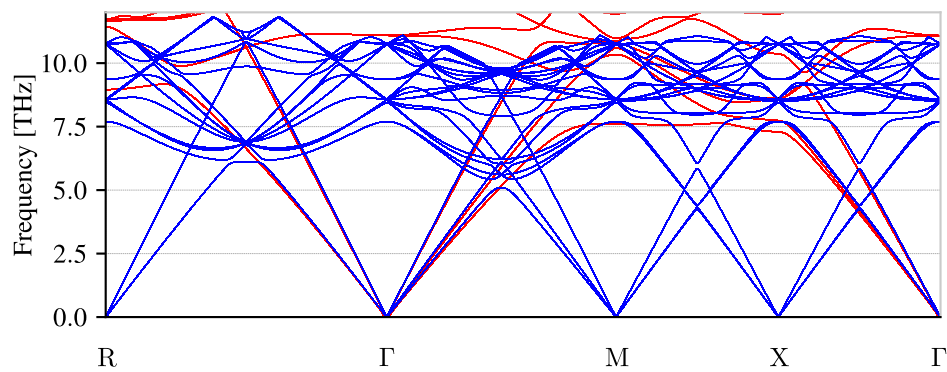


Figure 5.6: NV^- density comparison, a) and b) the blue lines correspond to a supercell containing 512 lattice sites and 1 NV^- center, the red lines show a cell of the same size containing 8 NV^- centers. b) Due to the smaller size of the primitive cell for the 8 NV^- center cell, the repetition of the Brillouin zone is plotted for the cell with 1 NV^- center to see the backfolded bands more clearly.

agree for typical phonon frequencies in the range of THz, but they differ when we approach the regime, where the group velocity reaches unreasonable values.

Phonon modes to consider in the calculation

In the actual calculation of the spin-lattice relaxation rate, we will try to compensate for the anisotropy of the phonon-dispersion by performing a calculation of the local velocity of sound for the 2.88 GHz phonons. The anisotropy of the phonon dispersion is depicted in Figure 5.8. As we saw in Figure 5.7, the velocities of sound are unreasonable for the low frequency regime. We will try to compensate for that, by calculating the velocity of sound in each direction for phonons with a frequency of 0.1 THz, where the calculated speed of sound has a reasonable value. The anisotropy for this elevated frequency is up to 10 % and therefore the shape of the isosurface differs from a sphere, as shown in Figure 5.9. When we model the local phonons, we will have to check, how large the influence of the polarization vectors is. For this reason, we will use the polarization vectors of the 2.88 GHz and 0.1 THz phonons even though the speed of sound for the first ones seems to be unphysical. The local speed of sound (in \mathbf{k} -space) will either be modeled by the calculated group velocity for the 0.1 THz phonons or by the values of a pure diamond crystal, if the nitrogen content in the crystal is supposed to be too small to alter the phononic properties of the system.

Localized phonon modes in the NV^- center

Due to the strong coupling of the spin with localized modes, we are interested in modes, where the atoms in the vicinity of the vacancy have a significantly bigger amplitude than the surrounding. These modes will give rise to a strong spin-lattice relaxation for the Orbach processes as we saw in Chapter 4. We obtain the localized phonon modes by randomly scanning the first Brillouin zone with a shifted Monkhorst-Pack grid, calculating the eigenvalues and the corresponding eigenvectors and keeping only strongly localized ones. As a measure for localization we consider x_{loc} , the ratio of the amplitudes of the atoms close to the vacancy and the rest of the cell

$$x_{loc} = \frac{\sum_{n \in N} |Q_n|}{\sum_{n \notin N} |Q_n|} . \quad (5.3)$$

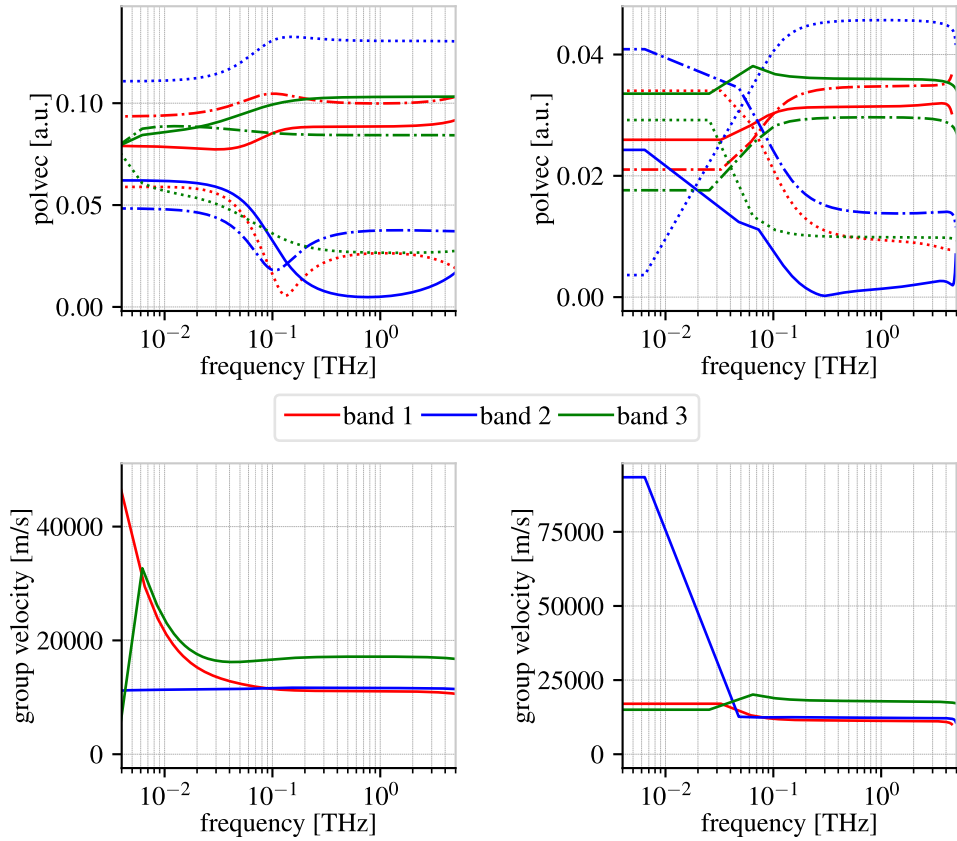


Figure 5.7: NV^- **phonons supercell convergence**, The polarization vectors and the corresponding group velocity for 3 different bands along a single direction in \mathbf{k} space are shown for the small supercell (64 lattice sites) on the left and the large supercell (512 lattice sites) on the right. The style of the lines corresponds to the x, y and z component of the polarization vector, whereas the colors denote the bands.

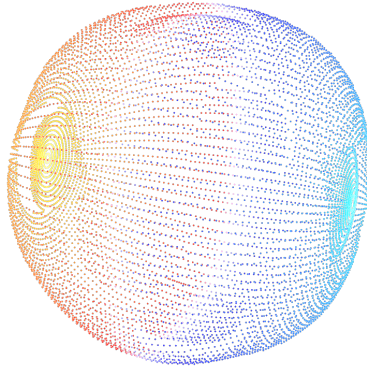


Figure 5.8: **2.88 GHz-isosurface of the third acoustic band**, The plot shows, that there are small anisotropies for the long wavelength phonons, if the calculations are performed for the 64-atomic cell. The velocity of sound is given by $\mathbf{c}(\mathbf{k}) = \frac{1}{\hbar} \nabla_{\mathbf{k}} E(\mathbf{k})$ and therefore dependent on the position in \mathbf{k} -space.

We will look for localized modes, if the number of neighbours is limited to the 4 atoms adjacent to the vacancy and for the case, where also the next nearest neighbours are participating in the localized mode. The result of the analysis is shown in Figure 5.10, where we see that the modes with $x_{loc} > 3$ are present in the frequency range of 14 THz to 22 THz. The maximum value of x_{loc} being 14 for a frequency of $\nu \approx 18$ THz. Taking a look at the symmetry of the vibrations, we see that the strongest localization is present for breathing modes, transforming as a_1 . The frequencies of the localized modes are in good agreement with another *ab initio* study by Gali, Simon, and Lowther (2011) and the measured rates presented in subsection 4.11.1.

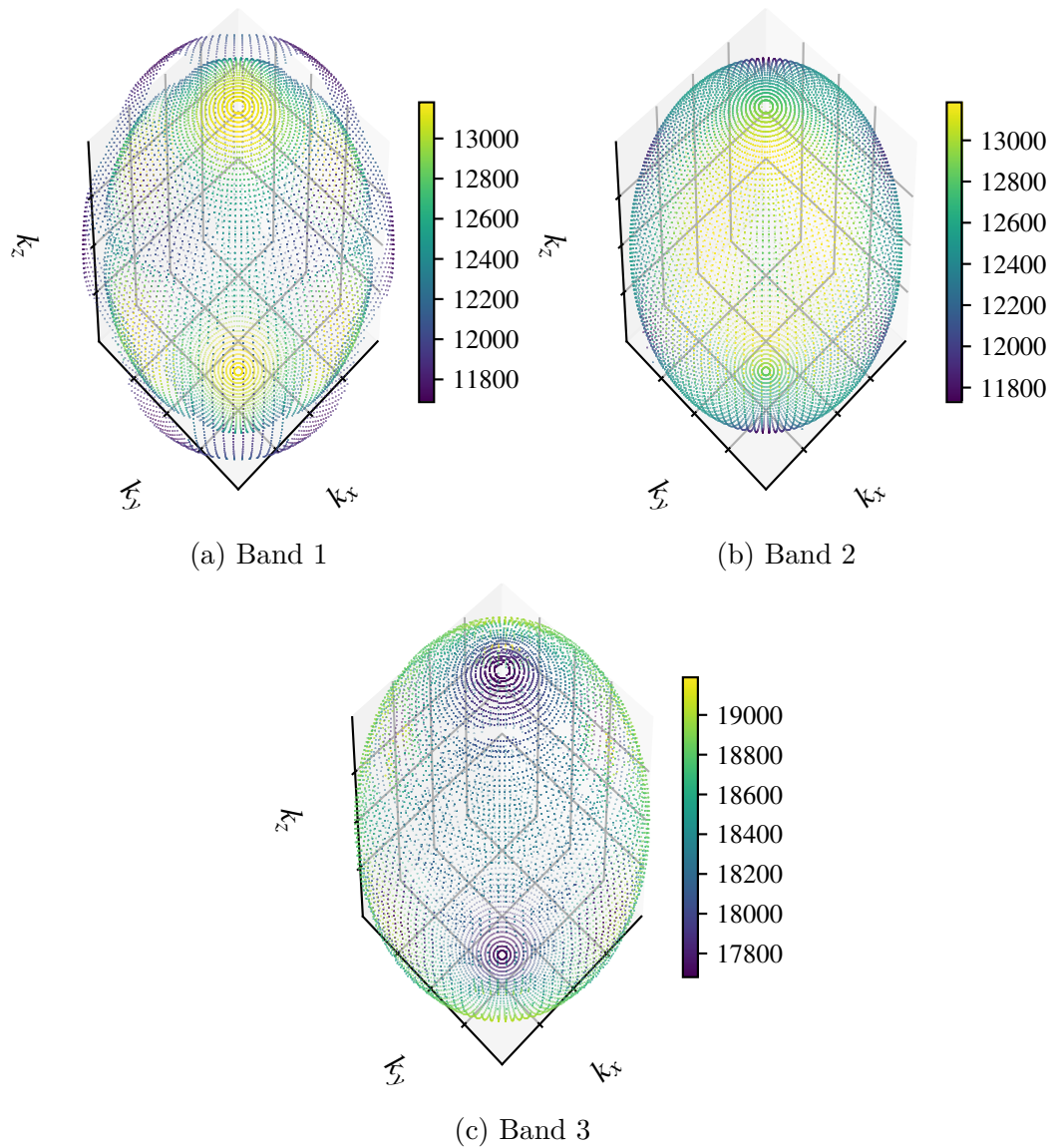
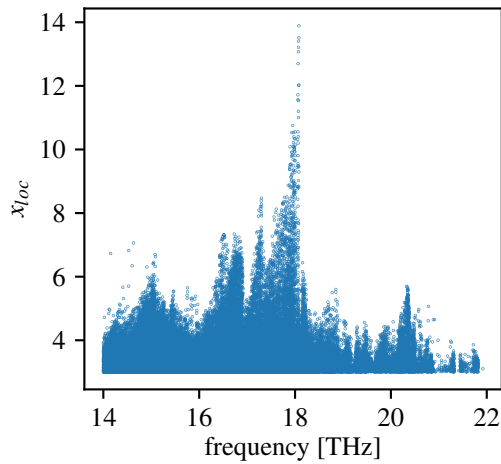
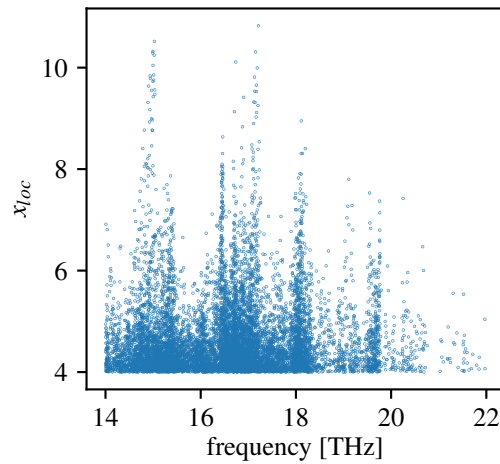


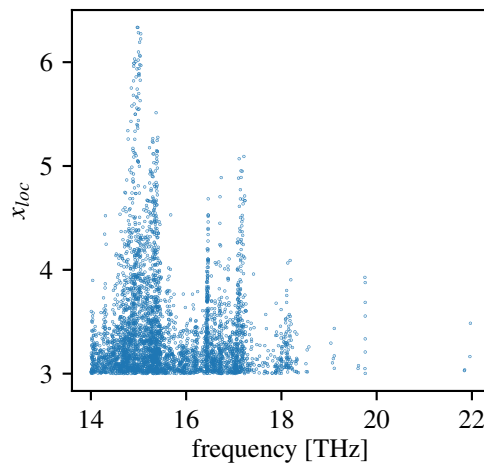
Figure 5.9: 0.1 THz-isosurface and group velocity, The isosurface of the 0.1 THz phonons, colored with the respective group velocity. We see, that the group velocities for different directions differ by up to 10 %.



(a) 64-atom cell - 4 neighbours



(b) 512-atom cell - 4 neighbours



(c) 512-atom cell - 16 neighbours

Figure 5.10: x_{loc} **analysis**, The random sampling of \mathbf{q} vectors in the first Brillouin zone yields modes with a localization factor > 3 only in the plotted frequency range. The criteria of localization for the upper plots (a and b) are a big displacement of the 4 nearest neighbouring atoms and a big displacement of the next nearest neighbours in the bottom plot (c).

5.2 The electronic properties of the NV⁻ center

In order to calculate the matrix elements for a transition between two m_s spin states in Equation (4.49), we have to calculate the matrix elements involving different powers and directions of the position operator \mathbf{r}_{ij} between two m_s states. A proper description of the relevant orbitals is thus necessary. As already stated in the introduction, the electronic properties of the NV⁻ center are well described by a 4 orbital model²: If the localized orbitals on the carbons and nitrogen atoms are denoted by c_i and n respectively, the orbitals of the center transforming according to the denoted representation of the C_{3v} group are given by

$$a_1(N) = n \quad (5.4)$$

$$a_1(C) = \frac{1}{\sqrt{3}\sqrt{1 + 2S_{cc} - 3S_{nc}^2}}(c_1 + c_2 + c_3 - 3S_{nc}n) \quad (5.5)$$

$$e_x = \frac{1}{\sqrt{3}\sqrt{2 - 2S_{cc}}}(2c_1 - c_2 - c_3) \quad (5.6)$$

$$e_y = \frac{1}{\sqrt{2 - 2S_{cc}}}(c_2 - c_3), \quad (5.7)$$

where S_{nc} and S_{cc} are the overlaps between the orbitals. The bandstructure plotted in Figure 5.11 is obtained by using the density of a HSE06 calculation and the structure of a PBE calculation, as a relaxation with HSE06 is computationally expensive. The calculations reveal that the bands arising due to orbitals located at the NV⁻ center interact with the neighbouring NV⁻ centers due to the periodic boundary conditions. The corresponding Bloch wavefunctions at a single \mathbf{k} -point are plotted in Figure 5.12, where we see that the spin polarized e_x and e_y orbitals as well as one of the $a_1(C)$ orbitals are localized and do not hybridize with the diamond bands, whereas the second $a_1(N)$ orbital hybridizes strongly with the bulk bands. To get rid of the translational invariant description and the spurious interaction with neighbouring NV⁻ centers, we will convert the description of the wavefunctions from \mathbf{k} -space to real space by using maximally localized Wannier functions.

²see for example Doherty et al. (2011)

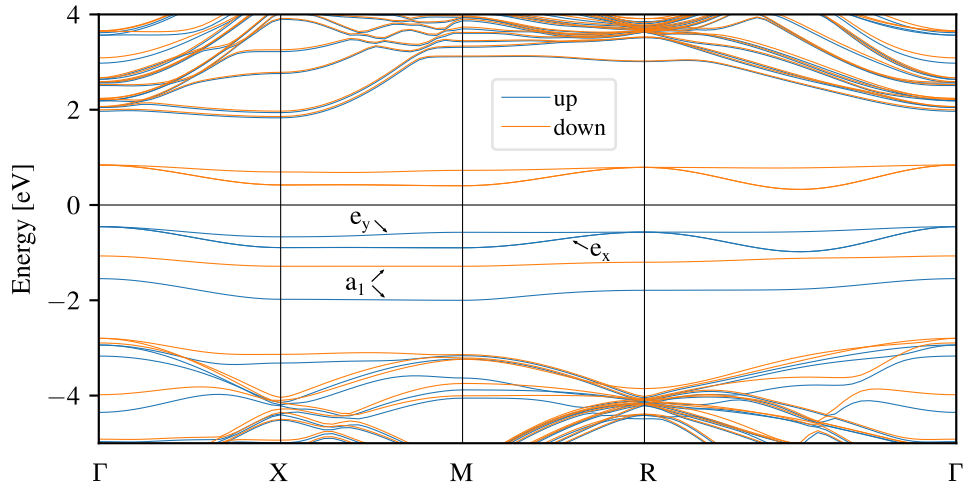


Figure 5.11: **Bandstructure of the NV⁻ center**, the spin polarized bands of the center are shown for a given path of high symmetry lines in \mathbf{k} -space. We can clearly see, that the e_x and e_y bands show a non-flat dispersion, resulting from the interaction with neighbouring cell wavefunctions.

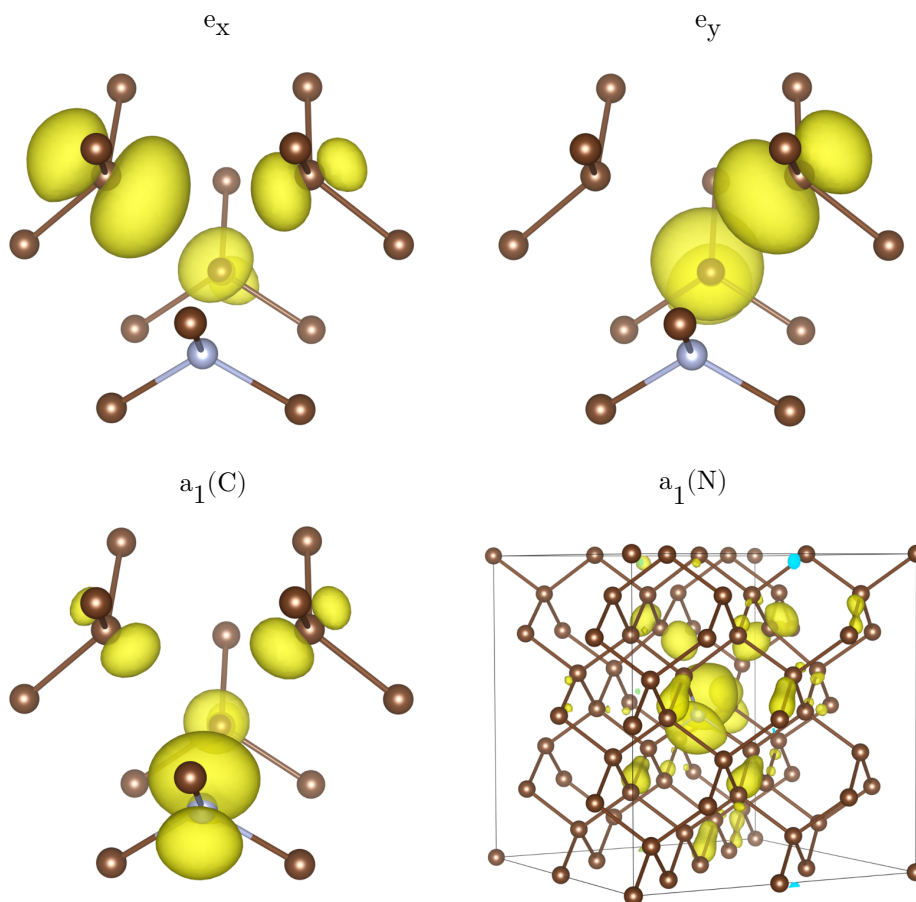


Figure 5.12: **Electronic orbitals of the NV⁻ center**. Shown are isosurfaces for the absolute value of the wavefunction.

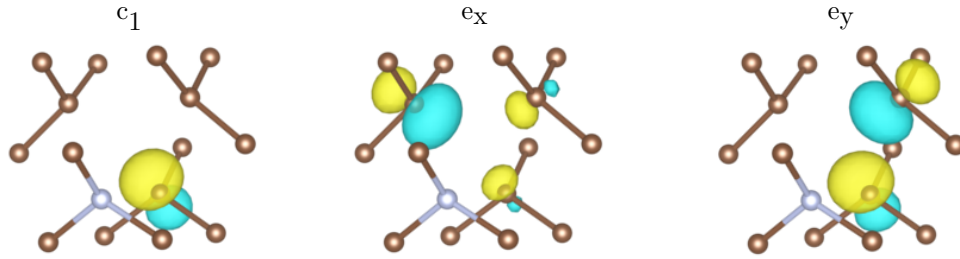


Figure 5.13: **Maximally localized Wannier functions**, the left panel shows the MLWF centered on a carbon atom and the other two panels visualize the resulting molecular orbitals e_x and e_y .

5.2.1 Maximally localized Wannier functions at the NV^- center

For the transition inside the 3A_2 ground state spin triplet, only the e_x and e_y orbitals have to be extracted. We will describe these spin states by calculating the maximally localized Wannier functions, located at the carbon atoms adjacent to the vacancy and will then add them up to fulfill the symmetry constraints. For the extraction of the orbitals, we use the bands which contain the localized states and end up with orbitals shown in Figure 5.13. A crucial point here is the choice of the bands containing the $a_1(N)$ orbital. The hybridization of this orbital with the diamond bulk bands is shown in Figure 5.12, where the site-projected density of states at the nitrogen atom is plotted for three different functionals. The peak arises from the $a_1(C)$ orbital, which has a big projected density of states on the nitrogen atom. In the case of the SCAN and PBE functional, the hybridization of the $a_1(N)$ orbital is very pronounced for a single band, whereas in the case of the HSE06 functional, this hybridization is visible for a number of bands, which thus have to be included in the wannierization procedure. The difference between the Bloch wavefunctions and the MLWFs is small for \mathbf{k} points, where the degeneracy between e_x and e_y is lifted but may be huge in the proximity of high symmetry points, where the orbitals are degenerate. The localization procedure leads to a smearing out of directional influences on the wavefunctions and therefore hopefully gives a better representation of the wavefunctions in real space.

5.3 Moving orbitals

One problem of the current theory is the arbitrariness of the volume around each ion, in which the electronic orbitals will follow the movements of the

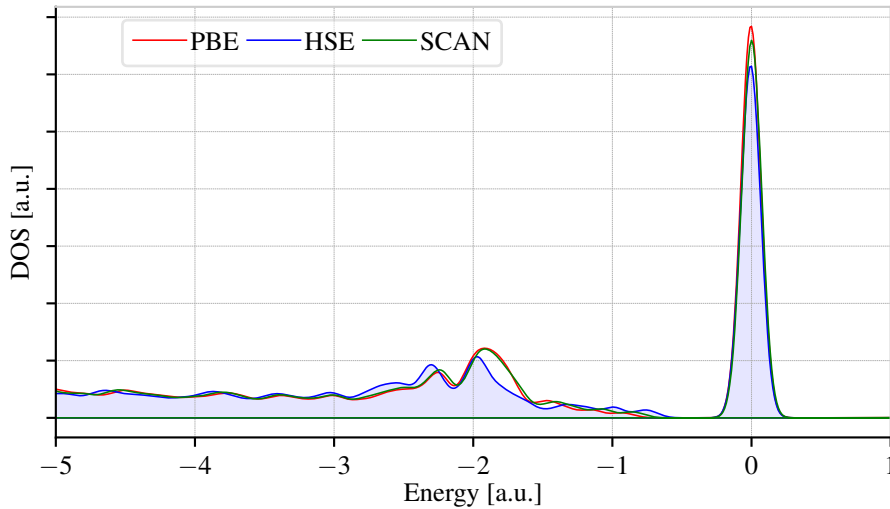


Figure 5.14: **Electron density of states at the nitrogen atom**

ions rigidly. In order to make the theory predictive, we will investigate on the moving region and check which volume partitioning is a realistic representation of nature.

5.3.1 Bader analysis

First we follow the chemists' convention to define an atom within a molecule by performing a Bader analysis: In his book *Atoms in molecules* Bader (1995) considered the separation of atoms based on the topological behaviour of the charge density $n(\mathbf{r})$. The charge density has local maxima at the positions of the nuclei, which come with a cusp as shown by Kato (1957). These maxima serve as attractors if we follow a trajectory $\mathbf{R}(t)$, constructed by choosing a starting point \mathbf{R}_0 and consecutively following the direction of the gradient of the charge density given by

$$\mathbf{R}(t) = \mathbf{R}_0 + \int_0^t \nabla n(\mathbf{R}(t')) dt' \quad . \quad (5.8)$$

An atom is now defined as the region Ω containing one point maximum of charge density and all the starting points, where the trajectories either end in the point maximum or in any surface between two maximum points. The boundary between two atoms is therefore determined by a surface S with normal vectors $\mathbf{n}(\mathbf{r})$, where the zero flux condition

$$\nabla n(\mathbf{r}) \cdot \mathbf{n}(\mathbf{r}) = 0 \quad \forall \mathbf{r} \in S \quad (5.9)$$

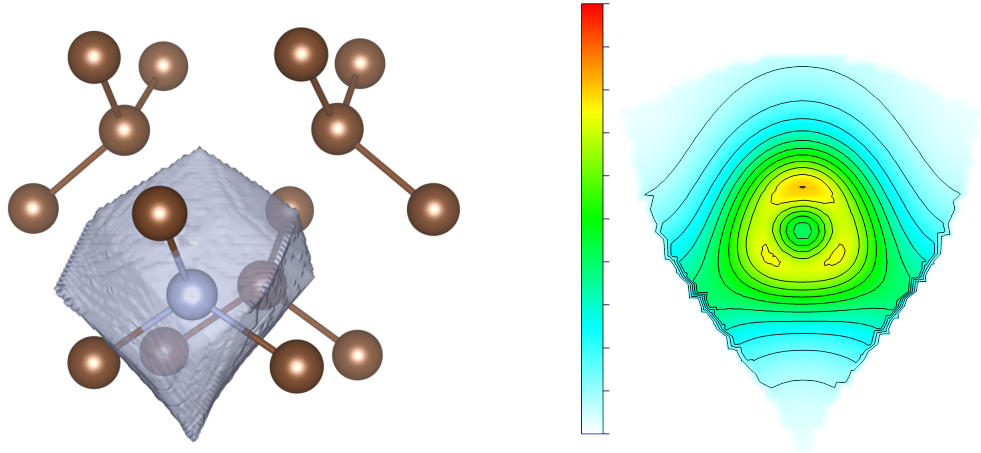


Figure 5.15: **Bader volume and charge density along the [111] direction of the nitrogen atom**

is fulfilled. Bader has shown, that the volumes Ω are suitable definitions of atoms even from a quantum mechanical point of view, because it allows for a definition of an average kinetic energy of an atom due to the fact that boundary integrals contain an integral over the zero-flux surfaces (for details see Bader, 1995, p. 176). For the Bader analysis we use the code developed by the Henkelman group (Tang, Sanville, and Henkelman (2009)) and end up with Bader volumes for all our atoms, one of which is shown in Figure 5.15.

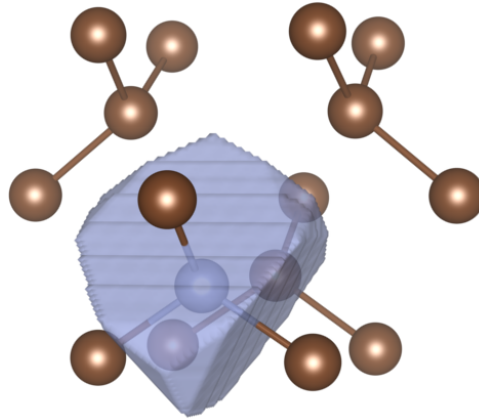
5.3.2 Geometrical separation

The second approach is to divide the volume in analogy to Wigner-Seitz cells by geometrical means. All the points which are closest to atom X belong to that atom, no matter how the charge distribution looks like. In our case, this picture may also yield good results because the nuclear charges of nitrogen and carbon do not differ drastically and the main contribution of the relevant orbitals resides on the carbon atoms.

5.3.3 Results for the Waller process

Using the obtained wavefunctions and the volumes of the previous subsection, we are in a position where we can calculate the five matrix elements of an initial electronic state $|m_s^i\rangle$ to a final state $|m_s^f\rangle$

$$\begin{aligned}
 I : & \quad \langle m_s^f | \Delta \Theta_{ij}^m \frac{3(r^x \mp ir^y)}{2|\mathbf{r}_{ij}|^5} | m_s^i \rangle \\
 II : & \quad \langle m_s^f | \Delta \Theta_{ij}^m \frac{3r^z}{2|\mathbf{r}_{ij}|^5} | m_s^i \rangle
 \end{aligned}$$

Figure 5.16: **Wigner-Seitz cell of the nitrogen atom**

Functional	Polarization-frequency	Group velocity	Moving Volume	Result [s^{-1}]
PBE	2.88 GHz	Diamond	Bader	1×10^{-5}
HSE	2.88 GHz	Diamond	Bader	2.24×10^{-5}
SCAN	100 GHz	Diamond	Bader	1.92×10^{-5}
PBE	100 GHz	Diamond	Bader	1.05×10^{-5}
HSE	100 GHz	Diamond	Wigner-Seitz	2.03×10^{-5}
SCAN	100 GHz	Diamond	Bader	1.76×10^{-5}

Table 5.2: Waller relaxation rates for the different theoretical approaches.

$$III - V : \quad \langle m_s^f | \Delta \Theta_{ij}^m \frac{15(r^x \mp ir^y)r^z r_i}{2|\mathbf{r}_{ij}|^7} | m_s^i \rangle \quad .$$

The matrix elements are multiplied by their respective components of the phonon polarization vectors for each ion. The sum over all polarization vectors is evaluated by accounting for the number of phonons by using a Debye model with the local velocities of sound, s.t. we account for the anisotropy of the phonon dispersion. The results depend on the supercell size, the exchange and correlation potential, the polarization vectors, the local speed of sound and the moving volumes. The calculated results for the largest feasible supercell, containing 512 lattice sites are shown in Table 5.2.

5.4 Ab initio Calculation of Γ_0 for the Elliott-Yafet process

This section is concerned with a quantification of the spin-orbit driven spin-lattice relaxation in the NV^- center. The starting point for the investigation

is the expression

$$\begin{aligned} \mathcal{H}_{\text{e-ph}}^{(2)} = & i\xi \sum_l \sum_{\mu, \mathbf{k}' \mu'} \sum_{\mathbf{q}, \lambda} l_{\mathbf{q}, \lambda}^l A_{\mathbf{q}, \lambda} \tilde{v}_{\text{eff}}(\mathbf{q}) c_{\mu \mathbf{k}' + \mathbf{q}}^\dagger c_{\mu' \mathbf{k}'} \left(\boldsymbol{\epsilon}_{\mathbf{q}, \lambda}^l \cdot \mathbf{q} \right) \cdot \\ & \cdot \frac{1}{\Omega} \int_{\Omega} d^3 r u_{\mu \mathbf{k}' + \mathbf{q}}^*(\mathbf{r}) [\mathbf{q} \times (\hat{\mathbf{p}} + \hbar \mathbf{k}')] \cdot \hat{\mathbf{s}} u_{\mu' \mathbf{k}'}(\mathbf{r}) \quad , \end{aligned} \quad (4.66)$$

which was derived in analogy to Baral et al. (2016) and Vollmar, Hilton, and Schneider (2017). The calculation of the phonons was already done in the previous section, so the only quantity to be calculated here is the matrix element

$$\frac{1}{\Omega} \int_{\Omega} d^3 r u_{\mu \mathbf{k}' + \mathbf{q}}^*(\mathbf{r}) [\hat{p}_j + \hbar k'_j] \cdot \hat{s}_k u_{\mu' \mathbf{k}'}(\mathbf{r}) \quad . \quad (5.10)$$

In the case of the NV^- center, the transition frequency between the triplet states only allows for a small \mathbf{q} and the broken periodicity for the defect results in a single \mathbf{k}' at the Γ point. Thus, we need to find the spinor wavefunctions $u_{\mu \mathbf{0}}$, that represent the spin-transition measured in the experiment. As we did not arrive at the correct wavefunctions up to now, we will present preliminary results, obtained by a \mathbf{k} -mesh, where each \mathbf{k} -point has a broken degeneracy for the e_x and e_y spinors. We construct the wavefunction to be in a superposition of Bloch-waves transforming as the a_1 representation, s.t. the representation of the resulting spinors is unchanged due to the assumption of periodic boundary conditions. Using these spinor wavefunctions, we calculate the gradients to obtain the momentum operator³. Using the expression of $\mathcal{H}_{\text{e-ph}}^{(2)}$ in Fermi's Golden rule results in a relaxation rate $9.0 \times 10^{-7} \text{ s}^{-1}$ and thus is smaller than the rates calculated in the previous chapter for the relaxation driven by the change of the spin-spin interaction. However, the calculated results are not published and taken to be a preliminary approach for a very demanding calculation, where a number of verification steps are still missing. Due to the smallness of the spin-orbit strength in the NV^- center, extensive care has to be taken to arrive at quantitative results.

5.4.1 Comparison with experiment

The results show that the calculation is able to explain the order of magnitude of the relaxation rate and that the highest obtainable rates are in proximity of the measured results for electron irradiated samples, as Figure 5.17a shows. For the case of the neutron irradiated sample, the measured relaxation rates

³The implementation of the gradient calculation in VASP was redone to fit our purposes by Prof. Andreas Grüneis, who shall be acknowledged for his help at this position.

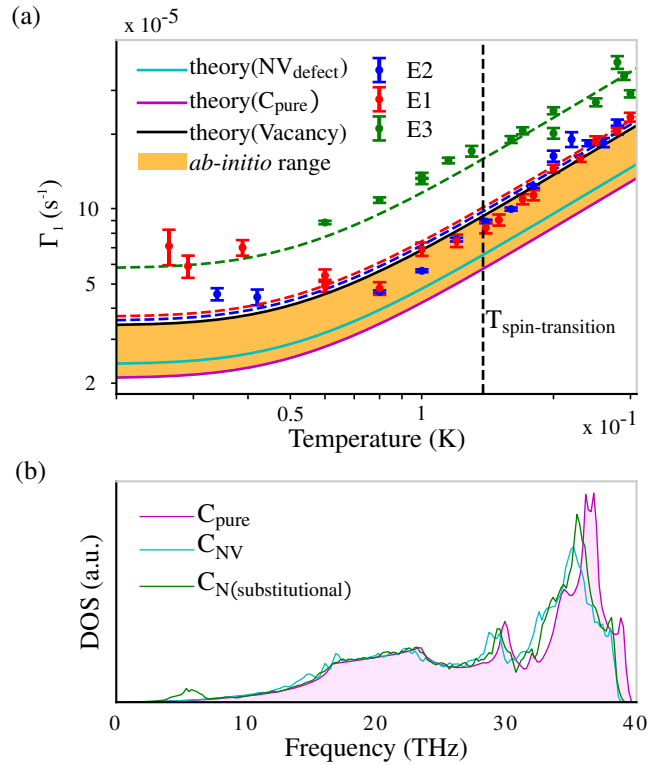


Figure 5.17: **Rates and phonon density of states,**

are an order of magnitude higher (sample H1b in Figure 4.4), which we explain by the high impact of neutron irradiation: If a neutron hits a carbon atom during irradiation, an average energy of 140 eV to 140 keV is transferred, s.t. a region of disorder of $\approx 45 \text{ \AA}$ is left behind⁴. The subsequent annealing procedure should cure some structural damage, however, our simulations indicate that the phonon spectrum is shifted towards lower frequencies, if the lattice structure is disturbed. The effect on the density of states is depicted in Figure 5.17b for the case of a NV^- center and a substitutional nitrogen atom. The theoretical understanding of this shift is most easily given by taking a look at equation (5.11): If we transform the sum over all the final states in our system to a sum over all the involved modes, we can use the thermodynamic limit and the Debye model, to see that the density of states is connected to the inverse of c^3 .

$$\sum_f \rightarrow \sum_{\mathbf{k}, \lambda} \rightarrow \frac{V}{(2\pi)^3} \int d^3k \rightarrow \frac{V}{(2\pi)^3} \int d^3(\omega/c) \rightarrow \frac{4\pi V}{c^3} \int \nu^2 d\nu \quad (5.11)$$

A big structural change in a diamond crystal will destroy the strongly bound structure and soften the material (experimentally seen by Damask (1958)), which yields a lower velocity of sound and thus increases the number of low

⁴data taken from Nöbauer et al. (2013) and Damask (1958)

energy phonons available for a spin flip. These considerations suggest, that the crystal structure has a big influence on the resulting relaxation rates and explains, why the electron spin-lattice relaxation times in diamond are among the longest ever observed.

References

- Bader, R. F. W. (1995). *Atoms in molecules*. Wiley.
- Baral, A. et al. (2016). “Re-examination of the Elliott–Yafet spin-relaxation mechanism”. In: *New Journal of Physics* 18, p. 023012.
- Damask, A. C. (1958). “Hardness of Neutron-Irradiated Diamonds”. In: *Journal of Applied Physics* 29.11, pp. 1590–1593.
- Doherty, M. W. et al. (2011). “The negatively charged nitrogen-vacancy centre in diamond: the electronic solution”. In: *New Journal of Physics* 13, p. 025019.
- Gali, A., M. Fyta, and E. Kaxiras (2008). “*Ab initio* supercell calculations on nitrogen-vacancy center in diamond: Electronic structure and hyperfine tensors”. In: *Phys. Rev. B* 77 (15), p. 155206.
- Gali, A., T. Simon, and J. E. Lowther (2011). “An *ab initio* study of local vibration modes of the nitrogen-vacancy center in diamond”. In: *New Journal of Physics* 13, p. 025016.
- Kato, T. (1957). “On the eigenfunctions of many-particle systems in quantum mechanics”. In: *Communications on Pure and Applied Mathematics* 10.2, p. 151.
- Monkhorst, H. J. and J. D. Pack (1976). “Special points for Brillouin-zone integrations”. In: *Phys. Rev. B* 13 (12), pp. 5188–5192.
- Nöbauer, T. et al. (2013). *Creation of ensembles of nitrogen-vacancy centers in diamond by neutron and electron irradiation*.
- Tang, W., E. Sanville, and G. Henkelman (2009). “A grid-based Bader analysis algorithm without lattice bias”. In: *J. of Physics* 21.8, p. 084204.
- Vollmar, S., D. J. Hilton, and H. C. Schneider (2017). “Generalized Elliott–Yafet spin-relaxation time for arbitrary spin mixing”. In: *Phys. Rev. B* 96 (7), p. 075203.

Chapter 6

Summary and outlook

In this thesis, we introduced the negatively charged nitrogen vacancy center as a quantum system with many potential applications and motivated the importance of an understanding of the spin-dynamics in this system. The theoretical toolkit for the treatment of the electrons and ions on a quantum mechanical level was derived and the spin of the electron was coupled to the movement of the ions. Out of the vast amount of spin-phonon couplings, only two, which could be responsible for the spin-lattice relaxation in the NV^- center, were calculated and the resulting relaxation rates agree well with the experimental observations for the case of the spin-relaxation due to a change in the dipolar spin-spin interaction between the electrons, when the ions are moving. The calculated temperature dependence of the relaxation rate motivated the measurement of the lifetime for temperatures below the spin-transition, where a coupling of the spins to the phononic vacuum was observed, resulting in a finite relaxation time in the limit $T \rightarrow 0$. This limit is governed by the spontaneous emission of phonons. This work lays the foundation for a numerical treatment of higher order relaxation mechanisms, which were introduced in this thesis and turn out to be rather difficult to be evaluated analytically. A full understanding of the spin-relaxation may allow for a tailoring of the spin-properties by a reduction of the relevant phonon modes with phononic band gaps. As $2T_1$ is the ultimate limit of the spin-coherence time T_2 , this may expand the field of applications of the NV^- center.

Appendix A

Response functions

A.1 Linear Response

In order to deal with the weakly inhomogeneous electron gas, the response of the density to an external perturbation has to be modeled. As we will see, this is conveniently done with response functions, whose application will be motivated in this section and their properties will be described in section A.2. In the case of the jellium model, the perturbing potential is caused by a redistribution of the positive background charge

$$\delta v(\mathbf{r}) = - \int d^3r' w(\mathbf{r} - \mathbf{r}') \delta n_+(\mathbf{r}), \quad (\text{A.1})$$

giving rise to the Hamiltonian

$$\hat{\mathcal{H}} = \underbrace{\hat{T} + \hat{W}}_{\hat{\mathcal{H}}_0} + \underbrace{\int d^3r \hat{n}(\mathbf{r}, t) \delta v(\mathbf{r})}_{\hat{\mathcal{H}}_I}, \quad (\text{A.2})$$

which consists of the unperturbed Hamiltonian $\hat{\mathcal{H}}_0$ and the perturbation $\hat{\mathcal{H}}_I$. The influence of the perturbation potential on the time evolution of the wavefunctions is modeled in the interaction picture, where the time evolution of wavefunctions and operators is given by the perturbed and unperturbed Hamiltonian, respectively. This is achieved by assuming a wavefunction of the form

$$|\Psi_I(t)\rangle = e^{i\mathcal{H}_0 t/\hbar} |\Psi_S(t)\rangle, \quad (\text{A.3})$$

where $|\Psi_S(t)\rangle$ is the wavefunction in the Schrödinger picture. The equation of motion of this state is given by a Schrödinger equation, where the Hamiltonian

consists of the time-evolved perturbation only:

$$i\hbar\partial_t |\Psi_I(t)\rangle = e^{i\hat{\mathcal{H}}_0 t/\hbar} (i\hbar\partial_t - \hat{\mathcal{H}}_0) |\Psi_S(t)\rangle \quad (\text{A.4})$$

$$= e^{i\hat{\mathcal{H}}_0 t/\hbar} (\hat{\mathcal{H}} - \hat{\mathcal{H}}_0) |\Psi_S(t)\rangle \quad (\text{A.5})$$

$$= \underbrace{e^{i\hat{\mathcal{H}}_0 t/\hbar} \hat{\mathcal{H}}_I e^{-i\hat{\mathcal{H}}_0 t/\hbar}}_{=\hat{\mathcal{H}}_I(t)} |\Psi_I(t)\rangle \quad (\text{A.6})$$

The time evolution operator $\mathcal{U}(t, t_0)$, which relates the interacting wavefunction at the times t_0 and t may be derived by inserting the ansatz

$$|\Psi_I(t)\rangle = \mathcal{U}(t, t_0) |\Psi_I(t_0)\rangle \quad (\text{A.7})$$

in the Schrödinger equation for the wavefunction (A.4-A.6):

$$i\hbar\partial_t \mathcal{U}(t, t_0) |\Psi_I(t_0)\rangle = i\hbar\partial_t (\mathcal{U}(t, t_0)) |\Psi_I(t_0)\rangle = \hat{\mathcal{H}}_I(t) \mathcal{U}(t, t_0) |\Psi_I(t_0)\rangle \quad (\text{A.8})$$

$$\rightarrow i\hbar\partial_t \mathcal{U}(t, t_0) = \hat{\mathcal{H}}_I(t) \mathcal{U}(t, t_0). \quad (\text{A.9})$$

This equation may be solved by integration

$$\int_{t_0}^t dt' \partial_t \mathcal{U}(t, t_0) = \int_{t_0}^t dt' \hat{\mathcal{H}}_I(t') \mathcal{U}(t', t_0) \quad (\text{A.10})$$

$$\mathcal{U}(t, t_0) = \underbrace{\mathcal{U}(t, t_0)}_{=\mathbb{1}} - \frac{i}{\hbar} \int_{t_0}^t dt' \hat{\mathcal{H}}_I(t') \mathcal{U}(t', t_0) \quad (\text{A.11})$$

and subsequent repetitions of this formula gives an expression for the time evolution operator:

$$\mathcal{U}(t, t_0) = \mathbb{1} + \frac{-i}{\hbar} \int_{t_0}^t dt' \hat{\mathcal{H}}_I(t') + \left(\frac{-i}{\hbar}\right)^2 \int_{t_0}^t dt' \int_{t_0}^{t'} dt'' \hat{\mathcal{H}}_I(t') \hat{\mathcal{H}}_I(t'') + \dots \quad (\text{A.12})$$

Since the perturbation to the jellium model is supposed to be small, we only take the first order term of this series into account, when calculating the perturbed density in the interaction picture. Turning on the perturbation at $t_0 = -\infty$, where we start with the unperturbed wavefunction $|\Psi_I^0\rangle = |\Psi_I(-\infty)\rangle$, we obtain

$$\langle \Psi_I(t) | \hat{n}(\mathbf{r}, t) | \Psi_I(t) \rangle = \langle \Psi_I(-\infty) | \mathcal{U}^\dagger(t, -\infty) \hat{n}(\mathbf{r}, t) \mathcal{U}(t, -\infty) | \Psi_I(-\infty) \rangle \quad (\text{A.13})$$

and therefore the change in the electronic density $\delta\hat{n}(\mathbf{r}, t) = \hat{n}(\mathbf{r}, t) - n_0(\mathbf{r})$ is given by

$$\delta\hat{n}(\mathbf{r}, t) = \int_{-\infty}^t dt' \langle \Psi_I^0 | \frac{i}{\hbar} [\hat{\mathcal{H}}_I(t'), \hat{n}(\mathbf{r}, t)] | \Psi_I^0 \rangle \quad (\text{A.14})$$

inserting the perturbation $\hat{\mathcal{H}}_I(t)$ from equation (A.2)

$$= \int d^3r' \int_{-\infty}^t dt' \langle \Psi_I^0 | [\hat{n}(\mathbf{r}', t'), \hat{n}(\mathbf{r}, t)] | \Psi_I^0 \rangle \delta v(\mathbf{r}') \quad (\text{A.15})$$

To simplify the response and be able to write it as a convolution, it is convenient to define the generalized retarded susceptibility

$$\chi_R(\mathbf{r}, t; \mathbf{r}', t') = \Theta(t - t') \frac{-i}{\hbar} \langle \Psi_I^0 | [\hat{n}(\mathbf{r}, t), \hat{n}(\mathbf{r}', t')] | \Psi_I^0 \rangle, \quad (\text{A.16})$$

which is only dependent on the time difference $t - t'$ because

$$\langle \Psi_I^0 | \hat{n}(\mathbf{r}, t) \hat{n}(\mathbf{r}', t') | \Psi_I^0 \rangle = \langle \Psi_I^0 | e^{i\hat{\mathcal{H}}_0 t/\hbar} \hat{n}(\mathbf{r}) e^{-i\hat{\mathcal{H}}_0 t/\hbar} e^{i\hat{\mathcal{H}}_0 t'/\hbar} \hat{n}(\mathbf{r}') e^{-i\hat{\mathcal{H}}_0 t'/\hbar} | \Psi_I^0 \rangle \quad (\text{A.17})$$

$$= \langle \Psi_I^0 | \hat{n}(\mathbf{r}) e^{-i\hat{\mathcal{H}}_0(t-t')/\hbar} \hat{n}(\mathbf{r}') | \Psi_I^0 \rangle e^{iE_0(t-t')/\hbar} \quad (\text{A.18})$$

$$\rightarrow \chi_R(\mathbf{r}, t; \mathbf{r}', t') = \chi_R(\mathbf{r}; \mathbf{r}', t - t') \quad (\text{A.19})$$

This time dependence is most easily exploited by taking the Fourier transform of the susceptibility

$$\chi_R(\mathbf{r}; \mathbf{r}', \omega) = \int_{-\infty}^{\infty} d(t - t') e^{i\omega(t-t')} \chi_R(\mathbf{r}; \mathbf{r}', t - t') \quad (\text{A.20})$$

since it restricts the time dependence to one single frequency variable ω . This function allows us to rewrite equation (A.15) in order to stress the response of the density as a convolution of the perturbation potential and the susceptibility

$$\delta n(\mathbf{r}) = \int d^3r' \chi_R(\mathbf{r}; \mathbf{r}', \omega = 0) \delta v(\mathbf{r}') \quad (\text{A.21})$$

This is the linear response to the perturbation we are using in the main text, where the homogeneity of the jellium model is exploited and the response function is therefore assumed to be dependent only on the difference of two positions, allowing for another Fourier transform of the susceptibility

$$\chi_R(\mathbf{q}, \omega) = \int d^3(r - r') e^{i\mathbf{q}(r-r')} \chi_R(\mathbf{r} - \mathbf{r}', \omega) \quad (\text{A.22})$$

and the convolution in equation (A.21) becomes a pure multiplication in Fourier space

$$\delta n(\mathbf{q}) = \chi_R(\mathbf{q}, \omega = 0) \delta v(\mathbf{q}). \quad (\text{A.23})$$

A.2 Properties of response functions

As we have seen, the retarded response function is of great importance, since it is the convolution kernel for a density response. Another useful density response function is the time-ordered response function

$$\chi(\mathbf{r}t, \mathbf{r}'t') = \frac{-i}{\hbar} \langle \Psi_0 | \hat{T} \delta \hat{n}(\mathbf{r}t) \delta \hat{n}(\mathbf{r}'t') | \Psi_0 \rangle \quad (\text{A.24})$$

where \hat{T} is the time-ordering operator which shifts all operators acting at earlier times to the right and later acting operators to the left. This response function is especially important because it obeys the Dyson equation

$$\chi(\mathbf{q}, \omega) = \Pi(\mathbf{q}, \omega) + \Pi(\mathbf{q}, \omega) v_{ee}(\mathbf{q}) \chi(\mathbf{q}, \omega), \quad (\text{A.25})$$

which is important for a perturbation series, because a repetition of equation (A.25)

$$\begin{aligned} \chi(\mathbf{q}, \omega) = & \Pi(\mathbf{q}, \omega) + \Pi(\mathbf{q}, \omega) v_{ee}(\mathbf{q}) \Pi(\mathbf{q}, \omega) \\ & + \Pi(\mathbf{q}, \omega) v_{ee}(\mathbf{q}) \Pi(\mathbf{q}, \omega) v_{ee}(\mathbf{q}) \Pi(\mathbf{q}, \omega) + \dots \end{aligned} \quad (\text{A.26})$$

shows that χ can be computed, knowing the building blocks Π of this series, which can be calculated using Feynman diagrams. While χ is easier to calculate than χ_R , the latter is simpler to interpret physically since it was derived from linear response. As a calculation of the exchange and correlation energy functional in the gradient expansion only requires $\chi_R(\mathbf{q}, \omega = 0)$, it is a relieving fact that this equals $\chi(\mathbf{q}, \omega = 0)$.¹

¹The proof thereof is found in the book of Engel and Dreizler (2011)

Appendix B

A short introduction to group theory

This section summarizes the most important formulas of group theory. Derivations of the stated mathematical formulas can be found in Dresselhaus, Dresselhaus, and Jorio (2008). A symmetry operation is an operation that leaves the system invariant. Famous examples of symmetry operations in physics are rotations, inversions, reflections and time reversals. Symmetry operations are described by the mathematical apparatus of group theory, because they usually obey the rules that describe a group: For all elements (g_1, g_2, g_3, \dots) in the group \mathcal{G} , the following axioms must hold

$$g_i \in \mathcal{G}, g_j \in \mathcal{G} \rightarrow g_k = g_i g_j \in \mathcal{G} \quad \forall i, j, k \quad (\text{closure}) \quad (\text{B.1})$$

$$(g_i g_j) g_k = g_i (g_j g_k) \quad (\text{associativity}) \quad (\text{B.2})$$

$$\exists e : g_i e = e g_i = g_i \quad (\text{existence of neutral element}) \quad (\text{B.3})$$

$$\exists g_i^{-1} : g_i g_i^{-1} = e \quad \forall i \quad (\text{existence of inverse element}) \quad (\text{B.4})$$

The product of two elements of the group therefore yields another element in the group. All the products of group elements may be summarized in a multiplication table. The elements of the group may be represented by matrices $D(g_i)$, if matrix multiplication preserves the structure of the multiplication table

$$g_i g_j = g_k \rightarrow D(g_i) D(g_j) = D(g_k) \quad (\text{B.5})$$

If there exists a subspace in all the representing matrices, that is invariant under the action of the group elements, the matrices will show a block structure and we call this representation reducible. If no such subspace exists,

the representation is called irreducible. The irreducible representations play an important role in group theory, because they are the building blocks of a general representation. As we will see, they also provide an important orthogonality relation, which allows to diagonalize a Hamiltonian only by means of symmetry.

The irreducibility of a representation is not easily seen, because every similarity transformation of the matrices will yield a new equivalent representation. Consider for example the rotation around the z -axis, which leaves all the z -components of the vectors invariant. In the Cartesian basis, where the vector \mathbf{e}_3 is pointing in z -direction, the rotation takes the form

$$D^z(\phi) = \begin{pmatrix} \cos(\phi) & -\sin(\phi) & 0 \\ \sin(\phi) & \cos(\phi) & 0 \\ 0 & 0 & 1 \end{pmatrix}. \quad (\text{B.6})$$

This may be rewritten as the direct matrix sum $D^z = D_2 \oplus D_1$, which highlights the block structure of this matrix. Choosing a different basis, this block structure will be lost. This makes finding the irreducible representations complicated. The problem of the similarity transformations may be solved, by considering the fact that the trace of a matrix is invariant under every similarity transformation. The trace of a representation matrix is called its character. Two elements of a group g_1, g_2 are called conjugate, if there exists a g_k , s.t.

$$g_1 = g_k g_2 g_k^{-1}. \quad (\text{B.7})$$

Conjugacy is an equivalence relation and the elements, which are conjugate with each other are said to be in the same class. The representations of the elements of the same class will have the same character, because equation (B.7), stated in matrix form is a similarity transformation. The number of irreducible representations equals the number of classes. In the case of the translation group, the elements commute and therefore each translation is a class itself and the number of irreducible representations equals the number of available translations. The physical interest in group theory arises from the fact, that there exists an orthogonality relation (the *Wonderful Orthogonality Theorem*) for irreducible inequivalent representations

$$\sum_i D_{\mu\nu}^{(\Gamma_j)}(g_i) D_{\mu'\nu'}^{(\Gamma_j)}(g_i^{-1}) = \frac{h}{l_j} \delta_{\Gamma_j \Gamma_j'} \delta_{\mu\mu'} \delta_{\nu\nu'}. \quad (\text{B.8})$$

Here the sum is over all the h elements of the group, Γ denotes the irreducible representation and l its dimensionality.

This orthogonality translates into an orthogonality for basis functions: We say that a set of functions $\{\phi^{\Gamma_i}\}$ transforms according to the representation Γ_i if the symmetry operator \hat{g} acts on them according to:

$$\hat{g}\phi_a = \sum_b D_{ab}^{(\Gamma_i)}(g_k)\phi_b. \quad (\text{B.9})$$

The functions $\{\phi^{\Gamma_i}\}$, that build up this representations are called partners and the *Wonderful Orthogonality Theorem* allows to deduce that two functions, which are either partners, or transform like two different irreducible representations are orthogonal

$$\left(\phi_a^{\Gamma_i}, \phi_b^{\Gamma_j}\right) \propto \delta_{ij}\delta_{ab}. \quad (\text{B.10})$$

This orthogonality may also be exploited, if the transformation properties of the Hamiltonian are known, because the matrix element between two wavefunctions transforms according to the direct product of the irreducible representations

$$\langle \phi^{(\Gamma_i)} | \mathcal{H}^{(\Gamma_j)} | \psi^{(\Gamma_k)} \rangle \propto \Gamma_i \otimes \Gamma_j \otimes \Gamma_k \quad (\text{B.11})$$

and it can be deduced, that the matrix element is zero, if $\Gamma_j \otimes \Gamma_k$ does not contain the irreducible representation Γ_i . In the case of the translational symmetry in the solid, the Hamiltonian transforms in a trivial way

$$\mathcal{T}_{\mathbf{R}}\mathcal{H}(\mathbf{r}) = \mathcal{H}(\mathbf{r} + \mathbf{R}) = 1 \cdot \mathcal{H}(\mathbf{r}), \quad (\text{B.12})$$

s.t. all matrix elements of the Hamiltonian between two Bloch functions $\psi_{\mathbf{k}}$ and $\psi_{\mathbf{k}'}$ vanish, except if they label the same irreducible representation, which is only possible if they differ by a reciprocal lattice vector $\mathbf{k} = \mathbf{k}' + \mathbf{G}$, in which case the energies are degenerate.

Appendix C

Time-dependent perturbation theory

This appendix aims to introduce the time dependent perturbation theory in order to understand the rate calculation in cases of single phonon (or direct) processes and many phonon (Raman or Orbach) processes. The starting point for the rate calculation is the time evolution of the quantum states and operators: Since the only constant in the formulation is the expectation value of an operator

$$\mathcal{O}(t) = \langle \Psi | \mathcal{O} | \Psi \rangle (t) = \langle \Psi | e^{i/\hbar \mathcal{H} t} \mathcal{O} e^{-i/\hbar \mathcal{H} t} | \Psi \rangle \quad , \quad (\text{C.1})$$

we have several possibilities to account for the time evolution of wavefunctions and operators:

In the Schrödinger picture, the operators are time independent and the wavefunctions are evolving with the exponential factor $e^{-i/\hbar t \mathcal{H}}$. In the Heisenberg picture, the time evolution is calculated for the operators. If the Hamiltonian

$$\mathcal{H} = \mathcal{H}_0 + \mathcal{V}_I(t) \quad , \quad (\text{C.2})$$

consists of a time independent part \mathcal{H}_0 , which is assumed to be solved, and a (possible time dependent) interaction $\mathcal{V}_I(t)$, the interesting part is to extract the temporal evolution induced by the perturbation $\mathcal{V}_I(t)$. For this reason, we try to eliminate the time evolution due to the unperturbed Hamiltonian in the Schrödinger wavefunction $|\Psi(t)\rangle_S$ to obtain a wavefunction in the interaction picture

$$|\Psi(t)\rangle_I = e^{i/\hbar \mathcal{H}_0 t} |\Psi(t)\rangle_S \quad (\text{C.3})$$

which has a time evolution only due to the time dependent perturbation

$$i\hbar \partial_t |\Psi(t)\rangle_I = e^{i/\hbar \mathcal{H}_0 t} (-\mathcal{H}_0 + \mathcal{H}) |\Psi(t)\rangle_S \quad (\text{C.4})$$

$$= \tilde{\mathcal{V}}_I(t) |\Psi(t)\rangle_I \quad (\text{C.5})$$

$$\text{with } \tilde{\mathcal{V}}_I(t) = e^{i/\hbar \mathcal{H}_0 t} \mathcal{V}_I(t) e^{-i/\hbar \mathcal{H}_0 t} \quad (\text{C.6})$$

as necessary for our purpose. This equation allows to derive an explicit form of the time evolution operator in the interaction picture, where

$$|\Psi(t)\rangle_I = \mathcal{U}_I |\Psi(t=0)\rangle_I \quad (\text{C.7})$$

The time evolution operator may be calculated iteratively, starting from the time evolution of the wave function mentioned above

$$i\hbar \partial_t \mathcal{U}_I(t) = \tilde{\mathcal{V}}_I(t) \mathcal{U}_I(t) \quad (\text{C.8})$$

which is integrated from 0 to t

$$\mathcal{U}_I(t) = \underbrace{\mathcal{U}_I(0)}_{\mathbb{1}} - \frac{i}{\hbar} \int_0^t dt' \tilde{\mathcal{V}}_I(t') \mathcal{U}_I(t') \quad (\text{C.9})$$

and solved by iteratively plugging in the previous solution as in the case of a Dyson or Born series, starting from

$$\mathcal{U}_I^0(t) = \mathbb{1} \quad (\text{C.10})$$

$$\mathcal{U}_I^1(t) = \mathbb{1} + \frac{-i}{\hbar} \int_0^t dt' \tilde{\mathcal{V}}_I(t') \quad (\text{C.11})$$

$$\mathcal{U}_I^2(t) = \mathbb{1} + \frac{-i}{\hbar} \int_0^t dt' \tilde{\mathcal{V}}_I(t') + \left(\frac{-i}{\hbar}\right)^2 \int_0^t dt' \tilde{\mathcal{V}}_I(t') \int_0^{t'} dt'' \tilde{\mathcal{V}}_I(t'') \quad (\text{C.12})$$

$$\vdots \quad (\text{C.13})$$

If we consider the correct ordering of the times the operators are acting at, we may rewrite the multiple integrals

$$\begin{aligned} & \int_0^t dt' \int_0^{t'} dt'' \dots \int_0^{t^{(n-1)}} dt^{(n)} \tilde{\mathcal{V}}_I(t') \tilde{\mathcal{V}}_I(t'') \dots \tilde{\mathcal{V}}_I(t^{(n)}) = \\ & \frac{1}{n!} \int_0^t dt' \int_0^t dt'' \dots \int_0^t dt^{(n)} \hat{T} [\tilde{\mathcal{V}}_I(t') \tilde{\mathcal{V}}_I(t'') \dots \tilde{\mathcal{V}}_I(t^{(n)})] \quad (\text{C.14}) \end{aligned}$$

Here the time ordering operator \hat{T} orders the operators in the bracket, s.t. operators acting at later times are to the left of operators acting at earlier times. With this result, we can formally write the time evolution operator in

an exponential form

$$\mathcal{U}_I(t) = e^{-i/\hbar \int_0^t dt' \tilde{\mathcal{V}}_I(t')} \quad , \quad (\text{C.15})$$

which has exactly the meaning as written in equation C.14. With the time evolution of a state in our hand, we are able to calculate transition probabilities between two eigenstates of the unperturbed Hamiltonian \mathcal{H}_0 . The transition probability may be calculated solely with the time evolution operator of the interaction picture due to

$$P_{f \leftarrow i}(t) = |\langle f | i(t) \rangle|^2 = |\langle f | \mathcal{U}(t) | i \rangle|^2 \quad (\text{C.16})$$

$$= \left| \langle f | e^{-i/\hbar \mathcal{H}_0 t} \mathcal{U}_I(t) | i \rangle \right|^2 \quad (\text{C.17})$$

$$= \left| \langle f | e^{-i/\hbar \epsilon_f t} \mathcal{U}_I(t) | i \rangle \right|^2 \quad (\text{C.18})$$

$$= |\langle f | \mathcal{U}_I(t) | i \rangle|^2 \quad . \quad (\text{C.19})$$

Here $|i\rangle$ and $|f\rangle$ denote the initial and final states, which are eigenstates of the unperturbed Hamiltonian:

$$\mathcal{H}_0 |i/f\rangle = \epsilon_{i/f} |i/f\rangle \quad . \quad (\text{C.20})$$

Using the expansion of \mathcal{U}_I to first order leads to Fermi's Golden Rule for the transition probability per time, which is the transition rate $\Gamma_{f \leftarrow i}$. In this thesis we only deal with harmonic and constant perturbations $\mathcal{V}_I(t) = V_0 e^{i\omega_p t}$ ($\omega_p = 0$ for a constant perturbation) and therefore derive Fermi's Golden Rule for this case

$$\Gamma_{f \leftarrow i} = \frac{P_{f \leftarrow i}(t)}{t} \quad (\text{C.21})$$

$$= \left| \langle f | \frac{-i}{\hbar} \int_0^t dt' \tilde{\mathcal{V}}_I(t') | i \rangle \right|^2 / t \quad (\text{C.22})$$

$$= \left| \langle f | \frac{-i}{\hbar} \int_0^t dt' e^{i/\hbar \mathcal{H}_0 t'} \mathcal{V}_I(t') e^{-i/\hbar \mathcal{H}_0 t'} | i \rangle \right|^2 / t \quad (\text{C.23})$$

$$= \left| \langle f | \frac{-i}{\hbar} \int_0^t dt' e^{i/\hbar \mathcal{H}_0 t'} V_0 e^{i\omega_p t'} e^{-i/\hbar \mathcal{H}_0 t'} | i \rangle \right|^2 / t \quad (\text{C.24})$$

$$= \left| \langle f | \frac{-i}{\hbar} \int_0^t dt' e^{i/\hbar \epsilon_f t'} V_0 e^{i\omega_p t'} e^{-i/\hbar \epsilon_i t'} | i \rangle \right|^2 / t \quad (\text{C.25})$$

$$= \left| \langle f | \frac{-i}{\hbar} \int_0^t dt' e^{i(\omega_{f_i} + \omega_p)t'} V_0 | i \rangle \right|^2 / t \quad (\text{C.26})$$

$$= \left| \langle f | \frac{-i}{\hbar} \int_0^t dt' e^{i(\omega_{f_i} + \omega_p)t'} V_0 | i \rangle \right|^2 / t \quad (\text{C.27})$$

$$= \frac{1}{\hbar^2} \frac{\sin^2\left(\frac{\omega_{f_i} + \omega_p}{2} t\right)}{\left(\frac{\omega_{f_i} + \omega_p}{2}\right)^2 t} \underbrace{|\langle f | V_0 | i \rangle|^2}_{V_{fi}} \quad (\text{C.28})$$

$$\lim_{t \rightarrow \infty} \frac{1}{\hbar^2} \delta(\omega_f + \omega_p - \omega_i) |V_{fi}|^2 \quad . \quad (\text{C.29})$$

The delta function accounts for the conservation of energy. In the case of the NV⁻ center, the electronic transitions in the ³A₂ groundstate may involve many final phonon states, which we consider by summation. The result for a time-independent perturbation follows for $\omega_p \rightarrow 0$. For the case of the second order transition, we first take a look at the transition probability

$$P_{f \leftarrow i}(t) = \left| \langle f | \frac{-i}{\hbar} \int_0^t dt' \tilde{\mathcal{V}}_I(t') + \left(\frac{-i}{\hbar} \right)^2 \int_0^t dt' \tilde{\mathcal{V}}_I(t') \int_0^{t'} dt'' \tilde{\mathcal{V}}_I(t'') | i \rangle \right|^2 \quad . \quad (\text{C.30})$$

The first order term was already treated above, so we will first focus on the second contribution before we merge them:

$$\langle f | \left(\frac{-i}{\hbar} \right)^2 \int_0^t dt' \tilde{\mathcal{V}}_I(t') \int_0^{t'} dt'' \tilde{\mathcal{V}}_I(t'') | i \rangle \quad (\text{C.31})$$

$$= \langle f | \left(\frac{-i}{\hbar} \right)^2 \int_0^t dt' e^{i/\hbar \mathcal{H}_0 t'} V_0 e^{i\omega_p t'} e^{-i/\hbar \mathcal{H}_0 t'} \underbrace{\sum_m |m\rangle \langle m|}_1 \int_0^{t'} dt'' e^{i/\hbar \mathcal{H}_0 t''} V_0 e^{i\omega_p t''} e^{-i/\hbar \mathcal{H}_0 t''} | i \rangle \quad (\text{C.32})$$

$$= \sum_m \left(\frac{-i}{\hbar} \right)^2 V_{fm} V_{mi} \int_0^t dt' e^{i(\omega_f + \omega_p - \omega_m)t'} \int_0^{t'} dt'' e^{i(\omega_m + \omega_p - \omega_i)t''} \quad (\text{C.33})$$

$$= \frac{1}{\hbar^2} \sum_m \frac{V_{fm} V_{mi}}{\omega_m + \omega_p - \omega_i} \left(\frac{e^{i(\omega_f + \omega_p - \omega_i)t} - 1}{\omega_i - (\omega_f + \omega_p)} - \frac{e^{i(\omega_f + \omega_p - \omega_m)t} - 1}{\omega_m - (\omega_f + \omega_p)} \right) \quad (\text{C.34})$$

The first term in the parenthesis has the same form as in the first order expansion, whereas the second term is oscillating due to the sum over all the intermediate states. In order to get rid of the oscillating term, we follow the treatment of Landau and Lifshitz (1981), reformulate the problem and assume the perturbation to be adiabatically switched on at $-\infty$ with a time dependence

$$V(t) = V e^{\lambda t} \quad \lambda > 0 \quad . \quad (\text{C.35})$$

At the end of the calculation we perform the limit $\lambda \rightarrow 0$, which allows to rewrite the transition probability with first and second order terms as

$$P_{f \leftarrow i} = \left| \frac{1}{\hbar} V_{fi} \frac{e^{i\omega_{fi}t + \lambda t}}{\omega_{fi} + i\lambda} + \sum_m \frac{1}{\hbar^2} \frac{V_{fm} V_{mi}}{\omega_{ia} + i\lambda} \cdot \frac{e^{i\omega_{fi}t + 2\lambda t}}{\omega_{fi} + i2\lambda} \right|^2, \quad (\text{C.36})$$

where the difference between two frequencies was denoted as $\omega_a - \omega_b = \omega_{ab}$ and the energy of the perturbation was added to the energy of the final state. Landau now performed some physicists math, denoted every λ as a 0^+ , which allowed to pull outside a common factor in the sum and end up with

$$P_{f \leftarrow i} = \frac{1}{\hbar^2} \left| V_{fi} + \sum_m \frac{1}{\hbar^2} \frac{V_{fm} V_{mi}}{\omega_{im} + i0^+} \right|^2 \frac{e^{2 \cdot 0^+ t}}{\omega_{fi}^2 + (2 \cdot 0^+)^2} \quad (\text{C.37})$$

which leads to a relaxation rate

$$\Gamma_{f \leftarrow i} = \frac{d}{dt} \frac{1}{\hbar^2} \left| V_{fi} + \sum_m \frac{V_{fm} V_{mi}}{E_i - E_m} \right|^2 \frac{e^{2 \cdot 0^+ t}}{\omega_{fi}^2 + (2 \cdot 0^+)^2} \quad (\text{C.38})$$

$$= \frac{2\pi}{\hbar^2} \left| V_{fi} + \sum_m \frac{V_{fm} V_{mi}}{E_i - E_m} \right|^2 \delta(\omega_f - \omega_i), \quad (\text{C.39})$$

where we used the relation

$$\lim_{\lambda \rightarrow 0} \frac{\lambda}{\omega^2 + \lambda^2} = \pi \delta(\omega) \quad . \quad (\text{C.40})$$

Using physicists induction, Landau proposed that the n -th order term of the perturbation expansion reads

$$\Gamma_{f \leftarrow i} = \frac{2\pi}{\hbar^2} \left| \sum_{a_1, a_2 \dots a_n} \frac{V_{fa_1} V_{a_1 a_2} \dots V_{a_n i}}{(E_i - E_{a_1}) \dots (E_i - E_{a_n})} \right|^2 \delta(\omega_{fi}) \quad . \quad (\text{C.41})$$

Appendix D

2nd order diagrams

This appendix shows all the possible diagrams that can arise, if we go to a second order Taylor expansion in the interaction potential and in time dependent perturbation theory. The transitions rate from an initial to a final state was derived in appendix C and reads

$$\Gamma_{f \leftarrow i} = \frac{d}{dt} \frac{1}{\hbar^2} \left| V_{fi} + \sum_m \frac{V_{fm} V_{mi}}{E_i - E_m} \right|^2 \frac{e^{2 \cdot 0^+ t}}{\omega_{fi}^2 + (2 \cdot 0^+)^2} \quad (\text{D.1})$$

$$= \frac{2\pi}{\hbar^2} \left| V_{fi} + \sum_m \frac{V_{fm} V_{mi}}{E_i - E_m} \right|^2 \delta(\omega_f - \omega_i) \quad . \quad (\text{D.2})$$

The interaction potential is chosen to be the second order Taylor expanded spin-interaction potential

$$V_{s-ph} = \sum_a \frac{\partial V(\mathbf{s}, \mathbf{r}, \mathbf{R})}{\partial \mathbf{R}_a} \mathbf{Q}_a + \sum_{a_1, a_2} \frac{\partial^2 V(\mathbf{s}, \mathbf{r}, \mathbf{R})}{\partial \mathbf{R}_{a_1} \partial \mathbf{R}_{a_2}} \mathbf{Q}_{a_1} \mathbf{Q}_{a_2} \quad . \quad (\text{D.3})$$

With these ingredients, we are able to change the phonon occupation by a maximum number of 4, using the second order interaction expansion and the second order time-dependent perturbation theory. The 20 possible diagrams, denoting all the excitation and de-excitation processes are shown in Table D.1 and Table D.2

The evaluation of the transition rate $\Gamma_{f \leftarrow i}$ for a given initial state is most easily done by a separation of the final phononic states. Taking a look at the interaction potentials, we see that there are a lot of redundant sums appearing in their evaluation. Consider for example a four phonon matrix element

$$\sum_f \langle f | \sum_{m_1} \sum_{m_2} \sum_{m_3} \sum_{m_4} (a + a^\dagger)_{m_1} (a + a^\dagger)_{m_2} (a + a^\dagger)_{m_3} (a + a^\dagger)_{m_4} | i \rangle \quad . \quad (\text{D.4})$$

For a given final state, only one set of modes $\{m_i\}$ allows for a non-zero transition matrix element, which means that the sums inside the absolute value of the Golden Rule expression vanish and the only sum to evaluate is the sum over all final states \sum_f . The temperature and magnetic field dependencies are given by the arising frequencies and the phonon-occupation numbers. To arrive at a transition rate for a given initial electronic state, we have to consider every initial state appearing in our spin ensemble. If there is no phonon-bottleneck, the sums over all initial states may be weighed by a Boltzmann-factor, resulting in the Bose-Einstein distribution for the phonon occupancies. In our summation, we will neglect the phonon-phonon interaction and assume the one particle Hamiltonian of phonons in the harmonic approximation is $H = \sum_m \hbar \omega_m (n_m + 1/2)$. Therefore, the product of two or more occupation numbers is just the product of Bose-Einstein distributions, meaning that there is no correlation:

$$\begin{aligned} \langle n_1 n_2 \rangle &= \frac{\sum_{n_1, n_2} n_1 n_2 e^{-H(n_1, n_2)\beta}}{\sum_{n_1, n_2} e^{-H(n_1, n_2)\beta}} \\ &= \frac{\sum_{n_1, n_2} n_1 n_2 e^{-(\hbar\omega_1(n_1+1/2) + \hbar\omega_2(n_2+1/2))\beta}}{\sum_{n_1, n_2} e^{-(\hbar\omega_1(n_1+1/2) + \hbar\omega_2(n_2+1/2))\beta}} \\ &= \frac{\sum_{n_1} n_1 e^{-\hbar\omega_1(n_1+1/2)\beta} \cdot \sum_{n_2} n_2 e^{\hbar\omega_2(n_2+1/2)\beta}}{\sum_{n_1} e^{-\hbar\omega_1(n_1+1/2)\beta} \cdot \sum_{n_2} e^{\hbar\omega_2(n_2+1/2)\beta}} \\ &= \frac{\sum_{n_1} n_1 e^{-\hbar\omega_1(n_1+1/2)\beta}}{\sum_{n_1} e^{-\hbar\omega_1(n_1+1/2)\beta}} \cdot \frac{\sum_{n_2} n_2 e^{\hbar\omega_2(n_2+1/2)\beta}}{\sum_{n_2} e^{\hbar\omega_2(n_2+1/2)\beta}} \\ &= \langle n_1 \rangle \langle n_2 \rangle \quad . \end{aligned} \quad (\text{D.5})$$

The temperature and magnetic field dependence is therefore deduced by keeping track of all the arising frequencies. We will show here, how the matrix element for the electronic de-excitation mechanism depicted in the upper left cell of Table D.2 looks like and how cumbersome an exact evaluation would be. The final electronic state may be reached either in first order perturba-

$ i\rangle$ — $ f\rangle$ ν_1 wavy \ominus —	$ m_0\rangle$ $ m_1\rangle$ $ m_2\rangle$	$ i\rangle$ — $ f\rangle$ ν_1 wavy \ominus — ν_5 wavy	$ m_0\rangle$ $ m_1\rangle$ $ m_2\rangle$ $ m_3\rangle$	
$ i\rangle$ — $ f\rangle$ ν_1 wavy \ominus — ν_5 wavy ν_6 wavy	$ m_0\rangle$ $ m_1\rangle$ $ m_2\rangle$ $ m_3\rangle$	$ i\rangle$ — $ f\rangle$ ν_1 wavy \ominus — ν_5 wavy ν_6 wavy ν_7 wavy	$ m_1\rangle$ $ m_2\rangle$ $ m_3\rangle$	
$ i\rangle$ — $ f\rangle$ ν_1 wavy ν_2 wavy \ominus —	$ m_0\rangle$ $ m_1\rangle$ $ m_2\rangle$	$ i\rangle$ — $ f\rangle$ ν_1 wavy ν_2 wavy \ominus — ν_5 wavy	$ m_0\rangle$ $ m_1\rangle$ $ m_2\rangle$ $ m_3\rangle$	
$ i\rangle$ — $ f\rangle$ ν_1 wavy ν_2 wavy \ominus — ν_5 wavy ν_6 wavy	$ m_0\rangle$ $ m_2\rangle$ $ m_4\rangle$	$ i\rangle$ — $ f\rangle$ ν_1 wavy ν_2 wavy ν_3 wavy \ominus —	$ m_1\rangle$ $ m_2\rangle$	
$ i\rangle$ — $ f\rangle$ ν_1 wavy ν_2 wavy ν_3 wavy \ominus — ν_5 wavy	$ m_1\rangle$ $ m_3\rangle$	$ i\rangle$ — $ f\rangle$ ν_1 wavy ν_2 wavy ν_3 wavy ν_4 wavy \ominus —	$ m_2\rangle$	
Intermediate states				
$ m_0\rangle$ \ominus \ominus	$ m_1\rangle$ \ominus ν_m wavy \ominus	$ m_2\rangle$ \ominus ν_m wavy ν_n wavy \ominus	$ m_3\rangle$ \ominus ν_m wavy ν_n wavy ν_k wavy \ominus	$ m_4\rangle$ \ominus ν_m wavy ν_n wavy ν_k wavy ν_l wavy \ominus

Table D.1: **2nd order excitation processes**, all the possible emission processes in second order are depicted diagrammatically and the involved intermediate states are shown in the right neighbouring column. The frequencies of the intermediate states are denoted by ν_m, ν_n, ν_k and ν_l . Whether these frequencies are arbitrary or have to include an initial or final phonon mode has to be considered separately for each diagram.

		$ m_0\rangle$ $ m_1\rangle$ $ m_2\rangle$		$ m_0\rangle$ $ m_1\rangle$ $ m_2\rangle$ $ m_3\rangle$
		$ m_0\rangle$ $ m_1\rangle$ $ m_2\rangle$ $ m_3\rangle$		$ m_0\rangle$ $ m_1\rangle$ $ m_2\rangle$ $ m_3\rangle$
		$ m_0\rangle$ $ m_2\rangle$ $ m_4\rangle$		$ m_1\rangle$ $ m_2\rangle$
		$ m_1\rangle$ $ m_3\rangle$		$ m_2\rangle$
Intermediate states				

Table D.2: **2nd order de-excitation processes**, all the possible de-excitation processes in second order are depicted diagrammatically and the involved intermediate states are shown in the right neighbouring column. The frequencies of the intermediate states are denoted by ν_m, ν_n, ν_k and ν_l . Whether these frequencies are arbitrary or have to include an initial or final phonon mode has to be considered separately for each diagram.

tion expansion with first order time-dependent perturbation theory of via a zero-,one- or two-phonon intermediate state. In formulas, this transition reads

$$\begin{aligned}
\Gamma_{m_s=0 \leftarrow m_s=\pm 1} &= \frac{2\pi}{\hbar^2} \left| V_{fi} + \sum_m \frac{V_{fm} V_{mi}}{E_i - E_m + i0^+} \right|^2 \delta(\omega_f - \omega_i) \\
&\propto \left| \sum_{\nu_5} \langle f | A_1 \frac{1}{\sqrt{\nu_5}} a_{\nu_5}^\dagger | i \rangle \right. \\
&\quad + \sum_m \sum_{\nu_n} \frac{\langle f | \frac{1}{\sqrt{\nu_5}} a_{\nu_5}^\dagger | m \rangle \langle m | \frac{1}{\nu_n} a_{\nu_n} a_{\nu_n}^\dagger | i \rangle}{\hbar\omega_i - \hbar\omega_m + i0^+} + \\
&\quad + \sum_m \sum_{\nu_n} \frac{\langle f | \frac{1}{\sqrt{\nu_5}} a_{\nu_5}^\dagger | m \rangle \langle m | \frac{1}{\nu_n} a_{\nu_n}^\dagger a_{\nu_n} | i \rangle}{\hbar\omega_i - \hbar\omega_m + i0^+} + \\
&\quad + \sum_m \sum_{\nu_n} \frac{\langle f | \frac{1}{\sqrt{\nu_5}} a_{\nu_5}^\dagger a_{\nu_n} | m \rangle \langle m | \frac{1}{\nu_n} a_{\nu_n}^\dagger | i \rangle}{\hbar\omega_i - \hbar\omega_m + i0^+} \\
&\quad + \sum_m \sum_{\nu_n} \frac{\langle f | \frac{1}{\sqrt{\nu_5}} a_{\nu_5}^\dagger a_{\nu_n}^\dagger | m \rangle \langle m | \frac{1}{\nu_n} a_{\nu_n} | i \rangle}{\hbar\omega_i - \hbar\omega_m + i0^+} \\
&\quad + \sum_m \sum_{\nu_n} \frac{\langle f | \frac{1}{\sqrt{\nu_5}} a_{\nu_n}^\dagger a_{\nu_n} | m \rangle \langle m | \frac{1}{\nu_n} a_{\nu_5}^\dagger | i \rangle}{\hbar\omega_i - \hbar\omega_m + i0^+} \\
&\quad \left. + \sum_m \sum_{\nu_n} \frac{\langle f | \frac{1}{\sqrt{\nu_5}} a_{\nu_n} a_{\nu_n}^\dagger | m \rangle \langle m | \frac{1}{\nu_n} a_{\nu_5}^\dagger | i \rangle}{\hbar\omega_i - \hbar\omega_m + i0^+} \right|^2 \delta(\omega_f - \omega_i) \quad . \quad (\text{D.6})
\end{aligned}$$

The further evaluation of this lengthy expression needs some comments: The sums over the intermediate states m only have a single non-zero component, where the intermediate state equals the initial phononic state plus the number of phonons created in the first step. Thus, one of the double sums (m, ν_n) vanishes. The second concern with this equation is the fact that the denominators could vanish, if the intermediate and initial state are degenerate or equal: Heitler (1954) followed an approach, which resembles the use of the self-energy in Green's function methods and introduced a lifetime-broadening. This approach is similar the treatment of the Orbach-process in the main text and in most of the cases the matrix elements will be considered in limiting cases, such that a temperature dependence may be derived.

Appendix E

Additional data for Chapter 5

This Appendix contains additional material, which shows the convergence of the crucial parameters of spin-lattice relaxation with respect to supercell size.

E.1 Eigenvectors and group velocities

In Figure E.1 we see the polarization vectors of the nitrogen atom and the corresponding group velocities for a line from Γ towards a non-symmetry boundary point in the Brillouin zone. As we see, the group velocities reach unphysical values, if the frequency is lower than 0.2 THz. Since we only deal with the acoustic bands, the polarization vectors are very similar for the different atoms in the unit cell.

E.2 Localized phonon modes

Depending on the definition of the localized mode, we obtain different modes which are maximally localized. As mentioned in the main text, we have chosen two types of localization criteria: Once we consider the amplitude of oscillation of the 4 atoms closest to the vacancy, and the other time we compare the oscillation of the 16 closest atoms with the rest. The results of the random scan of the Brillouin zone for localized phonons was shown in Figure 5.10. Here we present the localized displacements with the respective oscillation frequency.

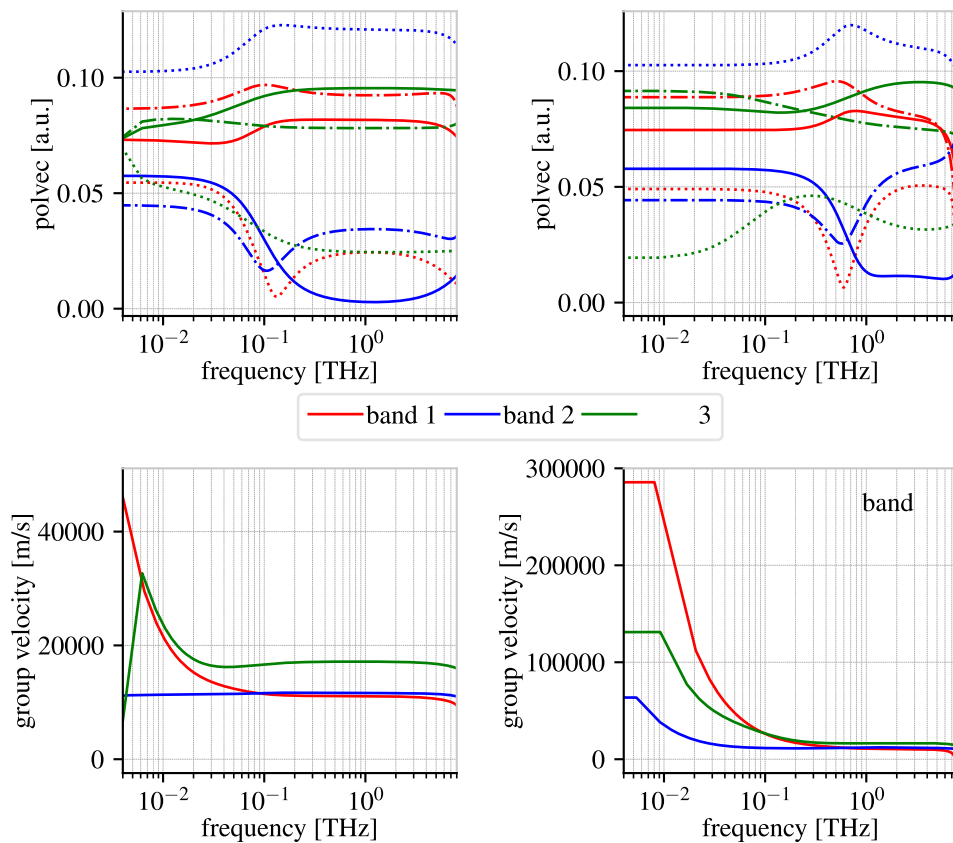


Figure E.1: **Supercell convergence**, the columns of this Figure show the resulting polarization vectors (top) and the group velocities (bottom) for the case of the $1 \times 1 \times 1$ supercell containing one NV^- center (left) and for the case of a $2 \times 2 \times 2$ supercell with 8 NV^- centers. The style of the lines in the top plots corresponds to the x- (solid) , y- (dashed) and z- (dotted) components of the polarization vectors

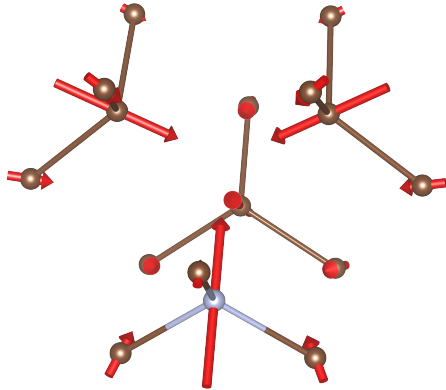
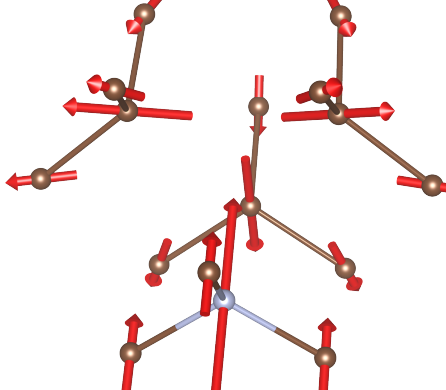
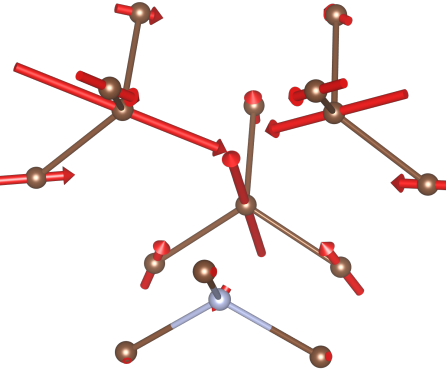
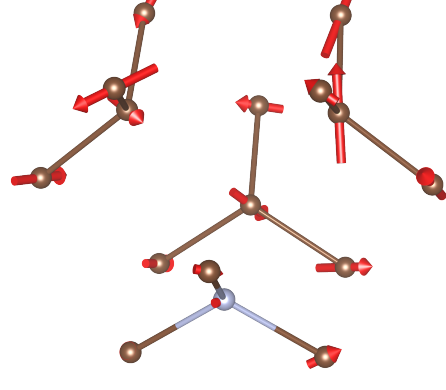
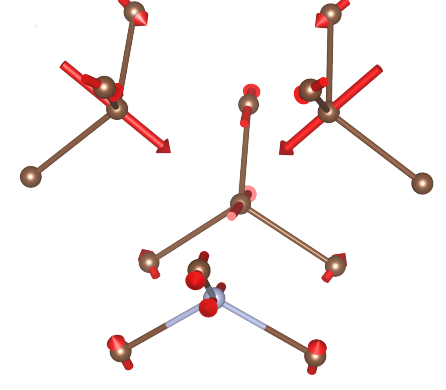
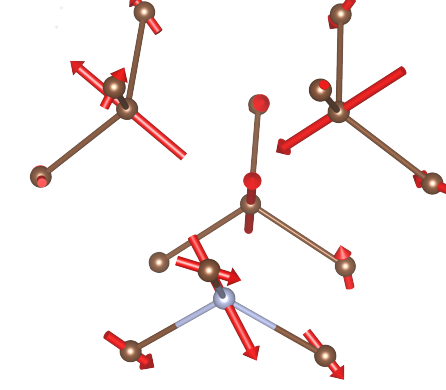
	
$x_{loc} = 10.00$ $\nu = 17.19 \text{ THz}$	$x_{loc} = 9.85$ $\nu = 15.01 \text{ THz}$
	
$x_{loc} = 9.13$ $\nu = 16.7 \text{ THz}$	$x_{loc} = 8.94$ $\nu = 18.11 \text{ THz}$
	
$x_{loc} = 8.63$ $\nu = 16.46 \text{ THz}$	$x_{loc} = 8.01$ $\nu = 16.69 \text{ THz}$

Table E.1: **Localized modes - 4 neighbours**, The most localized modes we found are listed with their oscillation frequency and localization factor x_{loc}

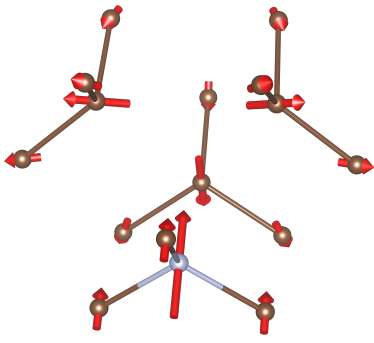
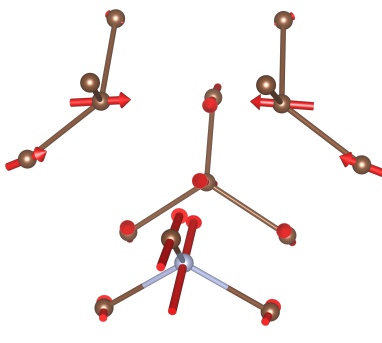
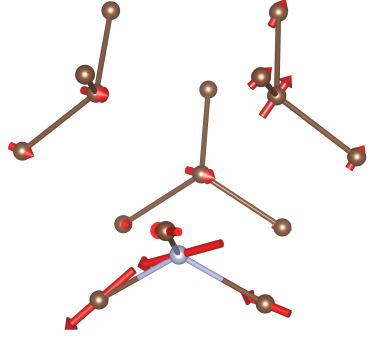
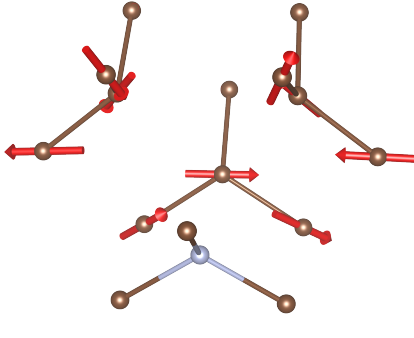
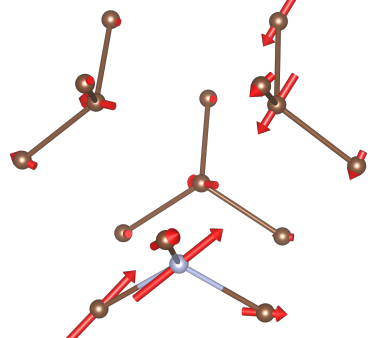
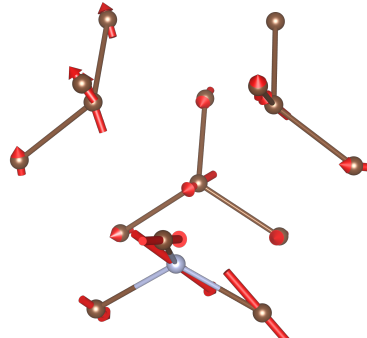
	
$x_{loc} = 6.4$ $\nu = 15.04$ THz	$x_{loc} = 5.51$ $\nu = 15.36$ THz
	
$x_{loc} = 5.42$ $\nu = 15.40$ THz	$x_{loc} = 5.33$ $\nu = 15.29$ THz
	
$x_{loc} = 5.26$ $\nu = 15.29$ THz	$x_{loc} = 5.14$ $\nu = 15.37$ THz

Table E.2: **Localized modes - 16 neighbours**, The most localized modes we found are listed with their oscillation frequency and localization factor x_{loc}

References

- Dresselhaus, M. S., G. Dresselhaus, and A. Jorio (2008). *Group Theory*. Springer Berlin Heidelberg.
- Engel, E. and R. M. Dreizler (2011). *Density Functional Theory: An Advanced Course*. Vol. 2011, pp. 499–515.
- Heitler, W. (1954). *The quantum theory of radiation*. Dover Publications.
- Landau, L. D. and E.M. Lifshitz (1981). *Course on Theoretical Physics, Vol 3*. Pergamon Press.

Johannes Gugler

Dipl.-Ing.

Personal Information

Date of birth September 16th, 1990
Nationality Austria

Education

1996–2001 **Primary School**, *Volksschule St. Peter in der Au*, grades 1–4.
2001–2009 **Secondary School**, *Öffentliches Stiftsgymnasium Seitenstetten*, grades 5–12.
2010–2016 **Diploma Studies**, *TU Wien*, Vienna, Master Thesis: Ab-initio Simulation von Bismut-dotiertem Silizium.
Supervised by Prof. Peter Mohn
2016–2019 **Ph.D. Studies**, *TU Wien*, Vienna, Ph.D. Thesis: Ab initio calculation of the spin-lattice relaxation time T_1 in the negatively charged nitrogen vacancy center.
Supervised by Prof. Peter Mohn

Work

2007–2008 **Internship**, *Hörmann Interstall*, Vienna.
2009–2010 **Civil Service**, *Landesverein für Sachwalterschaft und Bewohnervertretung*, Vienna.
2011–2013 **Internship**, *Landesverein für Sachwalterschaft und Bewohnervertretung*, Vienna.

Teaching

2018 **Tutor**, *Institute of Applied Physics*, TU Wien.
Tutor for the Fundamentals of Physics I
2018 **Mentor**, *Faculty of physics*, TU Wien.
Mentor for the

Publications

- [1] T. Astner, J. Gugler, A. Angerer, S. Wald, S. Putz, N. J. Mauser, M. Trupke, H. Sumiya, S. Onoda, J. Isoya, J. Schmiedmayer, P. Mohn, and J. Majer, "Solid-state electron spin lifetime limited by phononic vacuum modes," *Nature Materials*, vol. 17, no. 4, pp. 313–317, 2018.
- [2] J. Gugler, T. Astner, A. Angerer, J. Schmiedmayer, J. Majer, and P. Mohn, "Ab initio calculation of the spin lattice relaxation time T_1 for nitrogen-vacancy centers in diamond," *Phys. Rev. B*, vol. 98, p. 214442, 21 2018.
- [3] M. Pimon, G. Kazakov, J. Gugler, M. E. G. Valerio, N. Mauser, R. A. Jackson, P. Mohn, and T. Schumm, *²²⁹Thorium doped magnesium fluoride for nuclear laser spectroscopy*, 2018.